AURORAL INFRASONIC WAVES AND THE POLAR MAGNETIC SUBSTORM

A
DISSERTATION

Presented to the Faculty of the
University of Alaska in Partial Fulfillment
of the Requirements
for the Degree of

DOCTOR OF PHILOSOPHY

By
Roland Everett Johnson, B.S., M.S.
Fairbanks, Alaska
May, 1973

AURORAL INFRASONICS AND POLAR MAGNETIC SUBSTORMS

APPROVED:

K. B. Hoffman

Jack H. Wright

Jerry Wilde

Charles R. Wilson
Chairman

Roger Sheridan
Department Head

APPROVED: C. Black Date 5-16-73
Dean of the College of Mathematics,
Physical Sciences and Engineering

C. A. Pabst
Vice President for Research and Advanced Study

TABLE OF CONTENTS

ABSTRACT

The purpose of this thesis is to investigate the relationship of auroral infrasonic waves to the polar magnetic substorm. The major emphasis is to determine whether or not there are specific regions within the substorm where the infrasound is generated. It is found that the eastern end of the electrojet is a region which was very effective in generating infrasound, and was also a region in which supersonic auroras were observed to be propagating.

The magnetic substorm is represented temporally and spatially by use of sequences of contour maps of the total horizontal disturbance vector or the total magnetic disturbance vector. It is shown that attempts to locate the source region of the auroral infrasound generator are futile in the mapping study unless there is some knowledge of the transit speed between the source and observer. A mean horizontal transit speed is derived and found to be near the value of 243 m/sec.

Applying the mean horizontal transit speed to centers of intense magnetic activity within the auroral electrojet led to the capability of predicting the onset of coherent pressure disturbances at College, when the station was located near the eastern end of the electrojet. Only feeble infrasound emission was correlated with the western end of the electrojet.

Before analyzing the material for four data nights utilized in this study, recognition is given to the multiplicity of types of auroral infrasound and a system of classification is proposed.

ACKNOWLEDGEMENTS

A deep debt of gratitude goes to my Committee Chairman, Dr. C. R. Wilson, who provided the motivation for my continued research at the Geophysical Institute, and who, even during the trying times of disagreement over the research, always kept the faith.

To my wife, Penny, whose presence and efforts in support of my scholastic program, and who contributed the larger part of the typing to this document, I am also gratefully appreciative.

Much effort was contributed by my friends in the final days of preparing the typed manuscript and the preparation of figures. The large boost in typing came from Mrs. Jane O'Connor and supplementary aid from Miss Judy Holland. Drafting skill and uncompensated assistance was provided by Mrs. Shirley Wilson and Jimmy Burton, who came in a time of need. Excellent drafting assistance and general support as the deadline hours approached was also provided by Miss Hiroko Horiuchi, Mrs. Genny Edsall, and Mrs. Barbara Schleigh.

I am also indebted to Dr. Rostoker for provision of magnetograms from his chain of stations and a helpful discussion of electrojets early in the analysis of this report.

To Dr. R. L. McPherron I owe a vote of thanks for the data provided at Tungsten, a critical location for this investigation.

I am grateful for the funding which has made this thesis possible, and which has come from a small number of sources. I acknowledge the research supported by the U.S. Department of Commerce, NOAA geoacoustics group. I would also like to thank the Infrasonic Group at Pullman,

Washington, and the Infrasonics Group in Boulder, Colorado for providing pressure records for this study.

Research for this thesis was also supported by U.S. Department of Commerce Contract E22-45-70 (N) and National Science Foundation Grant GA-16821, for which I am thankful. My gratitude extends also to National Science Foundation Grant GA 2954IX which also supported this research.

My appreciation is extended to the Inuvik Research Laboratory which provided an excellent data collection, some of which was used in this study.

A final debt of gratitude goes to the people who staff the services at the Geophysical Institue, for they have indeed, captured the spirit that made my stay here more pleasant. Continual support was always offered by my friend and co-worker, Mrs. Nita Balvin, whose technical skills have been a blessing to the project.

To my friend, Paul Goodwin, my gratitude for the many penetrating technical discussions, and especially for his skill in developing the ray path program used in this endeavor.

LIST OF FIGURES

INTRODUCTION

For nearly two decades since their discovery, long period traveling pressure waves have been found to be emitted during geomagnetic disturbances. Subsequent research found that the onset of these pressure waves was associated with supersonic aurora which were themselves an integral part of the complex geomagnetic disturbance. Inasmuch as the regions of the geomagnetic disturbance which were most prolific in the production of infrasound was unknown, it became a motivational point of interest at which to undertake this investigation.

Before specifying the central aims of this study, it is significant to summarize the present state of knowledge, or ignorance as it were, of many important factors significant to the study of emission of infrasound by the aurora. There are many unknown quantities which are evident whenever an acoustic pulse is received from the geomagnetic disturbance or substorm. A partial listing of such unknown features is:

1. The region within the geomagnetic disturbance where the infrasound is generated.
2. The time of emission of the signal.
3. The input signal shape or frequency spectrum.
4. The amplitude of the signal at the source.
5. The propagation path and attenuation factors.
6. The acoustic structure of the atmosphere along the propagation path.
7. Threshold value of geomagnetic disturbance necessary for the production of infrasound.

8. The generation mechanism itself.

The main purpose of this thesis is to investigate the areas within the auroral and polar magnetic substorm disturbance which are significant to the production of auroral infrasound. The secondary effort will be directed toward studying the emission time within the substorm framework when the infrasonic pressure disturbances commence. These two objectives head the listing above, and it is hoped that the process of studying them sheds some light, however small, on some of the others.

Chapter I of this thesis reviews some of the pertinent literature related to the substorm an auroral electrojet.

Chapter 2 discusses the morphology of auroral infrasonic waves, as well as displays the multiplicity of types of other sources of natural infrasound. In recognition of the diverse types of auroral infrasonic signals detected in the auroral regions, a system of classification is proposed in order to direct some effort of future research towards understanding the processes associated with each.

Chapter 3 discusses pertinent information concerning the data analysis and instrumentation.

Chapters 4-7 are the sections in which the observations of particular nights are discussed and interpreted. Each of the nights was selected because of some peculiar feature of the data, and the attempt was made to select the widest variety of conditions of the infrasonic disturbance in order to broaden the scope of the study. In each of these data night chapters, the geomagnetic disturbances are represented

by contour maps in order to achieve an understanding of both the spatial and temporal variations of the substorm.

Chapter 4 is a study of the data night of 3. Oct. 1968. It was selected because of the long duration of intense pressure perturbations of geomagnetic origin detected at College, and because of infrasonic data available at three stations in the lower United States.

Chapter 5, the data night 25 June 1969, was chosen because of its relative simplicity as far as the auroral pressure disturbances are concerned: only a single signal was thought to have occurred at College that night. The data night was used in order to derive a mean horizontal transit speed for auroral infrasonic waves.

The data night 9 Nov. 1969, comprising the study of chapter 6, was selected for the presence of large amplitude auroral infrasonic pressure disturbances at the College station, and also another station located at Inuvik, N.W.T., Canada. It was also chosen due to the availability of magnetometer data from a large number of observatories in North America and its eastern environs.

The data night 9 November 1969, chapter 7, was selected for the fact that there was no auroral infrasound detected at both College and Inuvik, the observing conditions were relatively quiet at both stations insofar as background noise was concerned, and there was All-Sky Camera data available at a total of six stations in Alaska and western Canada.

The remaining chapter discusses the findings of this investigation, and concludes.

CHAPTER I

SUBSTORM PHENOMENA

Introduction

The appearance of an acoustic pressure pulse which has emanated from some obscure region of the geomagnetic disturbance, culminating in its dissipation by numerous atmospheric extinction processes, represents an end point of numerous dynamic phenomena whose origin may be traced back to the sun. Be it even a tiny fraction of the total energy of the various processes associated with its origin, a proper perspective of the chronology of the signal must at least mention in some way, however general, that this parcel of acoustic energy had an extra-terrestrial origin. Certainly myriads of energy transfer interactions transpired in order to yield the acoustic pulse, and it is equally certain that most of them will remain obscure for many years to come. Nevertheless, as research to the present has shown, the infrasonic pressure disturbance generated during polar magnetic disturbances has its atmospheric origin embedded somewhere in those processes characteristic of the polar magnetic substorm itself. Thus a researcher investigating this type of naturally-occurring infrasound must confront himself with not only some of the substorm phenomena themselves, but from point of view of overall perspective at least, must recognize the labyrinth of marginally-understood interactions on the solar surface which went into their creation. So, from point of view of form and chronology, this study commences with passing reference to those

significant solar processes which lead to the magnetospheric storm, names the various substorms currently recognized as such, studies some aspects of the auroral and polar magnetic substorm thought to be significant in the acoustic study, and then studies the auroral electrojet and the affected portions of the polar ionosphere.

Magnetospheric Storm

It would appear that the intent of the designation 'magnetospheric storm' is to apply a name to a large number of complex dynamic interactions in the upper atmosphere and magnetosphere which owe their origins in a more direct way to the energetic processes occurring on the sun. An exceptionally comprehensive work tracing the important solar disturbances and their relation to the earth's magnetosphere as well as providing an up-to-date summary of the findings of knowledge in this field has been presented by Akasofu and Chapman (1972). They show that the significant features of the solar surface which culminate in a magnetospheric storm are solar storms, the growth and decay of 'centers of activity' which affect the flow pattern and magnetic fields in the solar wind, and turbulent M streams which are associated with an alternate form of plasma emission by the sun that influences our 27-day recurrence tendency.

The solar storms are shown to be the focus of emission of electromagnetic radiations, corpuscular radiations of energy 1 KeV to 10 GkV, and then a shock wave in the solar wind which is followed by a plasma cloud. The magnetospheric storm is then shown to be caused by the interaction of this interplanetary shock-wave with the magnetosphere which compresses it, and also by the following plasma

cloud which contributes to those explosive processes embodied in the name substorm.

The authors have divided the magnetospheric storm into three phases: an initial phase, a main phase, and probably a recovery phase which does not appear to be specified as such. The onset of the initial phase is caused by the interaction of the interplanetary shock with the earth's bow shock which then leads to a compression of the magnetosphere. This interaction also leads to the storm sudden commencement which is frequently observable at ground-based observatories as a step-function-like increase or abrupt change in some magnetogram components in some cases, and sharp onsets and perhaps oscillations of a component in others. Following the sudden onset, there may be an extended relatively calm period which may last from minutes to a few hours.

There follows then the main phase of the magnetospheric storm which occurs after the plasma cloud, which drives the interplanetary shock, reaches the magnetosphere. This triggers the onset of the many dynamic processes which have been included in the name of magnetospheric substorm. Seven separate and interrelated processes have been recognized and described under the names magnetospheric or polar substorm (Akasofu, 1968). The names applied to these different processes are: auroral, polar magnetic, ionospheric, x-ray, proton aurora, VLF emission, and micropulsation substorms. Insofar as this thesis is concerned, the first three substorms designated here will form areas of principle concern, while the ionospheric substorm, in keeping with the Akasofu designation, contains the

infrasonic emissions which are the primary interest of this thesis.

Many observable features in the earth's magnetic field at the ground have been specified as well as such features of the upper atmosphere associated with the various phases of the magnetospheric storm can be discussed, for example see Paghis (Hines, et al., 1965), but will be overlooked here in favor of studying the substorm types of principle interest. To terminate this portion of the discussion, suffice it to say that the recovery phase of the magnetospheric storm represents a return to pre-storm conditions after an elapse of time. In low latitudes, the return of the H-component to pre-storm level is gradual, but fast compared to high latitudes which may take several days (Paghis, op cit.).

Polar Magnetic Substorm

One of the more interesting and challenging manifestations of the magnetospheric substorm is the sequence of magnetic disturbances which are incorporated under the title Polar Magnetic Substorm. This perturbation of the earth's magnetic field was identified after the invention of magnetic recording instruments in the last century. The early signature of the substorm detected at that time was given the name 'bay' which, according to Chapman and Bartels (1940) was first applied by the early researcher Chree (1919) who likened their appearance on magnetic records to geographic coastlines. It is not the intention to trace the history of the research on this phenomenon here, but to discuss some aspects of it which are pertinent to this study.

The motivation for the study of the polar magnetic substorm is

this investigation can be exemplified in Fig. 1-1. This figure shows two H-component storm magnetograms recorded at College, Alaska on the days indicated. Arrows placed along the base of the magnetograms indicate the times when coherent pressure disturbances were recorded at the station at College. The close association in time with the bays, which represent the polar magnetic substorms, are indicative of their geomagnetic perturbation origin. Though only a sketchy picture of these substorms in the generic sense will be attempted in this section, more detailed views of the substorms of particular nights will be presented in subsequent chapters with the emphasis on morphological features which might be significant to the production of infrasound.

Returning to the discussion of the polar magnetic substorm proper, one is confronted with a choice of initiation points when one considers the origin of the substorm itself. What is being referred to here is that a long sequence of events, each being caused by an earlier process in the chain, is significant to the discussion of the cause of polar magnetic substorms. There seems to be a consensus of opinion that one of the direct causes of the polar magnetic substorm is the enhancement of the westward electrojet (Rostoker, 1972; Akasofu, 1968; Akasofu, Chapman and Meng, 1965) which is an ionospheric phenomenon connected to farther reaches of the magnetosphere by the magnetic field lines. Other researchers have looked farther along the chain of causes for the magnetic substorm and have cited implosive recombination of field lines in the magnetotail along the neutral sheet (Atkinson, 1966, and others).

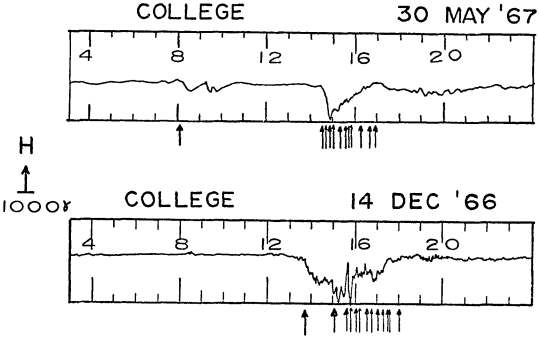

Fig. I-1 The association of infrasonic pressure disturbances with magnetic bays. (after Wilson, 1969).

Using this mechanism as a driving force, Axford (1969) applied a magnetospheric convection model to explain such variations as Sq, L, DP1, and DP2, where the DP1 variation itself appears to be associated with the auroral electrojet. On the other hand, substorm triggering mechanisms quite distant from the ionosphere were implied in the AST-1 satellite data taken at 6.6 Re (Cummings and Coleman, 1968). The references cited here certainly do not exhaust the literature of workers of their particular viewpoint, nor are they intended to. What is intended here is to trace a few characteristic features of the polar magnetic substorm and to look no farther away from the surface of the earth than the ionosphere, the seat of the auroral electrojet.

Because of their intimate relationship via causality, it is difficult and perhaps unfruitful to discuss the polar magnetic substorm as an isolated entity without lapsing into a description of particular features of the aurora and either equivalent current systems in general or the auroral electrojet in particular. Since separate treatment is given to these phenomena in this chapter, only brief general comments concerning the magnetic substorm will follow.

Despite the disagreement by some of the researchers in the field concerning the triggering and development of the substorm, it is probably safe to state that the polar magnetic substorm may in general be divided into at least two and possibly three phases. The first phase, a growth phase, is still in contention, but was suggested by McPherron (1970). During this phase, which may last a few tens of minutes, energy is taken to be injected into the nightside

magnetosphere. Following this phase, if indeed it does exist, there follows a less contentious expansive phase, which might be characterized by polewardly moving aurora which have just brightened. This phase may occur rather sharply and would typically last for only a few minutes. Following this phase is a recovery phase lasting one or two hours which ends as the auroral arcs return to their quiet time configuration.

Since an immediate cause of the polar magnetic substorm has already been specified as the auroral electrojet which is situated in the auroral oval, the magnetic disturbances around it typically occur as intense negative bays on the poleward side in the evening sector, and weak positive bays equatorward. Stations close to the auroral zone may frequently be located in a transition region between the two and may thereby encounter a combination of types (Akasofu and Meng, 1967) which are neither simple positive nor negative bays.

Having described in this simple way some of the general and typical features of polar magnetic substorms, it remains now to say that, using magnetograms to study this phenomenon, it is not always clear when the substorm actually begins, whether or not one considers the growth phase. Some light has been shed on this problem by Rostoker (1972) who has found that Pi micropulsations may be used to identify onsets for every substorm to within an accuracy of $\pm$ 1 minute!

The Auroral Substorm

This facet of the magnetospheric substorm has been studied very

extensively by Akasofu (1964). The sequence of observable features in his model are adopted here as the likely representation of the phenomenon on a given night. In terms of his model, this substorm is divided into two phases. The first, the expansive phase, begins with the brightening of a previously quiet arc near the midnight sector and its subsequent motion poleward. This poleward motion varies in speed depending upon the strength of the substorm. One of its consequences is an auroral bulge of the oval in the midnight sector which, in the case of fairly intense substorms, leads to an omnidirectional expansion of the bulge (Akasofu, 1966a). Into the evening sector the expansion of this bulge is manifest as a westward travelling surge which leaves a zone of negative bays behind it, and positive bays west and equatorward of itself.

A view of the various developmental stages into which Akasofu divided the expansive phase of the auroral substorm is afforded by the polar plots in Fig. 1-2. Since the various features of these diagrams are very well known, no further description of this phase will be given here other than to mention the speeds of the poleward expansions for 84 cases showed a distribution from less than 100 m/sec to greater than 1300 m/sec (Akasofu, 1966b). The most frequently occurring speeds were in the range 300-600 m/sec. It might also be mentioned that this entire sequence of auroral motions are taken to occur within the auroral oval and the bulges experienced from the midnight sector outwards is taken by Akasofu to be an actual expansion of the oval itself.

The second phase of the auroral substorm described by the

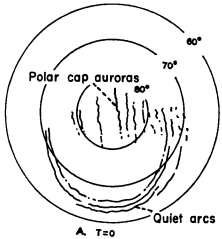

THE DISTRIBUTION OF THE AURORAS DURING THE QUIET PHASE.

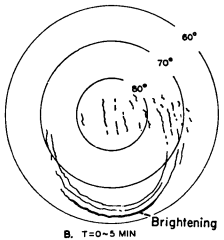

AURORAS DURING THE EXPANSIVE PHASE (STAGE I).

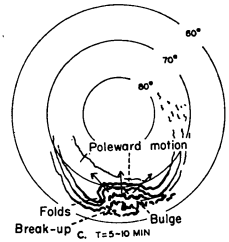

AURORAS DURING THE EXPANSIVE PHASE (STAGE II).

Fig. I-2. Diagrams of aurorae as seen from the geomagnetic pole during the quiet and expansive phases of the auroral substorm. (after Akasofu, 1964).

1964 Akasofu model is designated the recovery phase. It seems to come about typically between 10-30 minutes after the onset of the expansive phase, and is characterized by the arrival of the activated band at its northernmost latitude and its subsequent motion equatorward. Akasofu has also subdivided this phase into three stages, all of which seem to contain equatorward motion of arcs, and the final two stages of this phase is dominated by such movements. A polar plot of the first two stages of the recovery phase of the auroral substorm is shown in Fig. 1-3. As in the previous figure, the universality of the knowledge of this substorm model renders the figure mainly self-explanatory.

It is interesting to note here that according to the Akasofu model, the expansive phase of the auroral substorm at T=0, to the end of this phase occupies up to about 30 minutes, whereas the recovery phase would last up to 3 hours. Since the expansive phase is characterized by auroral motions north-, east-, and westwardly, whereas the recovery phase, at least in the final two stages, is dominated by equatorward motions, one would expect to see a preponderance of southerly motions during the expanse of the substorm.

The subject of auroral motions and their speeds is especially pertinent to the study of auroral infrasonic waves since the very earliest associations for an origin of the waves was through a supersonically moving arc (Wilson and Nichparenko, 1967) mechanism. Studying equatorward motions, Akasofu, Kimball and Meng (1966c) recognized three types of equatorward drift. For the one case of equatorward motion associated with the recovery phase of the auroral substorm, they measured the speeds for 76 examples of which 58

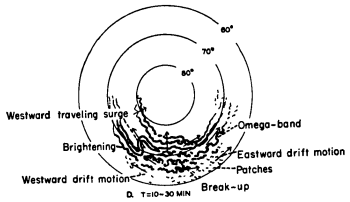

AURORAS DURING THE EXPANSIVE PHASE (STAGE III).

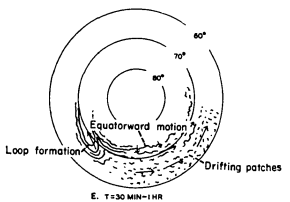

AURORAS DURING THE RECOVERY PHASE (STAGE I).

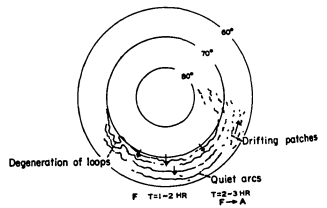

AURORAS DURING THE RECOVERY PHASE (STAGE II).

Fig. 1-3. The end of the expansive phase and the two stages of the recovery phase of the auroral substorm. (after Akasofu, 1964).

were less than 300 m/sec, and the remaining ones had speeds up to and including 800-900 m/sec. An earlier study (Bhattacharyya, 1960) of motions along and perpendicular to the geomagnetic parallels found that the peak number of occurrences for motions in the four cardinal directions were in the speed range of 0-150 m/sec. The largest speeds, i.e., greater than 700 m/sec presumably were associated with westward and southward motions as opposed to eastward and northward.

In a study of radar echoes of auroral motions at Saskatoon (Lyon and Kavadas, 1958) the authors found the motions mainly westward before midnight and eastward after. The westward-moving echoes were associated with positive bays, and the eastward ones with negative bays. The peak speeds reported in this study were 100 m/sec for westward motions and 250 m/sec for eastward.

In an all-sky camera study of auroral motions, Kim and Currie (1960) noting no significant variation that could be distinguished between north-, and southward motion, averaged their data into average values of meridional motion. Their data for the stations at Saskatoon, Flin Flon, Uranium City, and Aklavik showed an increase to maximum speed in the morning hours in the auroral zone for 358, 974, 642, and 237 observations respectively. All but two of their Saskatoon observations averaged out to be less than an acoustic speed of 300 m/sec. For motion normal to the geomagnetic meridians, they found average values of 527 m/sec. (31.7 km/min) for westward. Kim and Currie found, as did Lyon and Kavadas, that the speeds tended to increase with the level of magnetic disturbance

and associated their east-west motion with higher levels of magnetic activity. These findings do not disagree with Akasofu et al., (1966a) who found speeds of westward surges (order of 1 km/sec) to be less than the eastward speeds in the morning (approximately 10 km/sec).

In their study of auroral motions, Davis and Kimball (1960) observed a preponderance of southerly-moving motions over the northward motions, but did not study their relative speeds.

A recent study by Rostoker (1972) using all-sky cameras at Fort Smith and Meanook for the period August 1970-March 1972 in conjunction with his meridian chain of magnetometers, studied poleward and equatorward motions of auroras. He concludes that his observations of poleward motions depict jerky motions rather than smooth ones which he inferred from the Akasofu model. Moreover, he finds that his poleward motion observations show speeds in the 1-2 km/sec range for brief periods, which contrast to Akasofu's 200-800 m/sec speed for same. Aside from this lack of exact agreement - which might only be one of interpretation - a far more interesting and significant result is his observation of a continuous and persistent auroral electrojet after the bright aurora has vanished from the sky. At most during this observation, he noticed only faint, diffuse auroras in the vicinity where an intense electrojet was inferred. This finding, if not an atypical feature of electrojet and arc association, might have far reaching consequences insofar as analysis is concerned in the generation mechanism for auroral infrasound. It is significant to this study because, as the chapter concerning

the data night of 9 November 1969 will show, such an interpretation easily fits the data presented there during the poleward expansion.

The Auroral Electrojet

The basic concept of an ionospheric current system with field-aligned currents which cause polar magnetic disturbances was apparently first initiated by Birkeland (1913). Though not in agreement at that time with the idea of the three-dimensional current system, Chapman (1935) concluded that there were an infinity of solutions for the problem of locating the height of the electrojet by using magnetic observations alone, but reasoned that a study of the earth's role in the induction process would possibly unravel the dilemma. Monish (1938) also concerned himself with the height problem of the current system and was hampered by the lack of real knowledge of the role of induction.

Insofar as studies of this system in the past decade is concerned, Fejer (1963) described possible mechanisms for the formation of the jet citing a magnetospheric convection model of interaction with high energy particles or a high energy particle mechanism interacting with a magnetosphere co-rotating with the earth. Bostrom (1964) returned to the Birkeland field-aligned current idea by offering another three-dimensional current model for two separate cases. In the one case, he assumed a low density plasma driven by the wind and electric field of magnitudes 440 m/sec and 0.025 volt/m respectively. For the second case he selected a sheet current flowing into the south side of the auroral arc and out of the north side instead of flowing out of the eastern and western ends of the arc

as in the first case. Figure I-4 shows the model for the two cases which Bostrom studied. In both cases he assumed the current to be confined to the auroral arc, but added the restriction in case (1) that the plasma density was low and for case (2) that there was perfect conductivity along the field lines in the magnetosphere.

Following the Bostrom model, Akasofu, Chapman, and Meng returned to a two-dimensional model containing a westward jet around the entire auroral oval with return currents across the polar cap from the midnight sector north of the jet, and eastward return currents south of it beginning in the afternoon sector and rejoining in the midnight sector. This system was designed to explain the pattern of magnetic perturbations observed at the surface of the earth. Support to this model was given by Rostoker (1966) who, at that time, favored it while studying mid-latitude transition bays. His conclusions relative to this two-dimensional model were that this two-dimensional system and its return currents were the cause of geomagnetic bays whose intensity were dependent on both the temporal changes in the currents themselves as well as their motion with respect to the observing station.

By the following year, evidence of possible detection of field-aligned currents appeared in the literature (Cummings and Dessler, 1967) based upon the interpretation of localized magnetic fluctuations such as giant pulsations. Further support for a field-aligned model similar to the Bostrom model was given by Atkinson (1967) who viewed the auroral electrojet as causing magnetic bays by the

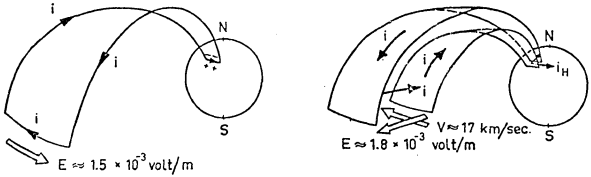

Fig. 1-4. Field-aligned currents of the auroral electrojets showing (a) the case of ionospheric transit through the ends of the auroral arc; and (b) the case of the ionospheric transit into the southern end and out via the northern. (after Bostrom, 1964).

superposition of its effects upon a Hall current system. Iijima and Fukushima (1968) discussed possible precursors in the form of increases in the H-component of about 10-15 gammas which herald the onset of the electrojet.

Bonnevier, Bostrom, and Rostoker (1970) decided "...there is no ionospheric source energetic enough to cover the energy losses of the electrojet." for the case of a two-dimensional model shown in Fig. 1-5. The new model, though similar to the earlier Bostrom model apparently made no restriction of flow into and out of the actual auroral arc, but specified only current flow into the ionosphere. The authors of this model claim that it accounts for the observed magnetic perturbations without meeting eastward return currents since the model was capable of producing positive H-component bays. They concluded from observations based upon their model that the ionospheric portion of the current both increased in length as well as broadened and expanded northward across the course of a substorm. Kisabeth and Rostoker (1971) again invoking the model of Bonnevier et al., inferred the possibility of double currents flowing during a substorm such that one might infer northward motion of an electrojet when, in actuality, there might have been an appearance of a new electrojet to the north of the one already in progress. Studying the electrojet with latitude profiles, they showed that the latitude of the location of the jet may be inferred from the moment, or the $\Delta z = 0$ crossing of the Z-component of the latitude profile. With other minor restrictions the width of the jet may also be inferred.

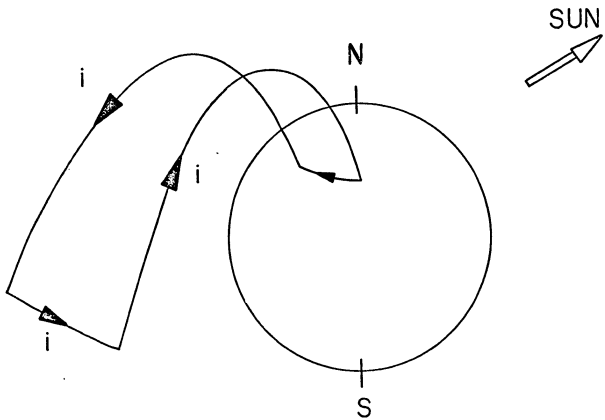

Fig. I-5. Proposed model current system showing field-aligned flow into the ionosphere (not arc). (after Bonnevier, et.al., 1970).

CHAPTER 2

INFRASONIC PRESSURE DISTURBANCES

2.0 Introduction

Since the fall of 1965, infrasonic waves have been detected and recorded at the Geophysical Institute, University of Alaska. The main thrust of the rearch has been the study of those pressure disturbances whose origin has been associated with the aurora, and which have become known as Auroral Infrasonic Waves (referred to hereafter as AIW). The main recording site has been located at College since that time, but supplementary recording sites have been supplying infrasonic data in support of the College staion at various periods. In particular, a station was operated at Palmer, Alaska for the period Oct. 1967-Oct. 1968; Inuvik, N.W.T., Canada, above the arctic circle, for the period Oct. 1969-March 1971; and Stevens Village, Alaska, Nov. 1971-April 1973 (this network referred to hereafter as the "Alaskan arrays").

In every case, the infrasonic array consisted of four microphone stations deployed in a quadrilateral shape whose dimensions were close to an average of 5Km. along the sides. From these stations more than 2500 signals have been scaled and recognized as being related to the aurora and the accompanying geomagnetic disturbance. Further remarks concerning the instrumentation used in these experiments will be presented in the chapter following this one.

Though higher and lower frequency channels were used at College

during the first two years, the one on which all the research concerning AIW has been based is the passband having the half-power points at 7 & 70 seconds. Thus the discussion of infrasound in this report is based upon those signals and noise which have been recorded in the 7 to 70 second passband.

In order to clarify the references to the records which are made in this chapter, a few words concerning their treatment are made here. A more detailed view of the overall data handling for this report will be provided in chapter 3.

The recognition of an infrasonic pressure disturbance as a travelling wave requires more than one station separated by a suitable distance. Otherwise, the pressure record from a single station would show an endless train of random pressure fluctuations admixed with the signal with no way of distinguishing between the two. Thus signal recognition is accomplished by superimposing the records from the four microphones from a given recording site, and observing the phase coherence in the record. These coherences are taken to be travelling waves when they can be recognized at three of the four observing sites and satisfy a plane-wave solution for time and direction of travel across the array.

Having recognized the presence of coherent travelling waves, computation is then made of their azimuth of arrival and horizontal trace velocity by utilizing the arrival time differences at the various stations. Since many waves arrive from a direction that is inclined to the earths' surface, the speed measured will in general be greater than the local speed of sound. This is due to the fact

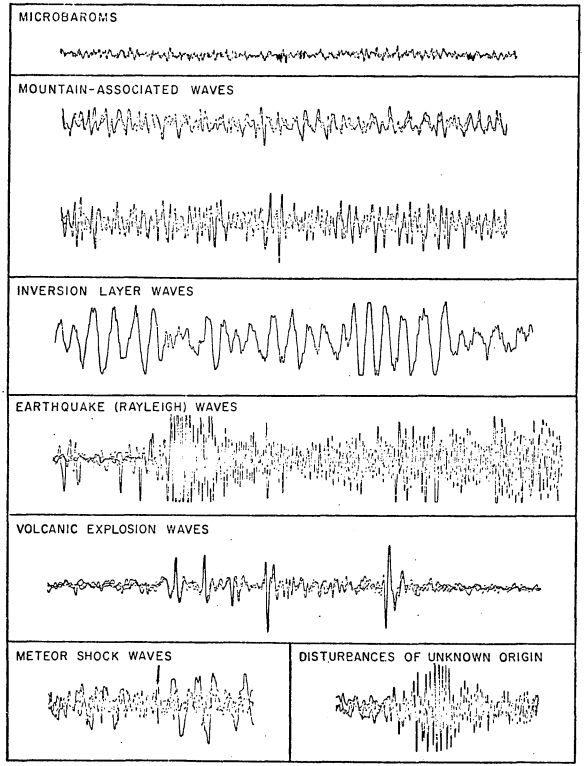

Fig. 2.1. Sources of natural infrasound unrelated to the aurora which are frequently observed on the 10-100sec. passband of the records at the Alaskan arrays.

that for the case of a plane wave inclined to the surface on which the detectors lie, the intersection of the wave with the surface is the actual form that the detectors 'see'. Thus one measures a horizontal trace velocity which is related to the sound speed at the surface of the earth by $V_t = C \sec\alpha$, where α is the angle between the wave normal and the horizontal, and C is the local speed of sound.

Before entering the discussion of AIW proper, it is in place to relate the fact that the passband of interest, the 7-70 second period range, is cluttered by not only background noise due to random pressure fluctuations and wind, but other types of infrasound from sources other than the one of principal interest. Thus it will now be shown that auroral infrasound is but one type of naturally occurring sources of infrasound of which there are many, both known and unknown. This means that some minimal knowledge of the other types is necessary in order to distinguish between those from diverse sources and those from the aurora.

2.1 Naturally Occurring Infrasound

A selection of the various sources of natural infrasound commonly seen on the 7-70 second range at the various stations of the network mentioned earlier is shown in Fig. 2.1. As they appear in the figure, the microbarom record is only a single trace from a single station at College, and the microbaroms appear as tiny wavelets of higher frequency superimposed on longer period waves. It turns out that on the 7-70 second passband at College and its associated stations, the microbaroms have only a nuisance value since they

contribute high frequency noise to the record and tend to obscure, though not completely obliterate other signals of interest. The record shown is typical, and they can always be identified by their appearance. They have been studied in depth by Lamont Observatory (Donn & Posmentier, 1967) and have been found to be generated by distant marine storms.

The inversion layer waves are gravity waves propagating along the surface of a temperature inversion. Temperature inversions are quite characteristic of the surface air in Fairbanks in all seasons but summer, however, frequently occur in late summer (Fahl, 1969). The inversion layer record shown in Fig. 2.1 is a trace from a single channel of the College array. Inversion layer waves are typically of large amplitudes often in excess of 100 microbars (full scale is 10 microbars on all records from the College and associated observatories) and completely obliterate the presence of signals of other types when they occur simultaneously. Inversion waves are easily identified by their waveforms and decorrelate rapidly between stations of 5 Km. spacing.

The remaining pressure traces in Fig. 2.1 are formed by superimposing the pressure versus time traces from four stations in the array in order to exhibit the phase coherence in the waves. Meteor shock waves have doubtlessly been recorded many times at one or the other of the stations of the infrasonic network, but only the one here was from a meteor that was visually observed. The meteor appeared on a photograph from the College All-Sky Camera. Their spasmodic appearance and short duration of the pulse has given them

nuisance value in the records. An observation of an infrasonic wave from a meteor was reported in the literature by Goerke (1966) using identical equipment as that at College.

The earthquake associated infrasonic wave shown in Fig. 2.1 is taken to be the result of ground motion in the vicinity of the recording array (Cook, 1971). The earthquake associated infrasonic waves as seen in Alaska thus far are typically, but not always, a high frequency group travelling at such high speeds (greater than 3 Km./sec.) that they cannot be scaled by the ordinary methods. They are always easily identified by their high speed (or short transit time across our array) and only seem to appear after large earthquakes greater than 7.0 on the Richter Scale.

The Mountain-associated waves and volcanic explosion waves shown in Fig. 2.1 are quite similar in physical appearance to the AIW, so greater care has to be taken in order to ascertain their true origin. As it turned out, some reasonable amount of observations had to be accumulated on the mountain-associated waves at each station in order to assess their true origin. Thus it happens that mountain associated waves arrive consistently from one to three direction bands as seen in Alaska. Their speeds are typically close to acoustic velocity and on many occasions they are known to continue for many hours and sometimes throughout an entire night or day. Waves of this type have been studied at Washington State University (Larson et.al., 1971). Triangulations from Pullman, Washington, Boulder, Colorado, and College, Alaska have located one source region in the mountains along the coast of British Columbia, Canada.

Volcanic signals have been observed at the Alaskan stations from explosions along the Aleutian chain in Alaska and from as far away as Galapagos Islands off the west coast of South America. The source of volcanic signals on the Alaskan records was identified early in the history of the array at College (Wilson et.al., 1966) and the identification of its origin may be easily distinguished from AIW by their azimuth, often by their time of arrival and their low trace velocity.

The final wave train depicted in Fig. 2.1 shows a signal of unknown origin. Physically it looks like the Rayleigh wave in Fig. 2.1, however it is also similar to some of the infrasonic waves which have been detected. Its slow trace velocity of 335 m/sec. shows clearly that it is not of Rayleigh wave origin. Its azimuth at Inuvik of 357°, (from straight across the polar cap) does not correspond to the direction of volcanoes known to be active by our observers. The arrival time of 0325 UT and pulse shapes of this unknown infrasonic signal make it non-auroral. The azimuth of the unknown signal coincide with the direction of Novaya Zemlya from Inuvik. Novaya Zemlya has been a location of nuclear-bomb testing in the past, but the signal itself is not typical of the atmospheric nuclear test signals which have been observed at the Alaskan stations. In any case, the signal is listed in our records as an "unknown" although it has the physical appearance of the type of wave resulting from an explosion. Many infrasonic signals of unkown origin have been recorded by the Alaskan array but their wave forms show that the one depicted here is by no means typical. In the typical case of signals of unknown,

their presence is merely recorded, scaled and archived, but no attempt is made to investigate whether they are a part of the natural infrasonic background, or artificially produced by a man-made explosion.

2.2 The Dispersion Diagram

The infrasonic waves discussed in this chapter may be categorized by the dispersion or diagnostic diagram which, for an isothermal atmosphere, separated them into three regions of a plot ω Vs K_x. Fig. 2.2 shows the diagnostic diagram which is separated by the curves $K_z = 0$ into an upper acoustic branch, an evanescent region, and the lower branch representing the internal gravity wave branch. The acoustic cut-off frequency is given by Hines (1960)

$$\omega_a = \frac{\gamma g}{2a}$$

and the Brunt frequency

$$\omega^2 = (\gamma-1)\frac{g^2}{a^2} .$$

The dispersion equation governing these curves is given by Pitteway and Hines (1965)

$$n_z = (1 - \frac{\omega_a^2}{\omega}) - n_x^2 (1 - \frac{\omega_b^2}{\omega^2})$$

where $N_z = \frac{aK_z}{\omega}$, $N_x = \frac{aK_x}{\omega}$, a = sound speed, γ = ratio of specific heats

g = acceleration of gravity.

The curves of constant K_z in this diagram are asymptotic to the line $\omega = aK_x$ for acoustic waves and ω_b for internal gravity waves. ω_a acts as a low frequency cutoff for the acoustic branch,

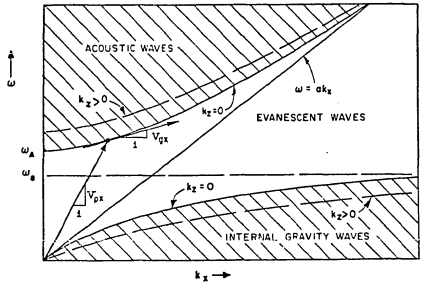

Fig. 2.2. Diagnostic diagram for an isothermal atmosphere. (after T. Georges, 1967).

and ω_b is the high frequency cut-off for the internal gravity wave branch.

The phase velocity $\frac{\omega}{k}$ is given by the slope of a line drawn from the origin to a point in the plane, whereas the group velocity, $d\omega/dk$, is given by the slope of the tangent to the point. As the diagram implies, phase velocity is always greater than group velocity for acoustic waves.

Generally speaking, most of the infrasonic pressure disturbances observed in the 10-100 sec. range at the Alaskan arrays lie in the acoustic mode of the dispersion diagram, whereas the boundary layer waves discussed in section 2.0 are located in the evanescent sector. The auroral infrasonic waves studied in this report are members of the acoustic branch also.

In the real atmosphere, temperature, sound speed, Brunt frequency, and the acoustical cut-off frequency are all a function of height. Moreover, the wavelengths of an acoustical pulse of auroral infrasound are long compared to the distance over which the properties mentioned change. Since all of these properties also change with time, a realistic dispersion diagram pertaining to a real atmosphere has not been studied. For this reason, the proper placement within the acoustical branch of the dispersion diagram of the auroral infrasound studied in this report is a bit nebulous at present.

2.3 Auroral Infrasonic Waves

(a) Waveforms

Despite the frequent occurrence of infrasonic events of various kinds in the records of the Alaskan arrays, the primary concern in the research at College has been the study of auroral infrasound. Now that the number of observations accumulated over the years since the inception of the project in 1965 has totalled more than 2500 AIW signals, it seems reasonable that the greater number of types of events have already been observed, and the subsequent observations will present few, if any, new types of AIW. This is not to say that more observations are not needed in order to gain a better insight of the many remaining problem areas in the study of auroral infrasound, but that the particular signals types themselves will probably not change significantly in the future. For this reason, it seems to be in place to initiate an attempt to classify the many types of AIW to see if the overall understanding of AIW can be enhanced by studying the separate groups.

An initial preview of the AIW records can leave one with the impression that the types of auroral signals are as diverse as the auroral forms themselves. Nevertheless, there are some properties of the signals that are quite common to many others such that the taxonomy might be simplified by merely describing the number of cycles in the signal, say. Other subdivisions may be achieved by noting whether the initial pulse is positive, negative, or indeterminate, and still further classification can be based on whether or not the cycles in question are accompanied by other cycles of successively higher or lower frequency. Such a classification is attempted here because of the need for such in order to present an overview of the various types

of AIW. The proposed classification system is presented in Appendix 2 of this thesis.

A view of some of the representative types of AIW are presented in Fig. 2.3. In brief, the signals have been arranged into two broad groups. The two largest groups of signals describe whether or not the signal consists of a single pulse, positive, negative, or both; or multiple pulses which begin with cycles of either sign. The latter group is subdivided depending on whether the signal has a few cycles (less than or equal to five) or many cycles (more than five). Further subdivisions can be followed by referring to the system as presented in Appendix I.

Returning again to Fig. 2.3, the separate traces shown in the various panels depict a sample of many of the diverse AIW signals observed at the Alaskan arrays. Each panel contains the superposed pressure traces for the four channels photographed for a particular event(s). The letters placed in the lower left corner of each panel classify each wave type by the scheme presented in Appendix I. The scalings for each panel are shown in the upper right corner of each frame and arrows have been placed in some of them in order to show the onset time of the signal. The signals will be discussed here by the large number shown in the middle of each frame.

The first four signals of part (a) of Fig. 2.3 are of the single impulse type: the first is a single positive pulse, the second a single negative one, and the other two contain both positive and negative components with a leading positive (3) and a leading negative (4)

pulse. Frame (5) of the figure shows an event having multiple pulses, but with fewer than 5 cycles and no associated additional dispersed cycles. Panel (6) of the figure shows another such pulse as (5), but with a leading negative cycle and no other discernible cycles. This particular example was chosen because it illustrates how the signal/noise ratio is not always a limiting factor in AIW wave detection. Here the ratio is obviously less than one, but the presence of the signal was easily discerned and quite routinely scaled. Frames (7) and (8) of the figure both show leading higher frequency pulses followed by wave trains of cycles of ever-increasing period. Such phenomena are described as dispersed wave trains here, and they appear as separate types of events only in that the former is preceded by a positive pulse, and the latter a negative one.

Part (b) of Fig. 2.3 shows 8 panels of the complex type of AIW event. Frame (9) shows a signal which appears to have multiple pulses, but less than five cycles. The way in which this event is embedded in the surrounding noise makes the onset time of the signal and the number of cycles in the wave train indeterminate and also raises the question whether or not the event itself is merely a chance coherence and not a real event at all. In such cases, some measure of confidence may be obtained by the way in which the signal can be scaled, and how spread in the four to five available solutions for speed and azimuth form the different triangles in the array. More will be said about the scaling techniques in the chapter discussing data analysis. Panel (10) of the figure shows another signal of the same type: fewer than five

cycles, but in this case, of sharp enough onset to be separated from the noise. The arrow in this and the previous frame show the location of the signal which was scaled, not the time of onset. Panel (11) of this figure shows the presence of two tiny wavelets (arrows) superimposed on a larger wave which is in itself, a part of a much more complex event. The records in this case are aligned for the wavelet on the left, whereas a different chart alignment would be required to show the phase coherence of the wavelet on the right. These small fluctuations have been considered a separate type of event because they are frequently present is some of the larger AIW events, and their scalings show that they appear to often have different azimuths or propagation and different trace velocities than the waves on which they are superimposed.

The panel showing frame (12) of part (b) of Fig. 2.2 depicts a dispersed wave train having more than 5 cycles. Frames (13) and (14) of the same figure shows wave trains of many cycles, but whose dispersion is indeterminate due to lack of certainty as to just where the wave trains begin. These are both taken to be different manifestations of the same type of event as proposed by the classification system mentioned earlier. Another interesting feature of these two panels is that they also show a characteristic feature of the infrasonic records recorded in summer and fall/winter by contrast. Summer records, and frequently spring ones, are typically less imbedded in high frequency noise, and the signals themselves seem to contain mainly longer periods. The winter records typically show higher frequency background noise and also higher frequency signals.

Frames (15) and (16) of the figure show events in which there is an initial pulse(s) which is followed by subsequent one(s) at a fairly regular interval later. Three such intervals have been recognized in the Alaskan array records, and they have been designated R_3, R_6, and R_{11}. The R_3 type, not shown in this figure, contains subsequent pulses from 2 1/2-4 minutes following the initial pulse; R_6 describes the appearance of pulses from 4-7 minutes following the initial one, and is depicted in (15) of the figure. The designation R_{11} is given to the event in which the repeated pulse comes from 8-12 minutes after the initial pulse, and this type of event is depicted in (16) of Fig. 2.3 (b). This type of repeated pulse event is not peculiar to auroral infrasound, but has also been observed in the case of some volcanic explosion waves. By referring back to Fig. 2.1, an example of both the R_3 and R_6 pulses may be seen in the panel depicting the volcanic explosion waves.

(b) Morphological Features of Classified AIW

Because the great diversity of AIW waveforms most probably contains an admixture of signatures of the AIW generator and the effects of atmospheric structure as well as the recording equipment, the grouping of signals into types in order to uncover a possible clue which might unscramble the three is obviously necessary. Only a brief digression into the morphology of the broad groups and two subgroups of AIW is attempted here.

In an attempt to observe the distribution of signal types collected

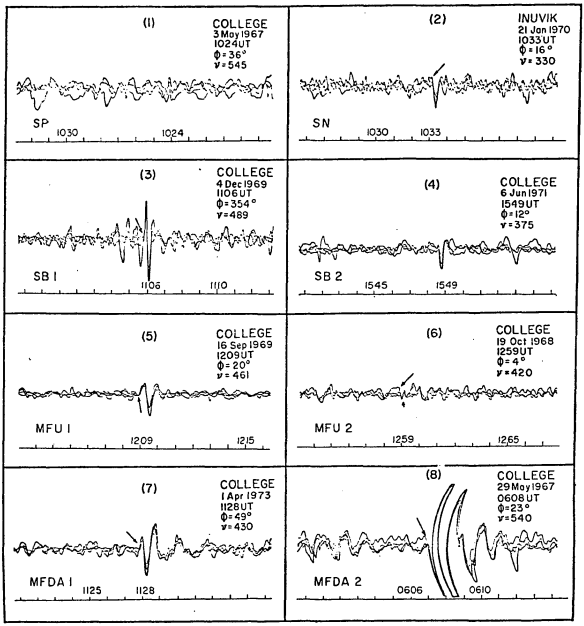

Fig. 2.3(a). Superimposed pressure traces of four stations to show phase coherence for single impulse AIW (1-4) and the simplest multiple impulse AIW (5-8). The date, time (UT), azimuth (ϕ), and trace velocity (V_+) scaling information is given in each frame along with a lettered classification code explained in Appendix I.

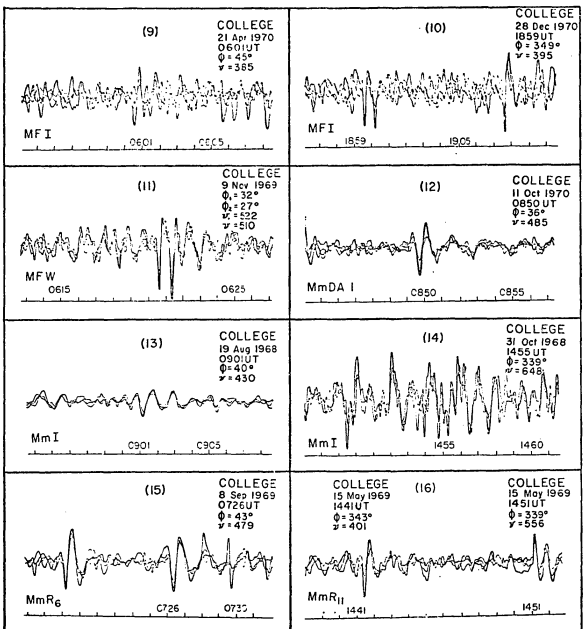

Fig. 2.3(b). Superimposed pressure traces from four microbarograph stations in each frame showing phase coherence for the more complex and frequently occurring types of AIW signals. Legends are identical to part (a) of this figure.

by the Alaskan array over the years, a survey of the year 1970 for the data collected at the College Observatory alone was undertaken. The system-search of the records for 1970 at College was undertaken in a cursory perusal of the entire data decks for all the Alaskan array in order to retain some impression of how typical the 1970 year at College was for the rest of the data. The type of signals studied in this effort were the broad groupings of single impulse events, and the two largest groupings of the multiple impulse events. Taxonomically, the single impulse groups and their various sub-types are designated by the initial letter S; the multiple impulse groups are preceded by the initial letter M followed by the letter f (few) if there are less than 5 cycles, or followed by the letter m if there are more than five. All group designations are followed by other letters which refer to other characteristics of the signal, but this information may be bypassed at this point until the full explanation of types as shown in Appendix II.

The results of the search of the 1970 College data for signal types S, Mf, and Mm showed that they represented 2%, 29%, and 69% of the data repectively. This says that for that year, the single impulse events were only a small part of the total data record, and the Mf types, having five cycles or less were a significantly large fraction. By far, the overwhelming majority of signal types were the Mm types whose number of cycles extended from six to innumerable ones which frequently ran for a few 'fives' of minutes, often for a few tens of minutes and less often, wave trains which continued for many

hours.

Since the preponderance of the data consisted of very complex wave trains having many cycles, a closer look at the various subdivisions was then made. As the 1970 data showed, the major subcategories were those described as indeterminate. Both of the two multiple impulse groups have such a category, and they are designated Mfl, and Mml, where the first two letters were described previously. The Mfl subgroup comprised 18 1/2% of the 1970 data and the Mml group represented 62%. Typical features of both indeterminate groups is that their onset time and cessation are frequently obscure and they often merge imperceptibly from the background noise and return into it in the same fashion. Because of these features it is very difficult or impossible to decide whether or not the waves which do stand out are preceded or followed by other shorter or longer period cycles, and thus the idea of a dispersed wave train is indeterminate. Since these two subgroups occupy 80% of the data, they must be accepted as the typical auroral signal as observed in the vicinity of the Alaskan array. Other signal types, though more definable in terms of onset times, wave form, or coherence, are typically the 'best looking' signals in which there is little doubt concerning its existence as a signal. Since the effect of propagation on the AIW is also undetermined, after it leaves the generator, it is obvious that a study is needed to help uncloud the puzzle of signal types. A final point related to the 1970 College data is that scanning of the records for all stations and years did not seem to alter the percentages greatly.

As stated earlier, a portion of the AIW signal must contain information of the AIW generator, the propagation path which intrinsically implicates the structure of the atmosphere, as well as the signal processing within the recording equipment itself. A very interesting and recent finding (Swift, 1973) infers that the recording equipment, by virtue of its band-pass characteristics, introduces spurious pulses into the chart records. Using an assumed input pulse the study showed that a secondary pulse would appear on the chart records nearly 11 minutes later-a striking similarity to the observations. However, the 11 minute period is a function of the particular geometry of the electrojet chosen in his model. Though the study did not explicitly discuss pulses repeated near 3 and 6 minutes also, there were sufficient numbers of spurious pulses to raise serious questions as to how much of the AIW chart records contain real data or spurious pulses. The answer to this question is well beyond the scope of this report because it was assumed that all obvious coherences having the known AIW features were real. Nevertheless, a token effort was made here to shed light on the enigma.

A survey of all the records from the Alaskan array was undertaken to observe the seasonal distribution of the R_6 and R_{11} events as well as to note any other morphological features. A total of 69 of these repeated pulse events were found. While this search was being conducted, a simultaneous search was conducted for the totality of single pulse events of all kinds.

The results of the search for single impulse and repeated pulse

events are shown if Fig. 2.4. Here histograms showing the frequency of occurrence vs. month of these types of events are compared to the total number of observations over all years at College, Inuvik and Palmer. First of all, it is interesting to note that the 63 single pulse events represent 2.7% of the total observations as seen at the stations mentioned which compares with 2% for this type of event in the 1970 data. This seems to support the conclusion that the 1970 percentages were probably representative for the various classes of AIW for the entire data span of the Alaskan array.

The interesting features of Fig. 2.4 concerning the single pulse events is that they have a greater tendency to occur in July and September, and that tendency exceeds by 7% the seasonal increase noted in the total AIW distribution. Despite an apparent seasonal maximum in the months mentioned, they did occur in all seasons and all months. No special or consistent features were noted insofar as their having any preferred azimuth, trace velocity, or arrival time outside the typical arrival times for AIW. In face, the only other slight tendency noted was that single pulses frequently tended to cluster across a given month. That is to say the records will show an absence of signals for from one to three months, and then when single pulses appeared, from one to five others might appear in the same month, or within a few days. This tendency typically occurred between May-Oct. and the single impulse events then usually appeared as isolated events in other months.

The repeated pulses R_6 and R_{11} which were studied in Fig. 2.3 also showed a tendency to increase in the late summer, Aug. and Sept.

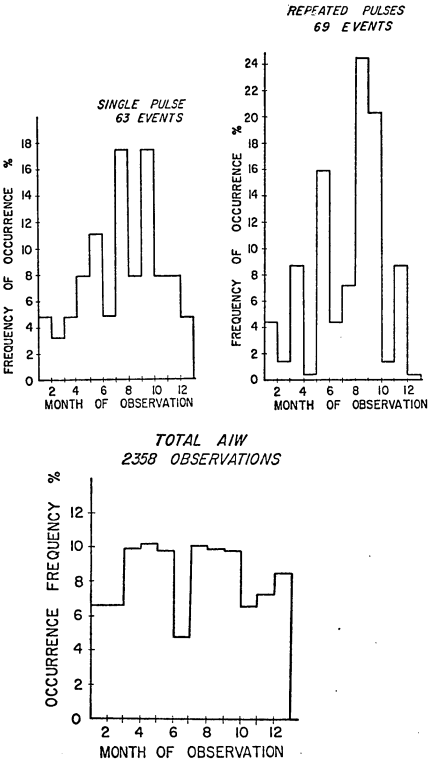

Fig. 2.4. Frequency of occurrence of specific types of AIW events compared to the frequencies of all types of AIW observations at College, Palmer, and Inuvik.

in particular. In fact, these two months comprised about 44% of the observations of the phenomenon, whereas the seasonal increase of the total AIW showed only about a 20% of the total observations of AIW for those months. The conclusion reached in this comparison is that there is a strong tendency for this type of AIW signal to maximize in Aug. and Sept. and to minimize in April and December in such a way as to exceed what would be expected merely on basis of the overall seasonal variations of AIW of all types.

This conclusion does not alter the possibility that the second pulse might not be real, but it does at least attest that the type of pulse which might generate such a signal does not follow the same morphology as the large numbers of recorded AIW signals. On the other hand, it is probable that the second signal is less a second impulse by the AIW generator than being a choice of atmospheric structural or equipmental origin. This viewpoint is maintained because the same type of repeated pulses are also observed in the case of volcanic signals (Wilson et.al., 1966). Thus the choice reduces to certain unique features of atmosperic structure which are frequently present in July and Sept., generally absent in April and December, or simply pulse shapes presented with the same seasonal frequency which result in the possibly spurious pulses. If it is indeed the latter, then it must also be borne in mind that the same input pulse shapes must also be produced by volcanics.

(c) General Morphology

Having specified the signal types which the AIW present to the

chart records of the Alaskan array, and having discussed some of the morphological characteristics of a few, we now turn our attention to the morphology of the entire ensemble of AIW without regard to particular types. From the time of the earlier associations of infrasonic pressure disturbances with geomagnetic activity (Chrzanowski et.al., 1961) it was noticed as far south as Washington, D.C. that the earlier arrivals of AIW came from the NE direction and progressed to the NW direction as the time passed from afternoon, to night, to early morning. Subsequent research at Ft. Yukon, Alaska correlated AIW micropulsation activity (Campbell & Young, 1963) and confirmed the azimuthal progression from E to W. Since that time many observations of AIW at the Alaskan array have upheld these early conclusions and uncovered many new interesting and problematical features of the phenomenon (Wilson & Nichparenko, 1967; Wilson, 1967: Wilson, 1968; Wilson, 1969a, 1969b, 1969c; Wilson, 1972; Johnson, 1972).

To summarize some of the major features observed in the Alaskan data, a few statistical plots are shown in Fig. 2.5. Part (a) of the figure shows plots of the number of observations vs. time UT at three of the stations of the Alaskan array: College (Col), Inuvik, (Inu), and Stevens Village (StV) for the periods indicated. The largest number of signals corresponding to the longest span of operation was received at College, thus its curve stands well above the others in the plot. It shows that there are two maxima in signal reception at College: one just after local midnight (10 UT) and another later in the morning. The largest number of signals, however, occur after local

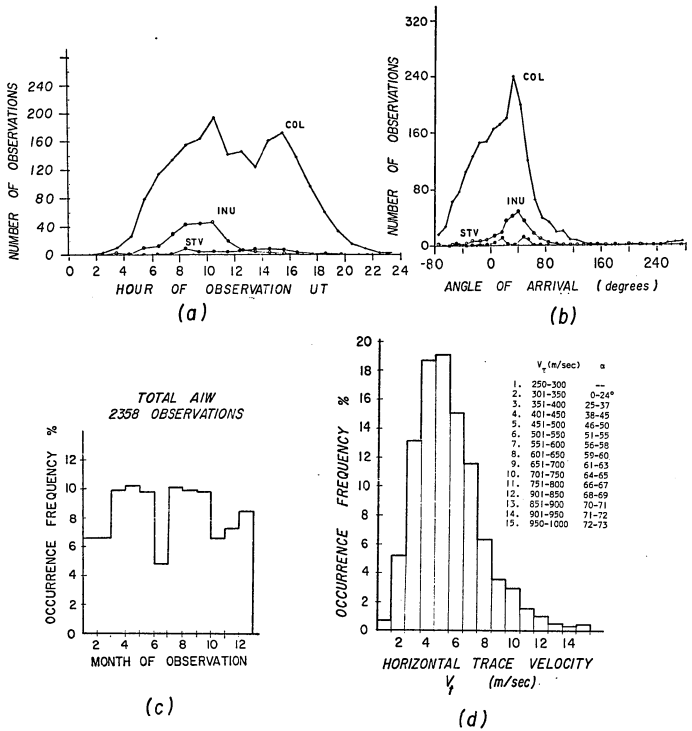

Fig. 2.5. General morphological features of all classes of AIW observed at College (COL), Inuvik (INU), and Stevens Village (STV).

midnight.

Part (b) of Fig. 2.5 shows one of the very outstanding and significant facets of the behaviour of AIW. The plot shows the number of observations vs. time of the signals for the three stations indicated. The first noteworthy feature is that the largest number of signals at College and Inuvik arrive from the direction of northeast close to the azimuth of 40°. The second and very important feature of this plot is that the curves drop close to zero for all stations for the azimuths representing most of the southern directions. This plot shows therefore that there is a very strong asymmetry in signal reception of AIW in which there are preferred directions and also forbidden ones.

The plots in Fig. 2.5 (c) and (d) are histograms showing the monthly occurrence frequency of AIW, and the occurrence frequency of measured horizontal trace velocity by 49, and 50 m/sec. groups. The former shows that there are two distinct maxima in the numbers of AIW received during the year separated by a minimum in June. The latter histogram (d) indicates that the most frequently occurring trace velocities are the groups numbered 4 & 5 which, as the legend to the right shows, corresponds to 401-500 m/sec. or 38°-50° inclination to the horizontal based upon a sound speed of 320 m/sec.. The plot also shows that there are a small fraction of AIW which, as group one shows, represent sub-acoustic velocities. The other end of the distribution shows that the highest trace velocities are near 1000 m/sec., which represents an inclination of about 73°. This points out another

interesting feature of AIW reception: they are never received from the zenith or within 10° of either side of it.

In discussing the morphological features as shown by these statistical plots, no attempt was made to account for the reason why each plot was distributed the way it was. The main reason for this is that the exact reasons for most of these features are not known but subsequent discussion in this chapter will show attempts to explain some of them.

(d) Significant Research Results

The major contributions to the study of auroral infrasound have been made at the Geophysical Institute at the University of Alaska by Wilson and colleagues. Other workers have added to the overall accumulation of knowledge on the subject, some of whose work pre-dates the Alaskan research, and others running concurrently. Basically their results are quite similar to the findings at the Alaskan observatory, but some interesting departures can be noted. A summary of these research efforts as well as findings by Wilson and colleagues at the University of Alaska now follows.

The findings of observers at lower latitudes have been quite consistent insofar as their correlation of AIW with geomagnetic disturbances in general and the increase of AIW with the planetary magnetic index Kp in particular (Chrzanowski et.al., 1961; Sachdev, 1969; Young, 1968; Cook, 1969). Young (1968) noted that when Kp was greater than 5, that chances of AIW observations at Wash., D.C. were quite good, whereas for Kp less than 4 they are infrequently observed if ever.

He also observed an apparent high frequency cut-off for AIW near 0.06Hz. Since his observations were aided by more filtered pass-bands for higher and lower frequency ranges than the Alaskan data of Wilson, he was also able to observe long period waves (of approximately 5 minutes) having amplitudes near 20 dynes/cm.^{2} on rare occasions. This latter observation contrasts greatly to the Alaskan data which shows the typical AIW has an average amplitude of about 5 dynes/sec.^{2} pk/pk. It might also be noted that the high frequency cut-off observed by Young could have been the result of propagation effects down to the latitude of his recording site in Wash., D.C. (38°53.5'N geogr.) since, as subsequent discussion here will show, higher frequencies are observed at higher latitudes.

Though the actual extent to which auroral pressure disturbances propagate into lower latitudes is unknown, the lowest latitude reporting such observations known to this investigator have been those of Sachdev (1969) from Bombay, India (18° 57'N geogr.). Using two microbarometers from which he did not seem to specify phase coherence of particular waves, he showed an overall unusual increase in amplitude and oscillations in the 25-65 second period range. These increases correlated with a rise in the Kp magnetic index, but apparently no significant analysis resulted from these observations.

The observations of Cook (1969) based upon data taken at Wash., D.C. as those of Young, cited previously, recognized two typed of AIW: those recorded at mid-latitudes as at Wash., D.C. and those at high latitudes as the Alaskan data. Though the features of both types seemed consistent with the AIW of the Alaskan arrays observations,

the period range of his mid-latitude category did extend from 20 to several hundred seconds, with a high frequency cut near 15 seconds, as in the case of Young's data. A possible reason that the longer period AIW has not been observed in the Alaskan data is that the pass-band of interest does not include frequencies that low.

There have been two separate observations of aurorally-associated infrasound in the frequency ranges above the cut-off frequency seen by Cook and Young. Procunier (1971), using a system of five Helmholtz Resonators sensitive over the range 1-16 Hz, detected over 100 events for his entire observational period which was in the month of January 1970. His equipment was located at Barrow, Alaska, and his typical auroral infrasound seemed to consist of impulses of from 1-3 cycles duration which occurred only during times of magnetic disturbance. He further noted that the events recorded by his higher frequency instrumentation was uncorrelated with the events seen near that time at College and Inuvik which utilize the lower frequency equipment as part of the Alaskan arrays. Owing to the low correlation of his events with supersonic aurora, he suggested a possible source mechanism to be associated with micropulsations.

The other confirmation of a higher frequency type of infrasound associated with the aurora has been offered by Liszka (1972). Using two tripartite arrays of piezoelectric microphones spaced at 2 Km. apart, he observed infrasonic emissions associated with geomagnetic activity at a frequency of 1.9 Hz. His observations showed persistent emission of infrasound for long periods of time during magnetic storms.

In studying the association of this high frequency emission with translational motions of supersonic electrojets, he did not find a very strong correlation. For the cases in which he did find correlation between the two, he found discrepancies in the direction of arrival of the infrasound and the position of the electrojet. Moreover, he observed infrasound emission when the jet did not move at all. He determined the electrojet motions from latitude profiles of the Z-component locating its position at any instant by the Z = 0 crossover, and computing its speed from the digitized magnetograms taken at one minute intervals. This gave him an idea of the latitudinal position of the jet, and the longitudinal part was assumed to extend indefinitely along a parallel of constant corrected geomagnetic latitude. Applying a ray-tracing procedure, he found that most of the infrasound emissions came from a zone between 64.5°-65.5° geomagnetic latitude.

The observations and conclusions of Wilson concerning infrasound in the 10-100 sec. region differ in a number of details from that of Liszka. Wilson's data shows a paucity of signals propagating northward, whereas Liszka's data of Aug. and Sept. 1971 shows a few signals from south of the station. Wilson's data, as other observers at lower latitudes mentioned previously, shows an azimuthal dependence on time which is not specified in the data of Liszka. It must also be borne in mind that the two observers are looking at different parts of the frequency spectrum, so it is not surprising that some of the observational details might differ.

From the very earliest published report concerning the AIW at the

Alaskan arrays, the association with supersonic auroral arcs was observed (Wilson & Nichparenko, 1967). The signals having durations of a few cycles led Wilson (1967) to propose a shock-wave model to describe the way in which a supersonically-moving aurora, by isotropic radiation from each increment of the auroral path, would result in amplification of the resulting signal to be received at the ground as a shock pulse having a positive leading phase.

Nichparenko (1967) correlated the reception of AIW with the motions of auroral surges, westward drifting loops, and faint omega bands moving rapidly eastward in the early morning hours. The common features of her correlations were that the forms moving supersonically were the ones which gave the infrasound, and such features as auroral brightness and auroral pulsations correlated poorly. Upon showing that a computer model simulating a fixed source with respect to the sun-earth line would not explain the diurnal variation in direction of arrival of AIW, she suggested the dominant westward drift of auroral forms in evening and eastward drift in the morning hours would explain the reversal in arrival direction of AIW after midnight.

Further studies by Wilson (1969) showed AIW to be related to the rapid auroral motions that occur during the breakup phase of the auroral substorm, and to the actual electrojet current system assumed to be located within the auroral arc (1969). A very interesting correlation between the azimuths of AIW with time and the changing position of the earth with respect to the auroral oval was made by Wilson (1972). This correlation is shown in the diagram in Fig. 2.6. Here the auroral oval for Q = 5 (Feldstein & Starkov, 1967) is shown plotted

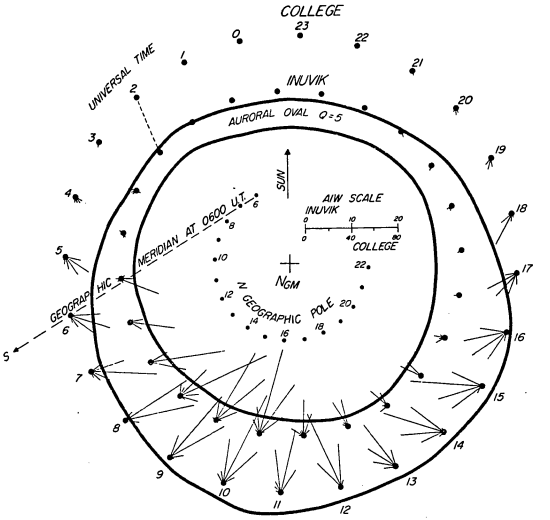

Fig. 2.6. Variation with time (UT) of the azimuths of arrival of AIW grouped by 20° increments (rays on dots) for the stations at Palmer, College, and Inuvik (dots). Successive geometric positions of these stations with respect to the auroral oval are simulated by each new set of three station dots representing each hour UT (outer numbers). (after Wilson, 1972).

against successive positions of the stations Inuvik, College and Palmer with respect to it. The plot in this way attempts to simulate the motion of the earth with respect to this huge statisically determined form which is fixed with respect to the sun-earth line. Small rays drawn from each station represent the direction and number of AIW as determined by the legend, while the time UT is shown by numbers along the outer perimeter. As the diagram shows, the arrival directions of the AIW at each station tend to follow the direction of the bulge sector in the oval belt. Moreover, Palmer is outside of this oval for the entire night, whereas College enters it near 0820 Ut and emerges in the late morning near 1630 UT. Inuvik is located near the oval even on the day side, and spends much of its time within the oval. Extrapolating beyond the figure, one can see that for still larger levels of auroral and magnetic activity, Inuvik could actually spend considerable time in the polar cap, and Palmer possibly be admitted into such an enlarged oval. Or on the other hand, for smaller levels of disturbance, both Palmer and College might be excluded from it, and most of the belt could lie poleward of Inuvik. Thus this diagram explains the diurnal morphology of arrival azimuths of AIW as seen at high and low latitudes if the source of AIW is assumed to be within the oval at all times.

(e) Generation Mechanisms

A small number of workers have attempted to offer possible models describing the way in which a pulse of infrasound is generated from the aurora. The earliest model was offered nearly a decade ago based

upon the observations of the phenomenon in mid-latitude Wash., D.C. (Maeda & Watanabe, 1964). Noting the wave trains of somewhat sinusoidal-like waves which appeared on the pressure records at the National Bureau of Standards in Wash., D.C. during periods of Kp greater than 5, they invoked a model of wave generation of pulsating aurora. They postulated that periodic auroral bombardment at 100 Km. lead to periodic heating of the upper air such that energy fluxes of 100 ergs/cm^2sec. would produce a pressure pulse of 1 dyne/cm^2 at the earth's surface.

Maeda and Young (1966) enlarged upon this model showing that after the periodic heating, the waves would propagate horizontally through ducting by the upper or lower sound channel in the atmosphere. Their model also predicted a gravity wave mode which would be excited due in part to the positive lapse rates in the stratosphere and thermosphere. The latter portion of the theory predicted waves of periods of about 5 minutes which were being observed at the Wash., D.C. station.

Another model based upon the concept of a pulsating aurora source of AIW generation was offered by Chimonas (1970). He envisioned an arc containing an electrojet having a current which was periodic in the same range of AIW, which coupled with the neutral atmosphere through both Joule heating and Lorentz force upon the ions. The collisional interaction of the ions with neutrals would then produce an AIW pulse as would also the Joule heating, and the two would produce pressure waves detectable within several hundred Km. of the exciting aurora.

The common feature of these three models is the inference that a

pulsating auroral source produces the observed AIW. In the years 1966-1967 very close All-Sky Camera surveys over some hundreds of AIW observations did not give a significant correlation of pulsating auroras with AIW when compared with supersonic aurora. Infact, in the period studied some 80% of the correlations were the supersonic auroras, while 3% of the signals occurred during pulsating auroras (Wilson, 1969a). For this reason the pulsating aurora generating mechanisms were not favorably considered as the probable source of AIW.

In order to explain the correlation of the impulse-like auroral infrasonic events with the supersonic motions of aurora, Wilson (1967) constructed a shock-wave model applying a numerical technique to the geometry of the moving aurora. He showed that a pressure pulse would be built up at an arbitrary observing point along the path of the aurora after the zenith crossing of the auroral form due to a superposition of wavefronts from each point along the motion. He later expanded this model (1969b) into a three-dimensional figure exhibiting 'front shock' and 'side shock' effects to explain differences between the AIW observations seen at two Alaskan stations, College and Palmer. An advantage of this extension to the earlier theory was the removal of the observing station from a position of uniqueness; it no longer had to be in the actual path of the moving aurora.

Chimonas and Peltier (1970) derived a mathematical model to show how the supersonic aurorae observed by Wilson could produce a pressure pulse at the ground. They replaced Wilson's concept of a shock wave with the term "bow wave" in order to avoid the nonlinear problems

associated with a shock. Using an infinitely long arc translating supersonically, they showed that there would be a twofold interaction with the atmosphere. On the one hand, Joule heating of the upper air by the electrojet would produce a positive pressure pulse at the ground, and on the other, Lorentz force coupling with the ions causing collisions with the neutrals would produce a positive or negative pulse depending on the direction of translational motion of the jet imbedded in the arc with respect to the current direction. The weakness in this model was the fact that there was no allowance for asymmetry in AIW reception as is actually observed. It showed an equal likelihood that a northward propagating form would produce an AIW as a southward moving one which is contrary to the way in which the observations at the Alaskan arrays have shown.

The failure of the Chimonas & Peltier model to account for the asymmetry in signal reception at the Alaskan arrays resulted in an alternate mechanism by Wilson (1972) in which the electrojet imbedded in a supersonic auroral arc is coupled by the Lortentz force on its ions to the neutral gas. When the arc has a component of motion parallel to the electrodynamic drift, an ionization collection process occurs which enhances the ion density at the leading edge of the arc. The resulting collisional interaction of the wall of ionization thus formed would cause an acoustic pulse during the supersonic motion of the arc. On the other hand, the Wilson model shows that should the auroral arc be moving anti-parallel to the neutral ionization drift, the neutral ionization density within the auroral arc tends to decrease. The latter

situation was taken to be the case insofar as polewardly-expanding arcs, were concerned, and accounted for the observation that no AIW signal is recorded for this northward motion. No attempt was made in this theory to account for the multiplicity of AIW wave forms or the wave form at the arc.

Fedder and Banks (1972) raised doubts concerning this latter model by Wilson on the basis that the ionization collection process crucial to the generation of the acoustic pulse in the Wilson view had never been observed. They also criticized the absence of a prediction of the resulting wave forms by Wilson, and proceded to develope a model similar in mathematical development to the one of Chimonas and Peltier. In addition to attempting to predict the resulting wave forms, they also attempted to account for the asymmetry in north/south AIW reception. They explain the asymmetry by three effects acting in concert. One includes a term which causes the Joule heat and the Lorentz force terms to add when the supersonic arc moves parallel to the convective flow, and to nearly cancel for motion opposite to the convective flow. A second effect is an outgrowth of their model which shows that higher mach numbers of the electrojet leads to diminished amplitudes of observable pulses. They then show that poleward expansions usually contain faster moving arcs which might enter far into this diminished pulse range thereby resulting in an undetectable AIW at the ground. Their third effect showed that poleward moving arcs tend to increase in width, and as their mathematical model showed, larger widths led to diminished amplitudes and longer periods. These three effects acting together would, in their view, cause an AIW pulse

caused by a poleward moving arc to be below the threshold of detectability.

The unpublished paper by Fedder and Banks contained a reliance on an eastward electric fields for their poleward moving arcs. Such a restriction is contrary to the barium release measurements of Westcott et.al., 1970) and raised serious doubts concerning the validity of the conclusions on this unfortunate assumption.

A very recent model of AIW generation by supersonic motion of an electrojet was offerred by Swift (1973). It is a nondispersive theory which couples the electrojet to the neutral atmosphere by both Lorentz force and Joule heating. The asymmetry problem is handled by additive Lorentz force and Joule heat terms when the electrojet motion is parallel to the electric field and which are subtractive when the motion is anti-parallel. It shows also, as did Fedder and Banks and Chimonas and Peltier, that higher mach numbers above mach 1 result in diminished amplitudes of the pressure pulse. Moreover, as an auroral arc would approach the speed of sound from below, an undetectably small pressure pulse would be produced, but for an arc velocity within a few hundredths of the sound speed, an extremely large high frequency pressure pulse would result.

A very intriguing aspect of the Swift development is the attempt to account for the filter characteristics of the detection equipment. His results show that for a supersonic arc having a specified current density profile, a pressure pulse in the vicinity of the arc would consist of a few cycles, but upon being processed by the filter in the

detection system, would result in many spurious cycles lasting from 10 up to 15 minutes for the cases examined. The implications of this result are far-reaching insofar as its effects on future analysis of AIW where is concerned. It was mentioned in section 2.1 (b) of this chapter that one of Swift's results was an alternate explanation for the 11-minute pulse frequently seen on the AIW records. Though the findings of Swift are much too recent to have been given an adequate treatment in this report, a logical jumping-off point for further research could be the implications of this very comprehensive model for the 11-minute pulse.

A summary of the attempts to model the generation mechanism of an acoustic pulse from auroral disturbances shows that the researchers have associated the AIW pulse with pulsating aurora or supersonic aurora. The problem of the north/south asymmetry was unknown to the earlier workers up to and probably including Chimonas and Peltier; consequently, having not anticipated such a morphological feature, they did not build it into their models. Of the three workers who did attempt to account for the asymmetry (Wilson, Fedder and Banks, Swift), all three seemed to favor a mechanism closely related to the generation or diminished generation of an acoustic pulse rather than a purely propagation effect. None of the models account for the wide diversity of AIW signal types, but the Swift approach does offer the possibility for explaining the wide variety of signals when the band-pass characteristics of the equipment are invoked. In any case, a lot of detailed research is needed on the AIW equipment itself to sort out whatever real and unreal pulses that might be

present to ascertain that the latter type has not and will not find its way into the AIW morphology.

Instrumentation and Data Analysis

3.0 Instrumentation

The instrumentation used for the detection of infrasound at the Geophysical Institute, University of Alaska and its satellite stations located at Inuvik, N.W.T., Canada, Palmer and Stevens Village, Alaska, was originally developed at the National Bureau of Standards, Washington, D.C.. A description of this type of equipment from the Alaskan arrays as well as other infrasonic stations from a world-wide net is given by Cook and Bedard (1971). Details of the equipment at College has been given by Nichparenko (1967).

In brief, the pressure pulse is detected by a capacitor microphone, whose input is mechanically connected to a 1000 ft. pipe, vented every five feet, so as to dampen out the wind noise. The microphone signal is sent to a central recording location from each of four such stations of the quadrilaterally-situated array, the FM signals are demodulated, amplified, and recorded in both filtered and unfiltered format. Portions of the unfiltered data go in part to a broadband tape not retained by the Geophysical Institute, but supplied to an associated station in Boulder, Colorado. The other portion of the unfiltered signal is processed by a digital data aquisition system designated the TC-200 which is described in the literature by Herrin and McDonald (1971).

The analyses conducted at the Geophysical Institute to date are based mainly upon the portion of the infrasonic signal which is passed through a filter 3 db down points at 10-100 sec. and which is then recorded on Esterline-Angus charts. The data used in the study of AIW in this report was recorded and analyzed from the chart records.

3.1 Data Analysis

(a) Infrasonics

The recognition of an infrasonic signal on the chart records at the Geophysical Institute is accomplished by manual methods and visual

inspection. Following the same procedure in this study, the chart records from each of the four stations were superimposed on a light table, time-shifted in order to ascertain the presence of phase coherence in the waves, and then scaled by recording the time differences of arrival of the signal at the various stations. The time differences can be converted, by assuming a plane wave solution, into an azimuth of arrival of the signal, and a horizontal trace velocity. In practice, this latter procedure is accomplished by means of nomograms which were computed for the geometry of the array. There are, in general, five independent solutions available from the geometry of a quadrilateral array. Four of them are independent triangles within the quadrilateral, and the fifth formed by the arrival time differences of the diagonally-located stations. The latter solution was not available on the nomograms for the earlier years of the study, so only four solutions were used in most of this report.

The process of obtaining visual correlation of coherence in the superimposed chart records is often somewhat tedious and possibly beset by errors which are difficult, if at all possible, to evaluate. First of all, matching the wave forms of a signal having fairly high frequency cycles for the 10-100 sec. passband, is generally the easiest to accomplish. If it is a visually-inspected 'good fit', the signal will appear as a single wave as seen by superimposing four records. Yet, the very best such fits, when solved by the various independent solutions on the nomograms, will frequently give a large range of azimuths and trace velocities for very well-aligned AIW waves. Many waves of longer period and noisier appearance frequently show smaller ranges of disagreement among the solutions. A first guess answer to this riddle is that perhaps the plane wave solution is breaking down because there is some finite curvature to the wave front for AIW signals generated close to the array. The actual answer to the problem is not studied in this report, but an effort to minimize the error range was done.

Before discussing the error minimization procedure used here, it can also be mentioned that large errors can also be made in scaling

simply be mis-aligning the charts, and misinterpreting the actual profile of the signal which leads to the same thing. This possibility is made more complicated if it happens that the wave itself undergoes some small changes in shape across the 5 Km average spacing of the stations. All of these possibilities lead to a large range of solutions as seen by the various independent triangles of the quadrilateral array.

In an effort to control the range of error of scaling of the AIW in this investigation, an arbitrary value of 10 degrees was selected as the maximum allowable error in azimuth among the various triangle solutions. In addition to acting as some measure of confidence in the scaled result, the 10 degree maximum allowable error also served as a criterion for ruling out the scaling of a chance coherence of the random fluctuations in the analog traces.

The act of reducing the error to an azimuth range of less than 10 degrees was accomplished by sequential scaling until the 'better' value was obtained. This procedure frequently led to 5 or 10 more attempts at realignment of the records in order to get a lower spread in azimuth. In following this procedure and recording the results each time, it was noticed that the lower azimuth range, $\Delta\phi$, was always accompanied by a lower spread in the trace velocity solutions. The very best scalings of azimuths led to a $\Delta\phi$ range of one degree and rarely, zero. For the lowest spreads of azimuth, $\Delta\phi$, the spread in velocity was still generally near 10 m/sec.. Thus that value is generally the best accuracy that can be expected for a trace velocity measurement. An error of 10 m/sec. trace velocity can amount to a small or large error in estimating the angle of inclination of the wave front to the earth's surface depending on the value of the trace velocity. Horizontal trace velocity, defined to be the speed of the intersection of the wave front with the surface of the earth, is related to the inclination of the wave normal by $V_{\dagger} = C\text{Sec}\,\alpha$, where α is the angle between the wave normal and the horizontal. The graph shown in Fig. 3.1 indicates the variation of trace velocity with angle of inclination α, for a local sound speed of 320 m/sec.

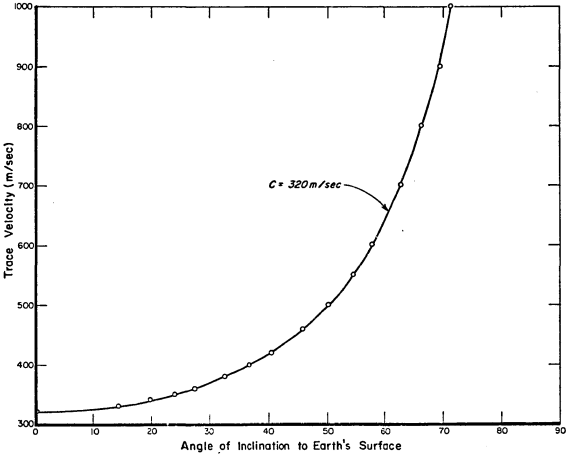

Fig. 3.1. Angle of inclination to earth's surface.

and 300 m/sec.. As can be easily seen from the graph, a scaling error of 10 m/sec. for a computed trace velocity average of 330 m/sec. would result in an 8° error in α; the same magnitude of error for and 800 m/sec. value would lead to less than 1° error in inclination angle.

In scaling the records successively in order to get a lower $\Delta\phi$, a very erratic and inconsistent feature of the azimuthal solutions was noted. In usual practice, once an accepted range of azimuthal solutions is obtained, the final value utilized is the average of the final solution from each of the four triangles. It is generally assumed that the actual azimuth from which the wave came is located somewhere between the two extreme values measured for the triangles, thus using a numerical average is justified. While successively scaling the same signal to lower spreads in azimuth, which means re-aligning the charts for a different visual fit, it was very frequently noted that the final scalings of low $\Delta\phi$ did not nessarily fall at all within the limits of the higher azimuthal spread. When it did, the process of scaling to successively lower $\Delta\phi$ resulted in erratic motion of the solutions thus obtained within the range of the larger azimuthal spread scaled earlier. A few examples of this behavior is shown in the graphs of Fig. 3.2 and Fig. 3.3.

Fig. 3.2 (a) shows the result of four successive scalings of the same AIW, each scaling of which is labelled $\Delta\phi_1$ thru $\Delta\phi_4$. As the graph shows, the first scaling indicated a $\Delta\phi$ of 22° spread between the azimuth range of from 320°-342°. (The vertical lines drawn from each azimuth spread show the separate azimuthal solution for each of the four triangles.) The second scaling of $\Delta\phi_2$shows a similar spread for the slightly lower $\Delta\phi$ 21°. The third and fourth scaling whose average between the four triangles is an arrival direction of 26°. The first scaling $\Delta\phi_1$ averaged to a value of 31°, while the final accepted value of 10° less and situated off to one side of the original scaling.

Part (b) of Fig. 3.2 shows the results of five scalings of an AIW which shift toward lower and then higher values until the final

Fig. 3.2. Changes in resulting azimuth for successive scaling of AIW records in order to achieve a lower error range in azimuth, $\Delta\phi$. (a) Four scalings of same signal to get resulting $\Delta\phi$ of 7°. (b) Five scalings yielding a final $\Delta\phi$ of 2°.

scaling is reached. The final azimuthal spread was 2° in which the four triangles, having two pairs of identical solution, average to an azimuth of AIW arrival of 10°. The original scaling, $\Delta\phi_1$, averaged to and arrival solution of 359°.

Fig. 3.3 shows a similar construction in which the first scaling resulted in a very wide error range of 81°. The next scaling shifted the error range to 34°, and the one following it, $\Delta\phi_3$, yielded a spread of 33°. Note however, that the next two scalings following the first one, $\Delta\phi_1$, resulted in solutions which fell on either side of it, and the final scaling ended with a spread of only 3°, but in no way a part of the azimuthal span of the first two scalings. This final scaling resulted in two pairs of separate values from the four stations, and they averaged to an arrival solution of 77°. The original scaling averaged to a value of 131°.

The lesson learned from these and many scalings like them is that the first scaling of an AIW, if it results in a $\Delta\phi$ greater than 10°, is likely to give an erroneous impression of the direction of arrival of the wave in question. Subsequent scalings do not necessarily fall within the span of azimuths given by the first one having a higher error range, but when the $\Delta\phi$ range becomes less than 10°, the lower azimuthal spread scalings generally fall close within a small range. Typically, an average of the four triangles scaling at an azimuth spread of 10°, or slightly less, will average within a few degrees, if not coincident, to the subsequent scaling of $\Delta\phi$ less than 10°.

(b) All-Sky Camera

The scaling of All-Sky Camera data was done by first viewing the film cinematically to observe times of interest. The lower borders of particular frames were then mapped by projecting the frames onto a standard sized grid. Each mapping was scaled at every 10° interval from the center of the frame, so as to render the resulting azimuths and range coordinates capable of being transferred to any map of known scale. In a few cases, the auroral form was mapped from a photographic

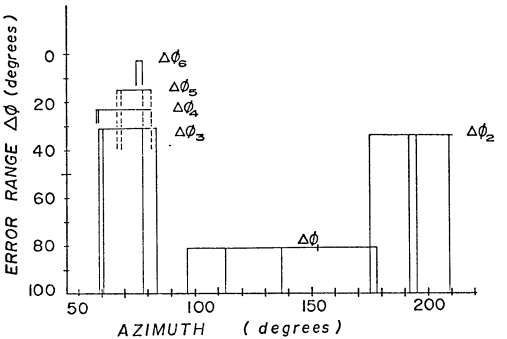

Fig. 3.3. Six successive scalings of the same AIW which terminated in an error range in azimuth of 2°.

print, and handled in the same fashion as the other data. Errors in this type if procedure are consistent with the extent to which the lower borders can be distinquished, and to the extent that the template used in standard practice for this purpose removes the non-linearity from the photograph.

(c) Magnetograms

In the various chapters of this report in which magnetograms were used, they were hand-scaled and digitized at periods varying from 10-minute intervals to 2-minute increments. Data from all available ovservatories in Canada, Greenland, Alaska, and the northern-most ones from the United States were used, and in one case, data from available European, Russian, and Japanese stations were also employed. The accuracy of scaling of the data varied with the quality of the magnetograms from each station and the accuracy to which the analogue trace could be seen and scaled. In the case of such stations as Rude Skov, Lerwick and some of the Greenland stations, timing errors were the major problem. Due to the system of time marking of their magnetograms, estimation of the time to the nearest 1-2 minutes would have been satisfactory. On the other hand, for stations like College, Kakioka, Memambetu, etc., timing to values somewhat less than a minute seemed possible.

In the process of scaling, the data was reduced in such a fashion that the total horizontal disturbance vector, $\Delta H^2 = \delta h^2 + \delta d^2$, or the total field disturbance vector, $\Delta F^2 = \delta h^2 + \delta d^2 + \delta z^2$, was computed. The quantities prefixed by δ represent the difference between the quiet day level and the value of the horizontal and vertical conponents, H, D, Z, shown on the records. The resulting data was then placed on maps of North America and environs and the field of mumbers from the stations were contoured.

(d) Contoured Maps

In the chapters of this thesis which the data for specific nights are investigated, the geomagnetic disturbances are represented by contoured maps of one of the two field vectors mentioned above.

The maps were based upon the data as hand-scaled from the magnetograms at varying time intervals over the periods of analysis. To construct a given map, the magnetic disturbance values for each time of interest and for each station were placed upon the maps. The resulting field of numbers were then hand-contoured by assuming a linear change in the field between stations, and connecting the resulting new field of numbers generated in multiples of 50 gammas by straight lines. The lines were then smoothed and all angular corners rounded out.

The role of subjectivity in doing a hand-contouring of any field of numbers is difficult, if not impossible, to ignore. On the other hand, a reasonable argument favoring the need for subjectivity can be presented when the objective approach, as would be followed by a computer, leads to results which contrast sharply with the known features of the field in question. An example of this type of consideration as well as the case when subjective reasoning was applied to the data is illustrated in Fig. 3.4.

Part (a) of Fig. 3.4 shows the contours of the total horizontal disturbance vector for the time near the substorm onset for the data of 31 Oct. 1968. This map was originally contoured by computer, but discarded due to the presence of errors other than the one to be discussed here. In its place, the hand-contoured model presented here was used, and the attempt was made to follow closely the objective features as done by the computer insofar as the rounding of straight line segments and gradients are concerned. As the map shows, the contours dip southwesterly after the western boundary of the United States is crossed. The gradient of the entire southern part of this magnetic disturbance 'cell' is considerably expanded and extended toward the south. A similar extension of the contours may be seen northeast of Alaska. This effect is purely a result of the station spacing and the resulting impression of the magnetic disturbance gradient over these two areas is most likely quite unreal. Yet, this extension was necessitated only because of objectivity which, as the case shows, could more realistically be rendered by subjective judgements. In this case, the stations at Honolulu and Mould Bay

led to the southern and northern extensions of the gradient respectively.

Part (b) of the Fig. 3.4 shows the case where the real situation was simply unknown, and a decision had to be rendered so as to make a reasonable guess. The case in point is the 300 gamma contour; does it close off into two separate cells as shown, or does it pass between the two arrows pointing to Ft. Churchill (lower) and Baker Lake (upper)? The separate cells can reasonably be connected if two (northern and southern) branches of it are drawn between the stations. In this case, it was decided not to connect them since no positive data to affirm the connection existed on the number field. However, should the electrojet have been quite narrowly confined in latitudinal extent, it could possibly have continued quite intensely between these stations and its presence be obscured by the poor station spacing.

The results illustrated by the foregoing figure show that departures from the real configuration of the gradient of the field, as well as small scale features of the spatial distribution of the disturbance, are obscured by any method of contouring. Yet the need for a temporal and spatial representation of the magnetic disturbance required that the contoured approach be used. As a general guide to reliability of the various features of the contoured study, a particular feature is seen to cross a station. The data between stations is actually an extrapolation and has to be handled as such. Such features as the width of a given cell then, can be considered only approximate, but a reasonable feeling of width may be had when the cell is extended across more than one station. Thus likening this procedure to the case of topographic mapping, the values at the magnetic stations may be treated as bench marks whose values are well known. Other measurements referenced to them are less well known.

All of the maps used in this study were contoured to a Mercator Map of the world of scale 1: 58,500,500. For purposes of practical study, once the contours were established in their final positions, the analysis was approached as if the entire two-dimensional

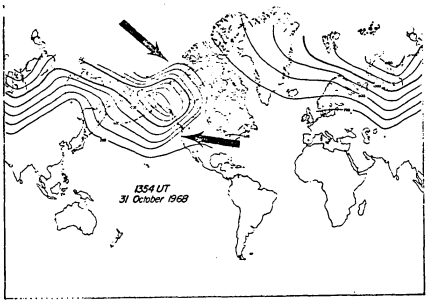

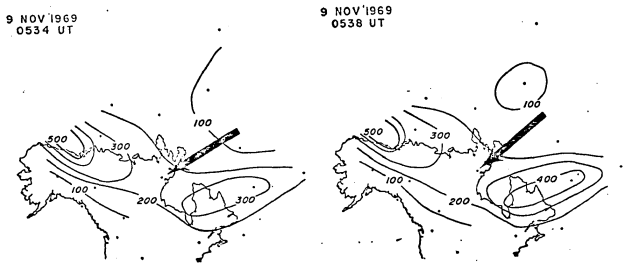

Fig. 3.4. Unreal and subjective considerations of the process of contouring. (a) Shows the unreal gradient spacing south and northeast of Alaska. (b) Questions the possible extension of the 300 gamma contour between the stations specified by arrows.

representation was real, but where unique features correspond to features observed by other physical quantities such as aurora or acoustical propagation, the approximate nature of many of the contoured boundaries and their limitations must be kept in mind. In no case was a measurement made of the rate of motion of a contour- though it could be when one crossed two successive stations- but rather instead, a distance measurement was frequently made to an area enclosed by the 'cells' of magnetic disturbance. In these cases, an error greater than half the width of the cell was considered unlikely.

(e) Relations of Contours to Auroral Electrojet

This section discusses the question of how well the most centrally disturbed portion of the magnetic contours used in the various chapters of this study represent the location of the auroral electrojet. The contours employed in the study were those of the total horizontal disturbance vector $\Delta H = \sqrt{\delta h^2 + \delta d^2}$, and the total magnetic disturbance vector $\Delta F = \sqrt{h^2 + d^2 + z^2} = \sqrt{x^2 + y^2 + z^2}$. The basis of this study is a comparison of the curves of ΔH and ΔF aginst theoretically constructed latitude profiles of the components, H, D, and Z. The theoretical latitude profiles used in this discussion are based upon constructions of Kisabeth (Ph.D. Thesis, 1972) applying the Biot-Savart law to three dimensional current systems in the ionosphere and magnetosphers.

The first comparison set of profiles is shown in Fig. 3.5. The current distribution is shown as a shaded box of 5° latitudinal width and represents an E-W current of 20° longitude in length. The latitude profiles are taken at 5° intervals of longitude east of the central part of the distribution and one profile 5° west. As the various profiles show, the curve for ΔH always peaks at the middle of this distribution while the ΔF curve peaks also within the distribution, but on the southern side.

The next set of profiles appear in Fig. 3.6. The perturbations represent the calculated distrubances for a three-dimensional sheet

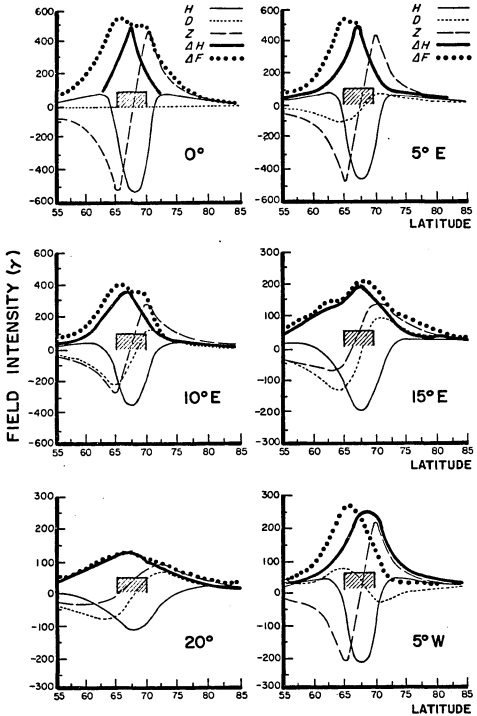

Fig. 3.5. Latitude profiles for an E-W current distribution (shaded box) which is of 20° longitude length and 5° latitude width. Successive profiles are taken at the stated intervals displaced from the meridian running though the center of the current. (after Kisabeth, 1972).

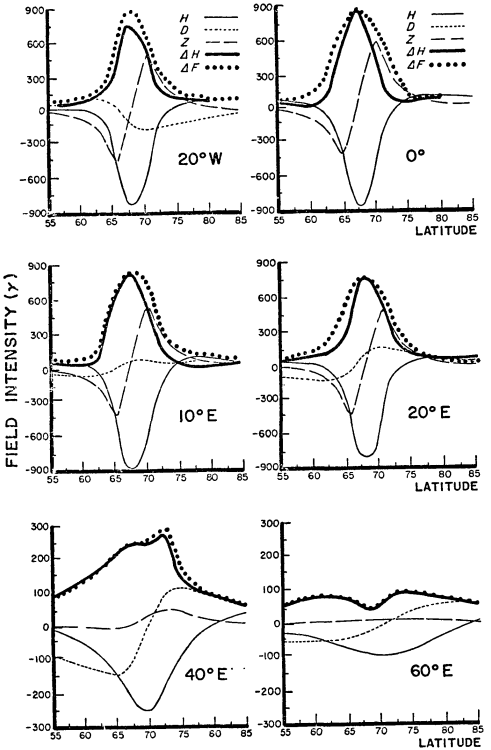

Fig. 3.6. Latitude profiles for a current distribution flowing along a parabolic arc in the auroral oval.

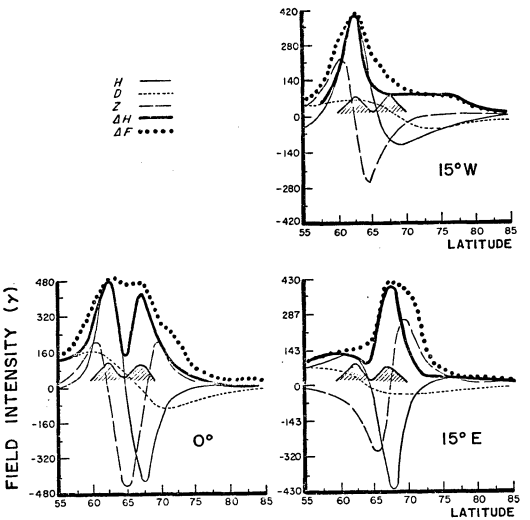

Fig. 3.7. Latitude profiles for a simultaneous eastward electrojet flow-south of a westward jet of equal intensity. Both jets are 40° long and each is 5° wide.

current flowing along the auroral oval in a parabolic arc located mainly between about 65°-70° latitude. The upper four profiles are across the current distribution but at various distances from the central meridian. The lower two profiles are located outside and to the east of the current distribution. As the profiles show, both ΔF and ΔH maximize above the latitudinal position of the electrojet for the cases when the profiles are across the actual body of the current distribution. For the cases where the profiles are taken outside the current 40°-60° east of the central meridian, ΔH and ΔF curves maximize slightly north and on either side of the current respectively. In the latter case, the disturbance peaks at a negative 100 gammas.

The final set of profiles is shown in Fig. 3.7. Here the current distribution shown in the shaded area is a double electrojet: the southernmost being easterly directed and the northernmost one being westward. Both currents are of equal intensity and are 40° long and 5° wide, while all three profiles are taken across the body of the current. (It is assumed, of course, that in all of the cases presented here that the currents are in the ionosphere and the perturbations are at the earth's surface.) In every case, both ΔF and ΔH maximize within the electrojet, but as the figure shows, the presence of the two currents is not very well displayed, if at all.

A number of other profiles having complex distributions of east-, and westward electrojets were also compared and proved to follow the morphology of the peak of the two vector components in question always fell within the current distribution of the electrojet. In fact, the only two exceptions to this rule were the final two profiles shown in Fig. 3.6, where the profile was taken well east of the current distribution itself, but where the maxima of ΔF and ΔH still fell within two degrees of the electrojet.

In the contoured representation of the substorms presented in this study, it was of interest to know the general location of the jet during many stages of the development. It was not necessary to know the exact width of the jet, and no attempt was made to infer it

Nevertheless, it appears that the location of the main current distribution can be ascertained by the maxima of ΔF and ΔH quite reliably, especially if one is near the central meridian of the current and is dealing with storms of more than 100 gammas. It is undeniable however, that for the cases of more than a simple line-current type electrojet, the contoured curves of ΔF and ΔH smear over many of the fine details of the electrojet development.

(f) Map of Invariant Latitude

Geophysical studies in the polar regions are often referenced with respect to some geomagnetic system of coordinates. The system chosen here is the Invariant Magnetic Coordinate system as discussed by Evans, et.al., (1969). No special use is made of this system in this thesis other than as a reference system of geomagnetic coordinates with which to compare the contour maps. A plot of the parallels of Invariant Latitude are shown in Fig. 3.8. Similar plots are supplied at the end of the large map sequences which are used in each data night chapter.

The fact that auroral arcs tend to lie along the narrow belt known as the auroral oval which is eccentric with respect to the dipole pole, a better coordinate system for auroral research would be based upon the oval (Akasofu, 1968).

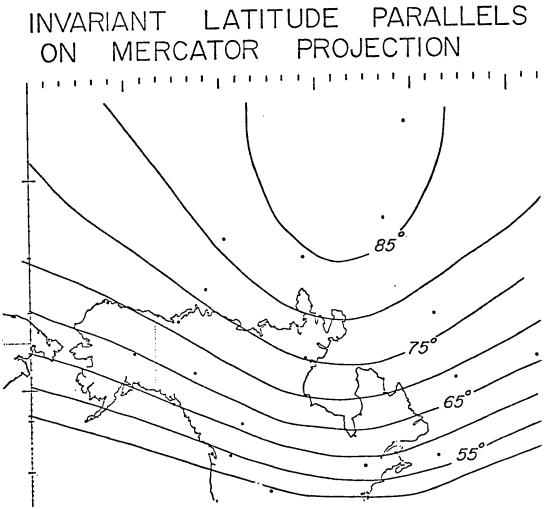

Fig. 3.8. Parallels of Invariant Latitude as they appear on a Mercator Projection.

CHAPTER 4

DATA NIGHT 31 OCTOBER 1968

4.0 Introduction

This chapter attempts to study the relationship of AIW signal reception to the morphology of the polar auroral and magnetic substorm. It utilizes contour maps of surface magnetic perturbations in order to achieve a temporal and spatial representation of the polar magnetic substorm. It also gives attention to the motions of the visual aurora since their supersonic motions have been related to their generation.

The substorms selected for study were successively-occurring substorms of the night of 31 October 1968. This night was selected because it was an occasion of exceptionally long duration of infrasonic disturbance at College, and it was also a night on which infrasonic data was available from three other station in the lower states of the continental USA.

The location of the stations whose data were used in this report is shown in Figure 4.1. Data was used from 29 magnetometer stations spanning two-thirds of the Northern Hemisphere, 13 riometer stations across the North American continent, 2 all-sky camera stations and four infrasonic stations spanning the continental USA and Alaska.

4.1 The 1000 UT Substorm

It has been observed that the break-up phase, the most violent phase of the auroral substorm, is generally observed around the midnight sector (Akasofu, 1964). From this it follows that the most intense part of the magnetic disturbance would also be located in this sector. Moreover, Akasofu has shown that the activation of auroral arcs originates in the

Fig. 4.1. Location of stations for the data used in this report.

midnight sector spreading equatorward-and-poleward from that locale. These characteristics seem to pertain in a general way to the substorm referred to herein as the 1000 UT substorm which, as is shown by the group of magnetograms from selected sectors of the Northern Hemisphere shown in Figure 4.2, is most intense between 1000-1100 UT at the western North America stations. (Local midnight occurs near these times in that area).

A closer inspection of this figure shows that in addition to the obvious large bay centered near 1100 UT, there is a smaller but correlatable deflection of the magnetic components near 1000 UT. Generally speaking, this deflection was correlatable to a greater or lesser extent in all of the magnetograms used in this study. Such a correlatable feature which, in this case, can be specified to occur within the five minute span from 0955-1000 UT at all stations, is taken to represent the onset of the 1000 UT substorm thus designated. If this selection is a valid one, then the magnetogram analysis shows that this substorm appears to have originated in western North American near Meanook, Canada.

(a) Magnetic Substorm

The growth and decay of the polar magnetic substorm is depicted in Figure 4.3 in a series of maps which show a contoured representation of the total horizontal disturbance vector ($\Delta H = \sqrt{\delta H^2 + \delta D^2}$) for selected times during the growth and decay of the substorm. The contour interval is 200γ. A given contour represents a line which was equally disturbed with respect to the value which was prevalent near 1000 UT.

As shown in the figure, the 1001 UT map depicts the earliest portion of the substorm originating within the 400γ contour around Meanook, Canada,

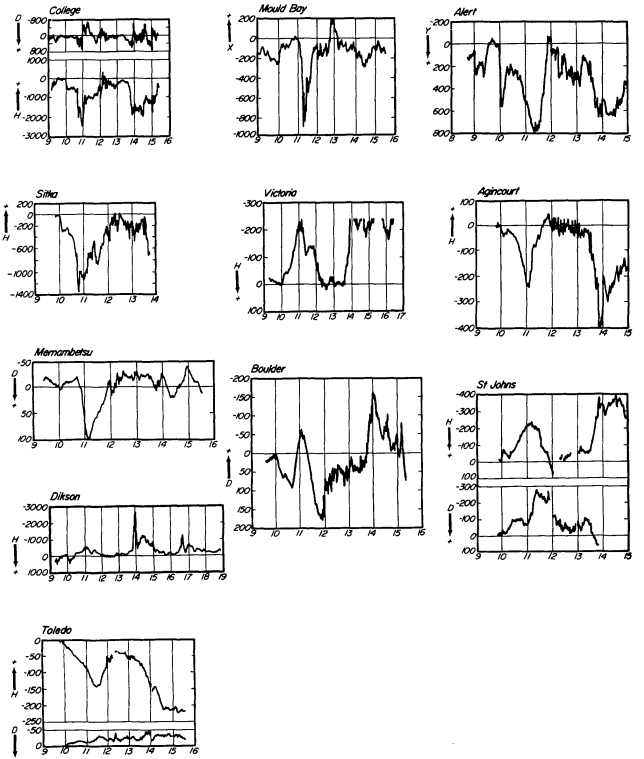

Fig. 4.2. A selection of magnetograms from various sectors of the northern hemisphere for 31 October 1968.

although there is also indication of a simultaneous disturbance in the high latitudes about the station at Alert, in northern Ellesmere Island. The adjacent map five minutes later in time shows the effects beginning to spread westward and eastward more rapidly than northward and southward (directions referring here to invariant coordinates). At 1042 UT it is seen that some of the earlier widespread portions of the disturbance - e.g., the 200γ and 600γ contour - have contracted arealy into a more intense compact bundle. It is at this stage that the onset of an auroral expansive phase of the type discussed by Akasofu (op. cit., 1964) occurs. The next three maps show that the following 18 minutes to 1100 UT represents a rapid, omni-directional increase of the disturbance favoring the most rapid expansion along a zone extending from east to west probably along an instantaneous auroral oval. The east-west expansion appears to be fairly uniformly distributed about the maximally-disturbed region at 1047 and 1056, but by 1100 UT, it is obvious that the effects of a westward expansion have exceeded those to the east. At 1100 UT the storm has reached its peak of development after which it begins to recover. Following the time of 1221 UT map, the area near College is occupied by pulsating aurora.

(b) Auroral Substorm

Superposed in the sequence of maps in Figure 4.3 are arrows which represent the general direction of motion of the auroral luminosity as seen by all-sky cameras located at College and Tungsten. Owing to the lack of necessary areal coverage by all-sky cameras as well as the imprecise nature of contours due to inadequate station spacing, no

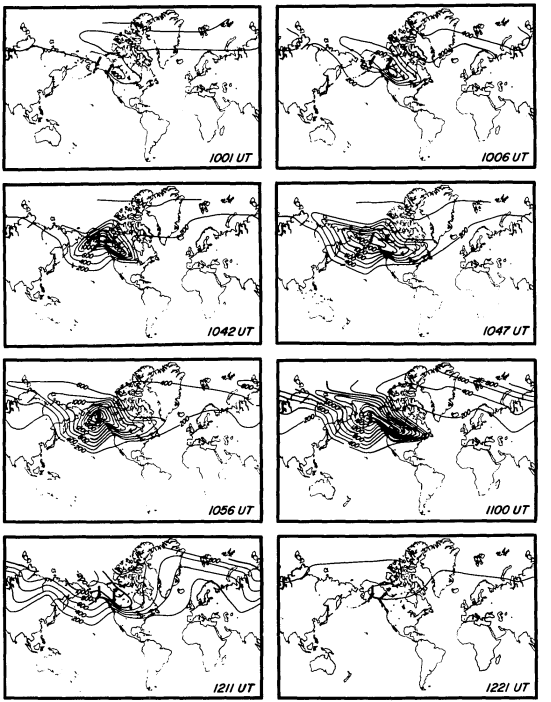

Fig. 4.3. Growth and decay of the 1000 UT substorm of 31 Oct. 1968. The contour interval is 200 gammas. See text.

definitive relationships between auroral motions and the substorm contours will be specified. Nevertheless, general features will be noted which may be of interest and possibly of significance.

The first two maps - 1001 and 1006 UT - show auroral motions along the local magnetic meridians at College and Tungsten during the early portion of the substorm. The aurorae seen at College at these times were very faint, while the Tungsten film showed brighter forms, but the changes in the level of brightness between the two at this time may be due to the different films and separate processings. At 1042 UT the expansive phase of the substorm has obviously begun. The all-sky camera showing this phase of the auroral substorm as seen at College and Tungsten is shown here in Figure 4.4.

The four frames from each station show poleward expansion at College and an eastward onset at Tungsten. The poleward motion seen at College is much more rapid than the easterly onset at Tungsten, but lack of discrete arcs at Tungsten makes it uncertain as to the exact quantitative difference. The average speed of the poleward arc at College during this period was 2760 m/sec. At both stations, within five to seven minutes following the onset, there occurred a change in the motion. At College, the nature of the change was an almost complete reversal in direction at 1046:30 UT in which fainter forms moved toward the geographic southwest for a few minutes and then commenced southerly motion. The average speed of the correlatable form from 40° was 508 m/sec. from 1046:30 - 1048:30 UT. At Tungsten the change in motion came at 1048 UT, but was so complex that a definite direction of motion could not be

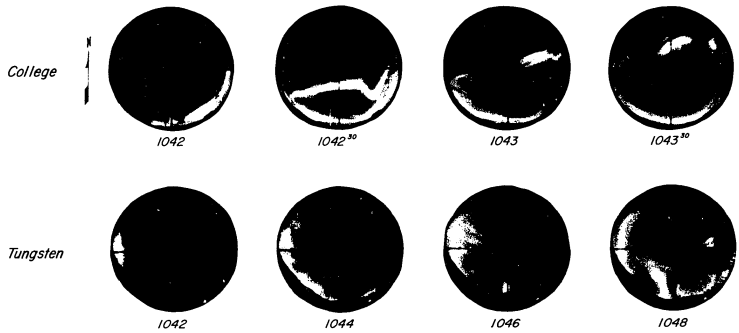

Fig. 4.4. Onset of the expansive phase of the auroral substorm.

ascertained. No attempt is made to represent picture frames of these motions here, because they are too subtle to be viewed by still pictures. However, it must be pointed out that this apparent reversal in the direction of motion following the poleward expansion as seen at College when the ASC film is viewed cinematically may be of considerable significance to the reception of AIW there.

As the arrows on the maps in Figure 4.3 show, the auroral motions at College were geographically southward from 1056 UT until the end of the substorm. Motions at Tungsten at 1056 and 1100 UT were indeterminate, but as the substorm began to subside in intensity at 1121 UT, distinct directions are shown.

(c) Infrasonic Disturbance Related to 1000 Substorm

Associated with the growth and decay of the 1000 UT substorm from its early origins in western North America to its eventual spread around the entire Northern Hemisphere, there were pressure disturbances generated in the atmosphere that propagated to the earth's surface. A portion of this energy was detected as the now familiar Auroral Infrasonic Waves (AIW) at Washington, D.C., Boulder, Colorado, Pullman, Washington and College, Alaska. Part of the pressure records for these stations, each containing an overlay of the records from three to four separate microphone sites time-shifted to display phase coherence, is shown in Figure 4.5. The microbarograph instrumentation utilized at these stations is described in the literature (Cook and Young, 1962).

As shown in the figure, coherent signals commenced near 1220 UT at Washington, D. C. and continued that way for at least the next three

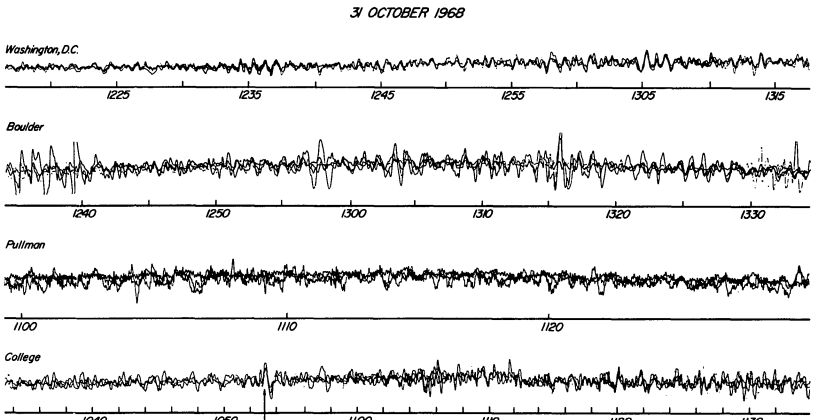

Fig. 4.5. Sections of the pressure records of AIW from the network of stations spanning continental U.S. and Alaska. (Note: Pullman records run at twice the chart speed of the others.)

hours (not shown). At Boulder, recognizable coherence began after 1240 UT amid much background noise probably of local origin. At Pullman, numerous microbaroms are evidently superimposed upon longer period AIW which began indistinctly and continued for some undetermined number of hours. At College, the first recognizable coherence seems to appear about 1048 UT as a multiple impulse event of a few cycles ($MFDA_1$, see Appendix I) and continues intermittently at other points to the three distinct waves near 1053 UT which were received just six minutes - in good agreement with the delay time for acoustical propagation from ionospheric heights to ground - following the 1047 UT reversal in motion of the aurora which followed the poleward expansion as seen at College. This example illustrates the asymmetry in signal reception at College in that poleward expansions do not seem to result in recognizable AIW detected at the ground when the system is south of College. Thus AIW signals from the south are rare, whereas, as this example shows, after the expansion has passed northward, AIW may be readily observable from auroral forms moving southward. The signals near 1053 UT were found to be arriving from an azimuth of 38° with horizontal trace velocity of 434 m/sec.

Scalings of the records from the four infrasonic stations are shown in Figure 4.6. A given ray represents the azimuth from which the AIW was received at the station in question. Also shown in the figure is a shaded region which represents the envelope of the resulting shapes formed by superimposing the contours representing the most intense area within the substorm for each map. This area then represents a sort of

Fig 4.6. Composite of the AIW azimuths scaled in conjunction with the 1000 UT substorm. Shaded area shows location of auroral electrojet as deduced from a composite of the contoured maps.

average location of the most intense portion of the magnetic substorm and therefore probably the zone which would most likely be associated with the location of the auroral electrojet.

One of the most inviting features of the display in Figure 4.6 is to associate some significance to the intersections of these rays from the various stations. Yet for AlW the meaningfulness of most of these intersections is unlikely owing to poor temporal correlation and, in terms of known behaviour of auroral infrasonics, poor spatial location.

In an effort to correlate the signals from the three stations in the lower states, some 28 intersections of these signals as shown in the figure were analyzed for travel time using both the measured trace velocity as calculated from the pressure records and a mean horizontal transit speed of 243 m/sec. - a value based upon a determination in Chapter 5 of this report. Such a calculation considers the travel time along each path and predicts an origin time for each intersection which must fall within reasonable limits to be credible. The time limit of error chosen for this determination was five minutes and as the calculation showed, none of the signals which intersect between Pullman, Washington and Washington, D.C. fell within these limits. On the other hand, three of them did correlate between Boulder and Pullman and these intersections are shown on the chart in Figure 4.7. The time of reception of each signal is displayed from top to bottom to represent the intersections from upper to lower. The predicted time of signal generation is shown by the dashed lines to the right of the intersections. It can be noted that the upper two intersections were

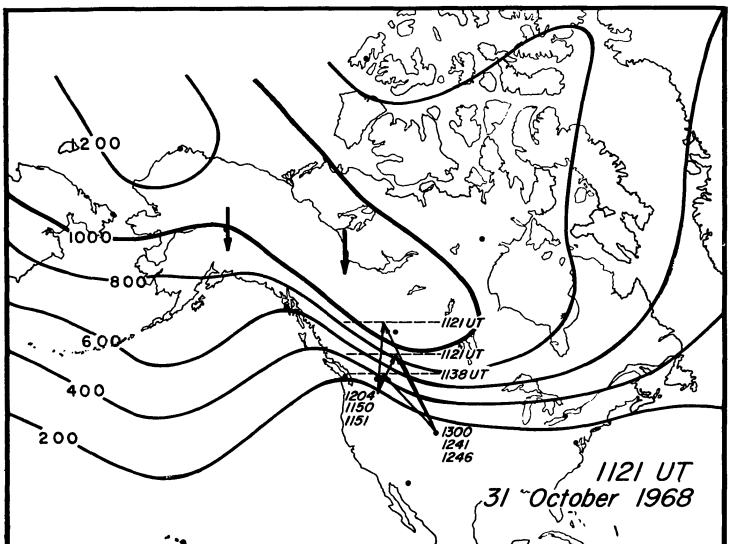

Fig. 4.7. Correlation of AIW waves generated from a common area as received at the infrasonic stations at Pullman and Boulder.

apparently generated from within and just south of a very intense part of the substorm at the time of that particular contour map. The other intersection had an origin time at 1138 UT - somewhat later. Auroral motions are shown by the heavy arrows in the figure and they indicate the motions as seen at College and Tungsten. If the same motions were prevalent further south near the azimuthal intersection, it would be a reasonable agreement with the generation of AIW propagating southward.

(d) Discussion of Results of 1000 Substorm

In a study relating AIW to the polar substorm, it would be most satisfying to either be able to specify the location from which each AIW was radiated within the huge areal form of the substorm, or to be able to follow the development or expansion and contractions of the substorm by a smooth succession of azimuths within the wave train received by a given station. Both of those two choices are difficult to achieve in the practical situation, however, because of the complex dynamics and geometry related to the generation of an AIW, as well as numerous factors involved in acoustic propagation detection and measurement. For example, the fact that when one makes a determination of speed from the pressure records, one is actually measuring the speed of intersection of a wave front with the earth's surface - the horizontal trace velocity, as it were -rather than the horizontal phase velocity. As it happens, V_t is generally larger than C and AIW may travel by paths which utilize the two sound channels in the upper atmosphere (Wilson, 1966) or AIW may travel downward, reflect from the earth's

surface (Wilson, 1969b) and be refracted downward from the thermosphere to possibly recycle again.

Moreover, depending strongly upon the height of generation, an acoustic signal may travel by any one or more of numerous paths (Barry, 1963) which depend upon horizontal and vertical sound speed gradients which are generally unknown and whose spatial and temporal variations during a substorm are also unknown. Thus in the practical situation, the actual path or multipaths over which an acoustic signal has propagated is nearly impossible to determine and one is left with simplified ray diagrams as a compromise and also an estimated transit speed in order to discuss long range propagation.

The AIW record as seen at a given station must represent a complex composition of waves from probably multiple sources, traveling by multipaths and generated at varying distances and times from the receiving station. An indication of this type of complexity can be inferred from a glance at the composite signals received at WDC as shown in Figure 4.6 and reference to the maps of the substorm at 1006 and 1100 UT. A signal generated over Hudson Bay at 1006 UT along the northern part of the 200γ contour at an azimuth of 340° would take about $2^h18'$ to travel to Washington, D.C. at 304 m/sec., to use an arbitrary transit speed. Yet a signal generated at the southern edge of the 200γ contour at 1100 UT along the same azimuth and same speed would take only 21 minutes to arrive there. Thus a signal generated within the substorm 54 minutes earlier but about 2500 km away would arrive at 1224 UT, whereas the signal generated later only 400 km away would

arrive at 1121 UT, more than an hour earlier. This simple calculation is specified to show that numerous sources generating at varying distances within the same substorm cause the AIW record to represent a complex admixture of coherent signals which are extremely difficult to interpret of correlate with regard to deducing the origin of a given AIW with pressure records alone. For this study extensive all-sky camera coverage in the southern and eastern parts of the substorm system in North America would be a necessity for any firm correlation.

4.2 The 1337 Substorm

(a) Magnetic Substorm

This substorm is named after the time which was taken to be its onset at College. Unlike the substorm discussed previously, there was no recognizable common feature which could be localized to a small span of time that was observable on the world-wide net of magnetograms other than a sudden bay disturbance occurring at most stations between 1300-1400 UT. The onset of the expansive phase at College is at 1337 UT which is the time the H component of the magnetogram commenced into a large negative bay. Taking such abrupt transitions to represent a common disturbance among the other stations, the contours for this substorm were based upon the time at which the most abrupt departure occurred in one of the magnetic components between 1300-1400 UT. Such a consideration led to the recognition of the onset as progressing westwardly from the midnight sector as a general feature, having an earlier onset in high latitudes near Alert than at most of the other stations.

The growth of the magnetic substorm is shown in the sequence of contour maps in Figure 4.8. This development is very rapid after 1337 UT and appears to have expanded primarily towards the west since very little eastward motion of the contours is observable throughout the storm. Unlike the earlier substorm, this one seems to have a broader areal development and a greater expanse of intense disturbance north of Alaska. In the process of growth it reaches its peak development at 1400 UT where the most intense part occurs in the evening sector near Cape Chelyuskin, USSR. From the time the substorm alternately declines at 1416 UT, intensifies again at 1428 UT, diminishes at 1444 UT only to intensify at 1507 UT after which it subsides again at 1521 UT and continues to do so afterward.

(b) Auroral Substorm

The onset of the auroral substorm was observable at both College and Tungsten all-sky camera stations. At College, the major aurorae came from the west moving easterly in the form of a broad band of rayed forms. Ray structure was generally observable in most of the visual forms throughout this substorm. At Tungsten there was a noticeable brightening of faint rayed forms 10 minutes after the onset time at College. Most of the advancing luminosity came from the southern sky at about 1400 UT at Tungsten proceeding towards the geomagnetic pole. At 1430 UT dawn came at Tungsten, thus leaving only the College all-sky camera available for the remainder of the substorm.

(c) Infrasonic Disturbance

The pressure disturbance propagated into the lower atmosphere by

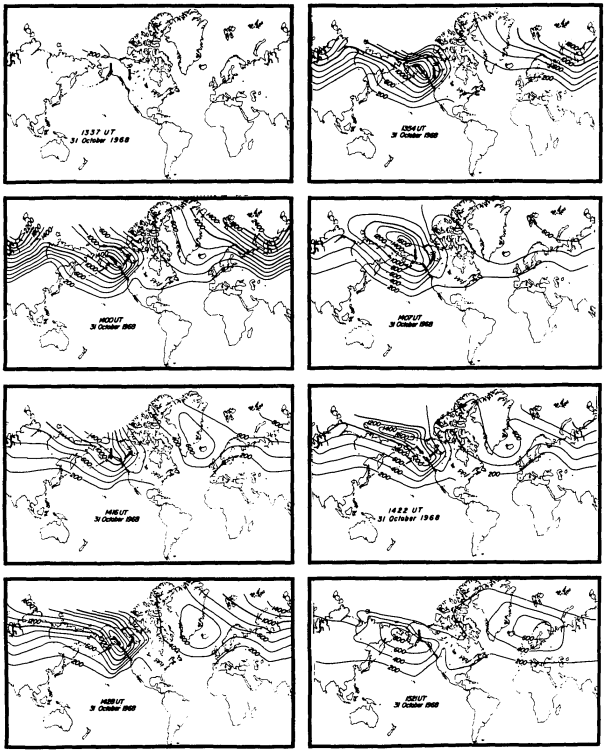

Fig. 4.8. Growth and decay of 1337 substorm of 31 Oct. 1968. Contour interval is 200 gammas.

this substorm was very intense at College, substantial at Pullman, Washington, undetected at Boulder due to local noise and indeterminate at Washington, D.C. due to a gap in the available data. A portion of the pressure records from Pullman and College are shown in Figure 4.9. Coherence in the pressure records at College associated with this substorm commenced in the final few minutes near 1350 UT as multiple impulse events of indeterminate dispersion (Mml) and quite unusually continued that way throughout both the remainder of the substorm as well as into subsequent substorm disturbances until their termination near 2300 UT. The pressure disturbance was very lengthy at Pullman also, but owing to both the difficulty in scaling their records which were run at twice the customary chart speed for auroral infrasonics as well as the problem of correlation of AIW between stations separated by such great distances as alluded to earlier in this paper, only passing treatment will be given to these data here.

Due to the exceptional length of the coherence in the infrasonic records at College, an attempt is made in this study to follow the morphology of the AIW as they progressed through the course of the substorm. The scaling of the records involved the laborious process of time-shifting the records by hand for each recognizably coherent cycle shown on the College record of Figure 4.9 in order to gain a solution for each wave in the wave train. Numerous scalings of each wave were done in an effort to keep the resulting solutions for azimuth below a 10° variation over the four independent solutions afforded by our four-station array (five are possible). In this effort, some 105 waves were

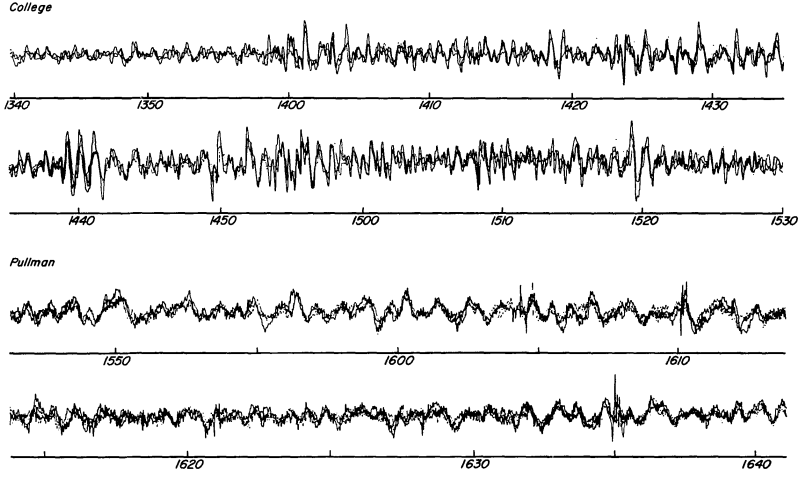

Fig. 4.9. Portions of the AIW records from College and Pullman showing events related to the 1337 substorm.

recognized and scaled between 1315-1504 UT of which 87 were scaled to an azimuthal spread of less than 10° and 53 of which showed a spread of less than five degrees.

As a reference again to Figure 4.8 will show, College was totally engulfed either in the most intense portion of the substorm or in one of the more intense regions. Scaling of the pressure record revealed that the pressure record was very complex and inexplicable unless the possibility of multiple sources generating disturbances which travel via multiple paths could be allowed. In fact, as the substorm progressed into its later stages, the dynamics of the generating mechanisms seemed to become more complex. An illustration of this fact may be seen in the graph in Figure 4.10. This graph shows a plot of the azimuthal solution as a function of time for each successively-scaled wave in the train having periods greater than 20 seconds. (Waves of shorter period were omitted because many were riding atop the longer-period waves and arrived at the same time, thus giving a second solution at the same time and causing a disconnected plot.) This figure shows that the variations in azimuth were smaller in the early expansive phases of the substorm, however, as the storm seemed to abate near 1444 UT, the differences in azimuth between succeeding waves was as much as 63° in one case. Thus it appears that from this consideration, the pressure record represents an admixture of disturbances from many sources located in and around the vicinity of Alaska. It is also noteworthy that despite the apparent central location of College in the midst of the substorm disturbance, by far the major portion of the record shows

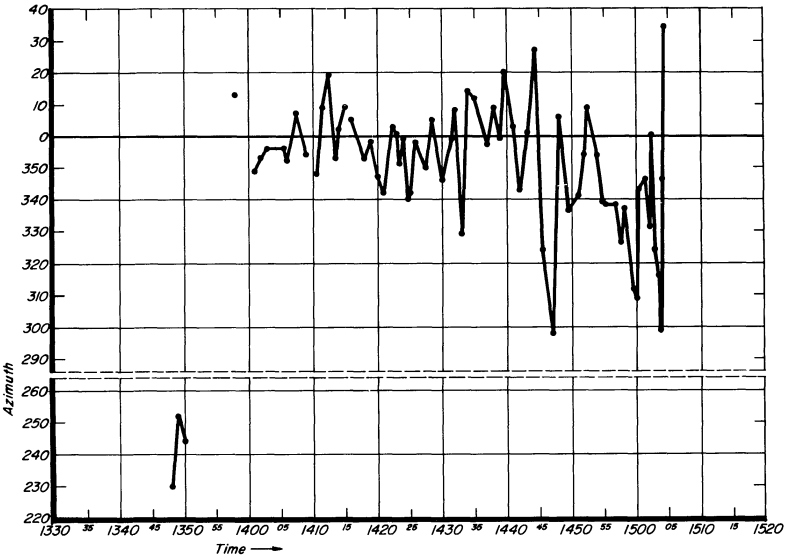

Fig. 4.10. Variation in azimuth of AlW at College as shown by each successive wave of wave train.

disturbances ranging between the azimuth of 35° to 298° along the sector which includes geographic north, but very little south of a line running east to west. This is typical of the asymmetry in the azimuthal statistics at College accumulated over the entire 5 1/2 year span of data collection, and remains a fact that AIW from the southerly quadrants even during poleward expansions are extremely rare.

Along with the possibility of multiple sources generating AIW during the substorm must come also the possibility of mutual wave interference along the propagation path. Interpretation of the pressure record at College led this investigator not only to infer the presence of dynamic interference among the waves themselves, but to recognize the presence of tiny wavelets, as it were, which are significant AIW and not microbaroms or random small instrumental or localized fluctuations in the atmosphere. An example of these phenomena is shown in Figure 4.11 (A,B). In Figure 4.11, (A) shows an example of a wave of period 52 sec measured from trough-to-trough as shown by the bar and designated 48, is aligned and scaled as in the upper wave train, then it was realigned and scaled for the coherent wavelet (marked by the arrow) which rides on top as seen in the middle trace designated 48B. (That it is realigned is evident when noting the rearrangement of the negative spike on the left side of the wave.) A second realignment was then made for the wavelet marked by the arrow on the bottom trace designated 48c. The resulting scalings are shown in the accompanying table where $\Delta\phi$ represents the spread in azimuth. From the small spread in azimuths as seen by the four independent-triangle

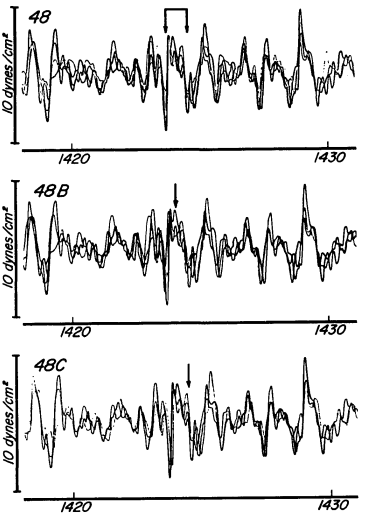

	Azimuth	Speed	Period	Δφ
48	359°	823 m/sec	52	8
48B	358°	1313 m/sec	14	5
48C	18°	520 m/sec	19	3

(A)

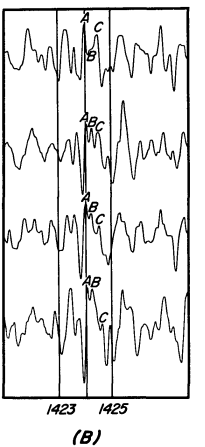

(B)

Fig. 4.11. (A) Independent wavelets (48B & 48C) advancing across a longer period wave (48). (B) Separate records of wave train as seen at each station. Lettered waves display interaction of wavelets during propagation.

solutions, and the variation in speed and/or azimuth as scaled for each wave, it becomes quite apparent that these little wavelets are as real a part of the AIW as are the larger, longer period types. Numerous wavelets of this type were scaled in this study, many of which were isolated between larger waves, or riding on their troughs or crests. A possible reason for their small amplitude may be due to the fact that their periods ranged from about 25 sec. down to 8 sec., which gets close to the low end of the 3 db down points - 7 to 70 seconds - for the pass-band of our equipment.

In the same figure, section B shows this same wave group shown by the superposed time-shifted pressure traces of II A, but in this diagram, the record from each individual station is shown with the various components in question labelled A, B, and C. The sequence from top to bottom is the sequence in which the wave designated 48C, or simply C here, traveled across the four-station array. In the upper trace, component B is first seen emerging from component C. As B grows in amplitude and increases its distance from C the top to the lower trace shown, C diminishes in both amplitude and period progressively as it propagated, almost as if the growth of B were coming at the expense of C. Numerous such wave interferences of various types were observed in this study which were out of phase from channel-to-channel between the various cases, thus eliminating instrumentality as being the sole causative factor. No attempt will be made to examine this phenomenon in depth here, because a very detailed quantitative approach is needed in order to give even fair treatment to the subject.

Relation of AIW to the Structure of the Substorm

The geometry of the AIW with respect to the magnetic substorm is shown in Figure 4.12, which depicts the sequence of signals which began an acoustical delay time of 6 minutes following each map in question. The possible signal associations are drawn as rays labelled by their arrival time along the azimuth from which the AIW were received. An arrow drawn below the station at College indicated the general direction of motion of the visible aurora at the time of the map.

Possibly due to the absence of a fixed relationship relating the geometry of the auroral motion with respect to the magnetic disturbance contours as interpreted for this substorm, there did not appear to be a firm relation between the directions of AIW and the orientation of the contours. For example, at 1354 UT the associated AIW appear to bridge directly down the gradient, while later at 1416 UT, many of them emanate from along it. The general trend, however, seems to be across the gradient, but then College was located well within the central part of the disturbance during most of the substorm. The general direction of the auroral motions as given by the arrow on each map agrees fairly well with the directions from which the AIW came. It is of interest to note on the 1354 UT map that as the time elapsed from 1400-1405 UT, there is a steady shift from NW to NE of the AIW, that is, allowing the 1403:30 signal as the exception. Most of these signals can be related to the passage of a series of rayed arcs as shown in the sequence of ASC photos shown in Figure 4.13.

Fig. 4.12. Geometry of azimuths of AIW at College with contoured structure of the polar magnetic substorm of 1337 UT. Rays show time and direction from which AIW were received. Arrows show general direction of auroral drift during period.

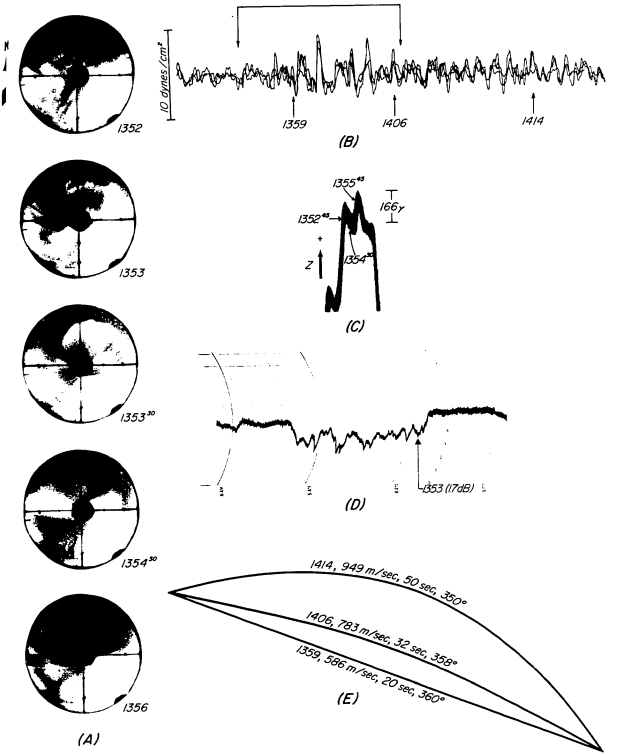

Fig. 4.13. Associated phenomena with the zenith passpage of a series of arcs at College. (C) Reversals of Z component of magnetic field. (A) AIW train associated with arcs. (B) All-Sky photos of auroral forms. (D) Enhancement of cosmic noise absorption during event. (E) Possible ray paths for three waves shown at 1354, 1406, and 1414 in (A).

This figure attempts to show a sequence of observable phenomena associated with the reception of a group of AIW (Section A) at College. Cinematic viewing of the all-sky camera film showed that there was a change in direction towards the southeast at 1352 UT. There followed the zenith passage of an arc near 1353 UT -- as shown in (B) of the figure -- a sudden brightening in an arc, and ensuing supersonic motion towards the zenith at 1353:30. A second fainter arc located in nearly the same position as the former which then moved supersonically towards the zenith crossing it between 1355:30 and 1356 UT as shown in the last frame of the figure. Reversals in the Z component of the magnetic field associated with those zenith crossings are shown in (C) of the figure, as well as the associated enhancement in cosmic noise absorption in (D) at the time of brightening and subsequent motion of the arc. The diagram (E) of the figure based upon earlier ray tracings by Barry (op. cit.) suggests a possible ray path configuration to explain the reception of three signals (lower arrows in "A" of the figure) which were close in azimuthal spread, but differing in period and speed. Here the longer path would cause a larger period due to finite collision rate processes in the upper atmosphere and the higher speed would be an indication of a steeper inclination angle of the wave front to the earth's surface. The arrival time, speed, period and azimuth are shown in the suggested ray diagram in the figure. Numerous such multipath associations showing even closer azimuthal spread were observed in the course of this substorm.

Another identification of AIW with the motion and subsequent zenith

passage of a rayed arc is shown in Figure 4.14 A to E. The sequence of events was similar to the earlier case in that brightening of an auroral arc was followed by sudden zenith-ward motion of the arc along the azimuth from which the AIW was received. In this case, however, the arc appeared to brighten both at 1414 UT and again at 1415:30 UT along azimuth 358°, each brightening resulting in rapid uneven motion of the arc in a zenith direction along the azimuth containing the AIW. The associated magnetic effects, cosmic noise absorption and a possible ray path configuration are also offered in the figure.

The direction of motion of the aurora is shown above the ray diagram as an arrow, and the time above the arrow is taken to be the time of signal generation. These coincide with the times when the aurora brightened and commenced rapid motion. Note that the 1424:40 signal is an AIW wavelet riding atop the wave mentioned earlier in Figure 4.11.

(d) Conclusion

An attempt was made in this chapter to relate the reception of AIW to the morphology of the polar substorm as well as to present a picture of the spatial and temporal development of the polar magnetic substorm itself. Of the four infrasonic stations whose data were used in this investigation, three were south of the more intense areas of the substorm, and the one, College, was totally within it. The most intense part of substorms studied here were initiated in the midnight sector spreading east- and west-ward in the earlier one (1000 UT) and primarily expanding westward in the later (1337 UT) substorm. Owing to the complex dynamics of AIW generation and propagation and the absence

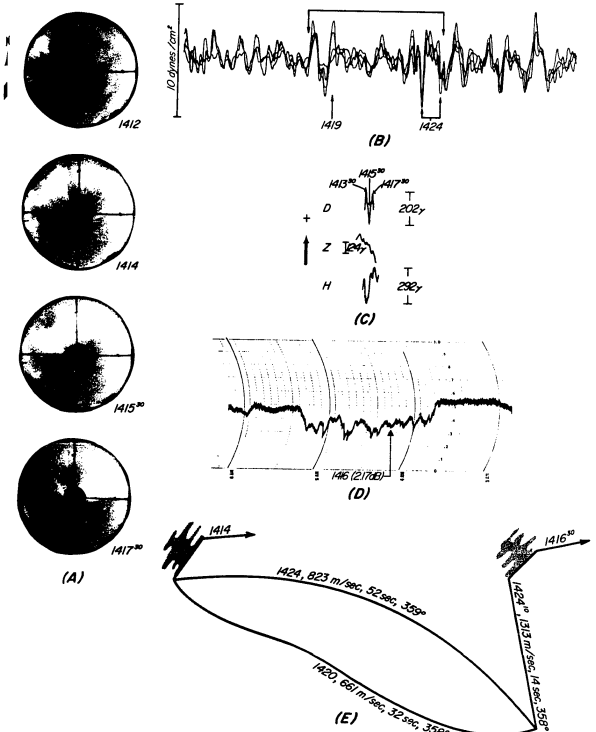

Fig. 4.14. Phenomena associated with the passage of a rayed arc near College. (A) All-Sky frames of rayed arc. (B) AIW train associated with arc. (C) Magnetic disturbance due to passage of arc. (D) Enhancement of cosmic noise absorption during transit of arc. (E) Possible ray paths associated with signals shown by arrows at 1419 and 1424 UT in (A).

of all-sky camera coverage in eastern Canada due to clouds, a likely location for the origin of the signals at Washington D.C. is uncertain. For reasons stated earlier, it is a conclusion of this study that simple triangulation by intersecting azimuths from the various stations simply does not lead to a meaningful result in many cases, and in any case for correlating the signals at Washington D.C. to the other stations on this night.

Reference again to Figure 4.6 shows that AIW azimuths received at Washington D.C. intersect with the other stations in an area well outside the most intense area of the storm. It is unlikely that this area would be the region containing the most active aurora which typically produce the AIW as seen at College. The shaded zone representing the most intense part of the substorm as shown in the figure probably represents the area in which the most active aurora are contained, and if this is so, probably represents a region in which much infrasonic energy is liberated. Good correlation is shown in the figure with the azimuths of the AIW from Boulder and Pullman and as was pointed out earlier, the only meaningful intersections arose within or just south of this zone.

Because the azimuths of the AIW at Washington D.C. do not intersect the substorm until 1047 UT which is just 13 minutes before the peak development of the substorm, it is a further conclusion of this study that most of the AIW received at Washington D.C. related to this substorm arose during the expansive phase and perhaps recovery phase of the substorm.

In a study of this nature in which the substorm is represented by disturbance contours, we try to find some firm geometrical relation between the motions of the aurora within the substorm and the contours by which it is portrayed. Since a general relationship of the motions of the aurora to the radiated AIW is known, i.e., the signal propagates in the direction of motion of the aurora or at an acute angle to it as a bow wave, then perhaps a useful relationship could be resolved relating the radiated AIW to the disturbance contours. This would then lead to better judgements in localizing the probable generating regions within the substorm when comparing it with AIW azimuths. Unfortunately, insufficient aerial coverage by all-sky camera in this study did not permit a definite statement of the relationship of the direction of auroral motion with respect to the contours of $\Delta\vec{H}$. If such a relationship does exist, subsequent studies of this effect are needed in order to ascertain it.

Insofar as the AIW themselves are concerned, it is a further conclusion of this study that closer attention needs to be given to the interference of the waves in order to form better ideas of the propagation effects. As a result of wave interference, major changes of wave structure may occur in times comparable to propagation times across a single array of microphones spaced about 5 km apart as at College. These effects are more pronounced in the cases of the short-period waves designated as wavelets in this study, thus further attention should be given to them.

The development of the polar substorm itself by use of disturbance

contours seems to be a useful one for expressing temporal and spatial growth. It is evident from these maps that both the growth and decay or expansion and recovery, whichever, does not proceed smoothly, but pulsates to wider and smaller areal expanses in all stages of development.

A few words need to be said concerning the generation of AIW and the sequence of observable events related thereto. Compared to the number of AIW received at College during the full span of its operation, the number of positive correlations of the AIW with a specific auroral form are small. One reason for this is the small areal coverage of an all-sky camera as compared with the vast expanse of the substorm over which an AIW may be generated. For this reason it is still of interest to relate the sequence of observable phenomena associated with reception of a signal. The final two figures of this report make such an effort, but perhaps the most logical sequence shown for the two correlations with specific forms given in this study may be stated thusly: there is an enhancement of cosmic noise absorption undoubtedly due to a new influx of auroral particles which leads to a brightening of the auroral form, sudden motion of the arc with associated magnetic effects, and then reception of the pressure disturbance. Thus the pressure disturbance appears to be a final end-product of this sequence which is detected at the ground some propagation-time later.

From point of view of spatial location within the substorm from which the AIW seem to have emanated, a comparison of the contoured maps in Figures 4.3 and 4.8 with the pressure records in Figures 4.5 and 4.9 respectively, shows that when the most disturbed portion of the

substorm; i.e., the auroral electrojet was above or in the northern sector from the station, coherent infrasound was received at the station at College. During the 1000 UT substorm, the few cycles of coherent infrasound near College began near the expansive phase of the substorm, or close to the time when the electrojet was both overhead and starting a rapid westward and less rapid eastward motion of magnetic disturbance. A study of the disturbance vectors (not shown) indicated that the main jet was westward.

In the case of the 1337 UT substorm, review of the latter figures mentioned above shows that slightly coherent infrasound was occurring at College while the jet is developing southeast of College, but the main pulses began and continued when the jet was both overhead and northwest of College. In fact, the continuation of the pressure pulses at College was occurring while the most intense part of the jet was northwest of College, and the station was actually near the western end of the electrojet system. Whether this geometry is the preferred one which produces the most prolific supply of AIW at the ground cannot be ascertained from the data of this night alone, but continued detailed analysis using the contoured representation of the magnetic disturbance might be a useful approach to continue.

CHAPTER 5

DATA NIGHT 25 JUNE 1969

5.0 Introduction

From the point of view of auroral infrasonic disturbances, the night of 25 June 1969 was not uniquely active for the production of infrasound. On the contrary, the pressure record as seen at the College observatory showed only a few, rather low-amplitude coherences which could be determined to be of geomagnetic origin. The reason that this night was selected for analysis was due, in fact, to its relative simplicity insofar as the pressure record was concerned, and also due to the relatively low intensity of the polar magnetic substorms. It was mainly chosen after these considerations, in order to elicit a value for a mean transit speed from the point of origin of the AIW to the location of the College recording array.

Since the speed of sound varies along the entire travel path of the emitted AIW, the absence of real time ambient measurements of this quantity makes the travel speed an unknown. On the other hand, interpretation of the pressure record with the geomagnetic disturbance contours at a particular time and location require some knowledge of the transit time or speed from the place of generation to the listening array. With this value firmly affixed, then if an origin time can be inferred by any other means, when coupled with the arrival times and azimuths deduced from the pressure record, a likely location can be found from which the AIW was generated. Or on the other hand, if by any other consideration a likely location of origin of the AIW is found, then coupled with the pressure records an origin time may be specified

thereby aiding ultimately in the correlation with other related processes which may have occurred at that particular time which may uncloud the picture centered around the AIW generator.

5.1 Geomagnetic Activity

The geomagnetic disturbances studied in this section are based upon the magnetograms from the 16 stations shown in the location chart in Figure 5.1. Magnetograms from some eastern European stations were also scaled, but when their effect to the overall analysis was found to be minimal, they were discarded from the investigation.

A sample of the most disturbed component of some of the magnetograms used for this analysis are shown in Figure 5.2. The actual study period is delineated along the time axis of the figure by two arrows. As it would appear in this composite plot, the substorm-type magnetic bays appear to be somewhat localized and not very coincident with one another in time. A sharp onset at Barrow during the study period correlates with bays at College and Godhaven, but their onset and recoveries do not correlate well with the bays and general perturbations at the other stations. No attempt is made to specify a particular substorm here, but the overall developmental pattern of the geomagnetic disturbance is studied, and the parts of it which can be reasonably ascertained as being the location of the auroral electrojet is of interest.

The spatial and temporal development of the geomagnetic activity for the night of 25 June 1969 is followed here, as it shall be in subsequent chapters of this investigation, by contours showing those lines along the earth's surface taken to be equally magnetically disturbed at a particular instant. Such a sequence of maps are displayed in Figure 5.3 (a) thru (d). The contours represent the total magnetic

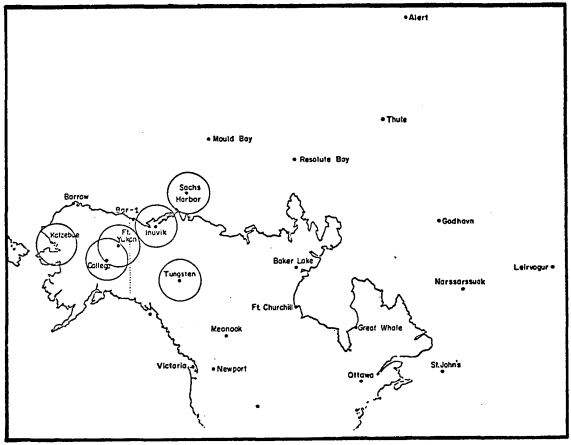

Fig. 5.1. Location of magnetometer stations whose data were used for the magnetic perturbation analysis for 25 June 1969.

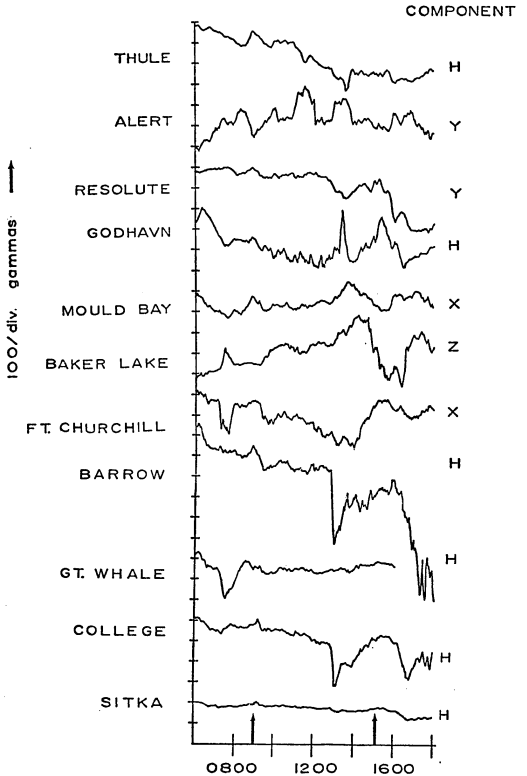

Fig. 5.2. A composite plot of the most intensely disturbed components of the magnetogram traces for 25 June 1969. Arrows along the time axis show the period of interest for this study.

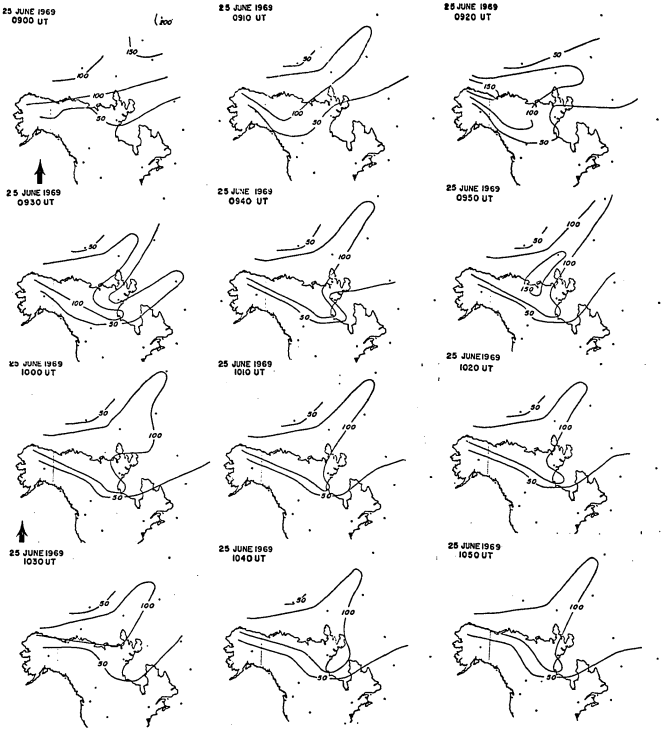

Fig. 5.3 a-d. Contour maps of the total magnetic perturbation vector for 25 June 1969. The contour interval is 50 gammas.

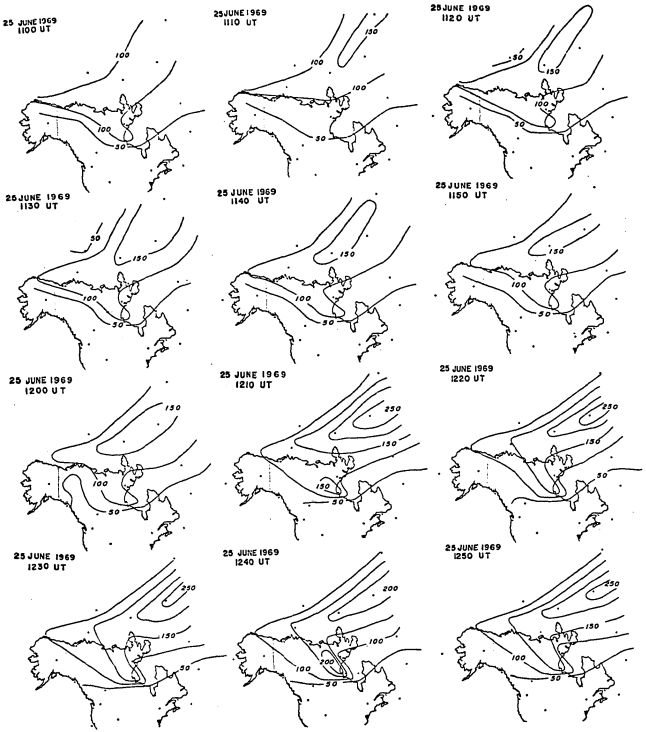

Fig. 5.3 b. Contour maps of the total magnetic perturbation vector for 25 June 1969. The contour interval is 50 gammas.

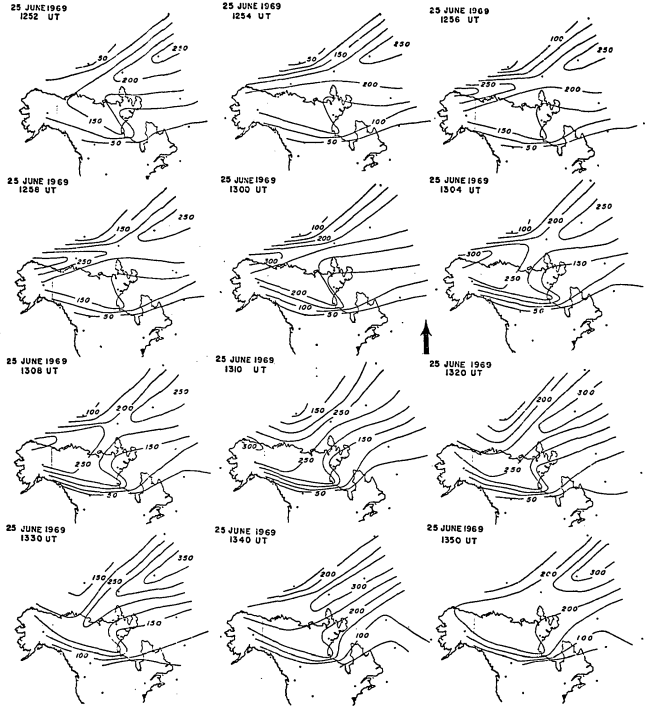

Fig. 5.3 c. Contour maps of the total magnetic perturbation vector for 25 June 1969. The contour interval is 50 gammas.

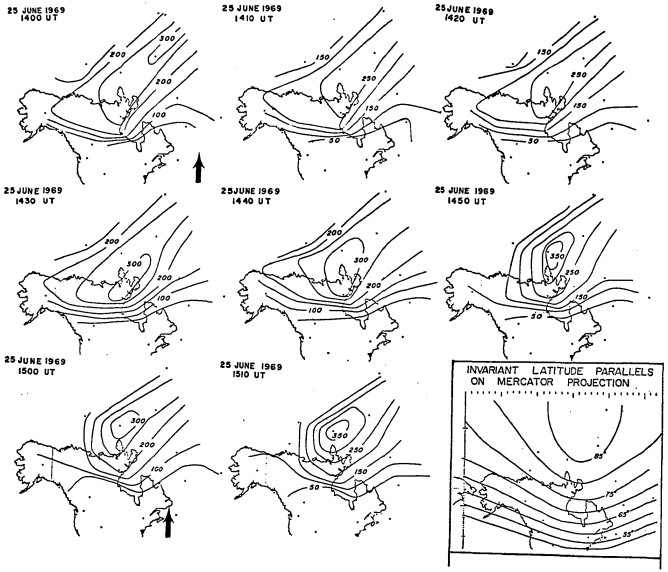

Fig. 5.3 d. Contour maps of the total magnetic perturbation vector for 25 June 1969.

perturbation vector $\Delta F = \sqrt{\delta h^2 + \delta d^2 + \delta z^2}$ for the period 0900-1510 UT. The input data for these 45 maps are based upon data which was hand-scaled and calculated from the magnetograms some of which were depicted in the earlier Figure 5.2. The contours on the maps were hand-smoothed from data which assumed a linear change in the value of the field between stations, and they are represented at an interval of 50 gammas throughout the entire study period. At 0900 and 1000 UT, the maps show an arrow along the lower border to represent the position of the line of local midnight, whereas the maps for 1300, 1400 and 1500 UT have such arrows depicting the location of local noon.

Returning now to the map sequence itself, the total span of time coverage is the period from 0900-1510 UT. At the beginning of this time period, College, Alaska was in the midnight sector and it is evident that magnetic perturbations were already in progress especially in the higher latitudes. The progress of the increase in intensity of the geomagentic activity is very slow until near 1110 UT when an increase in disturbance level initiates in high latitudes. The increase remains gradual, but nevertheless steady as a slow trend of increasing magnetic disturbance pushes its way westward from the high latitude afternoon sector. By 1254 UT a fairly well defined electrojet is flowing across the north Alaska border, and it intensifies fairly quickly thereafter. The disturbance has already expanded westward toward the midnight sector by this time, and expansion southward is also evident. By 1304 UT, greater intensity expands southward and the disturbance reaches peak level over Greenland near 1330 UT. From that

time to the end of the observation period at 1510 UT, the most intense parts of the disturbance appears to contract eastward toward the noon sector whereupon it begins to intensify again. This apparent contraction eastward need not imply motion of auroral forms of any kind eastward other than a progressive cessation of disturbance in the west which itself moved towards the east. The K_p index increased from 1+ to 2 across the study period, and ΣK_p for the day was 18-.

5.2 Infrasonic Activity

The pressure records for the night of 25 June 1969 were acquired during quiet wind conditions and only moderately disturbed geomagnetism as shown earlier. The time span of analysis of the records extended from 0945-1630 UT. During this time the background noise was averaged for the four channels in composite by 10-minute groups and was found to have reached the level of one microbar amplitude peak-peak for a single 10-minute span, and was less than this value for the remainder of the record. A histogram of this record is shown in Figure 5.4 where some of the blocks are shaded to show times in which coherence appeared in the record or in which nearly-coherent periods--vague coherences--were present. The unshaded areas represent incoherent times.

At this point, it is in place to define a tripartite description of the pressure records based upon a subjective visual inspection of coherence.

1. Incoherent--no correlation between the four channels of the infrasound records thus showing random phases received at the array at a particular time.

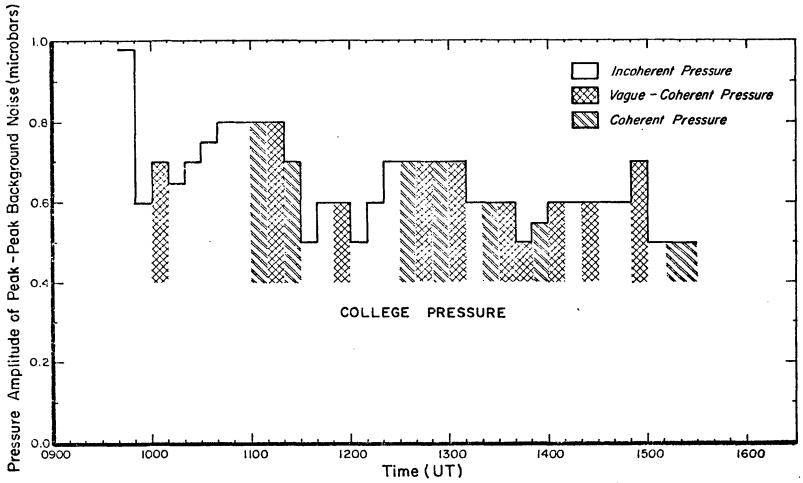

Fig. 5.4. Variation in amplitude of noise background with time for a section of the pressure of 25 June 1969.

2. Vague Coherence--an apparent attempt at some order in phase coherence between the channels, but insufficiently so for accurate scaling.
3. Coherent--correlation of phase of the AIW waves between three or all four channels thereby yielding a reliable solution for speed and azimuth.

For reasons of expedience and absence of such state-of-the-art hardware such as an autocorrelator (see Brown, R. F., 1963) only subjective visual inspection of the records was used to determine the three types of coherence reported here.

As an illustration to show the subjective categories of AIW just described (Figure 5.5) is presented containing strips of the pressure records during the analysis period. The designation "Incoherent", shown by the number 1 above the superimposed traces from the four channels as shown in the figure, is best seen in Part (a) of the illustration. Part (b) of the figure shown a period of "Vague Coherence" specified by the number 2 with arrows delineating its approximate time duration. Part (c) of this figure shows "Coherent" waves in the range covered by the number 3 and also periods of lesser or vague coherence as previously defined.

In light of the categories of coherence thus-defined, the College pressure records for the night of 25 June 1969 over the period of interest from 0950-1630 UT, was characterized by low amplitude background noise interspersed by erratic areas of vague-coherent to coherent infrasonic disturbances.

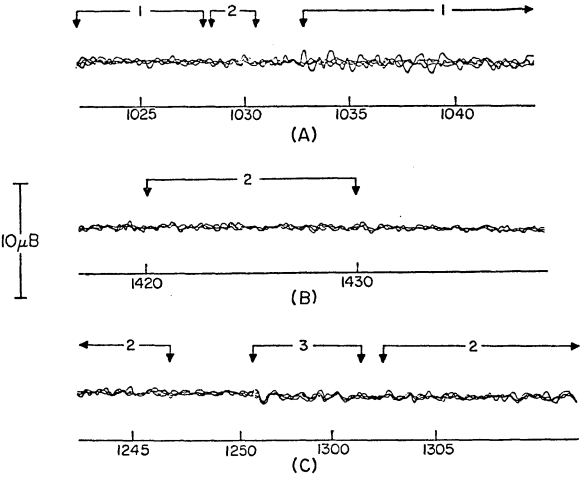

Fig. 5.5. Illustration of the types of coherence categories discussion in the study. (A) A brief period of vague coherence (2) sandwiched by periods of incoherence (1). (B) Vague coherence (2) spanning many minutes. (C) A small, low-amplitude coherent wave packet (3) preceded and followed by short stretches of vague coherence (2) to incoherence.

An effort is made in this study to include the morphology of those AIW signals which lie at the low end of the correlation spectrum which, because of either their low amplitude, high noise or poor correlation, have been excluded from earlier work at College. Many of the signals scaled on this night lie in that category, and with the subjective judgements which interpret their existence being always open to question, a photograph of each of the signals scaled for that night is entered in Figure 5.6. The numbers entered above the superposed traces of the four channels label the location of coherent waves where scaling were attempted. A given wave in this figure may appear less so merely because a realignment of the charts may be necessary to shown a particular phase coherence not well-illustrated for the particular instant shown.

The scalings for the waves shown in this figure are illustrated in Table I. When the scaling for a particular wave resulted in a range of greater than 10° among the four solutions available from our array, then the scaling was discarded and the wave was excluded from further consideration in the study except that its name lable was retained in the figure and table displaying them. Many of the waves whose scalings appear in this tabulation are collected in groups to show that the same chart alignments and thus the same speed and azimuth solutions applied to each member of the group. This revealed a rather interesting property of the scalings of the AIW signals from this small substorm: the coherent waves appeared to occur in small unidirectional packets. This leads to the conclusion that the packets shown by the successive wave groupings as displayed by Figure 5.6 are probably associated with a

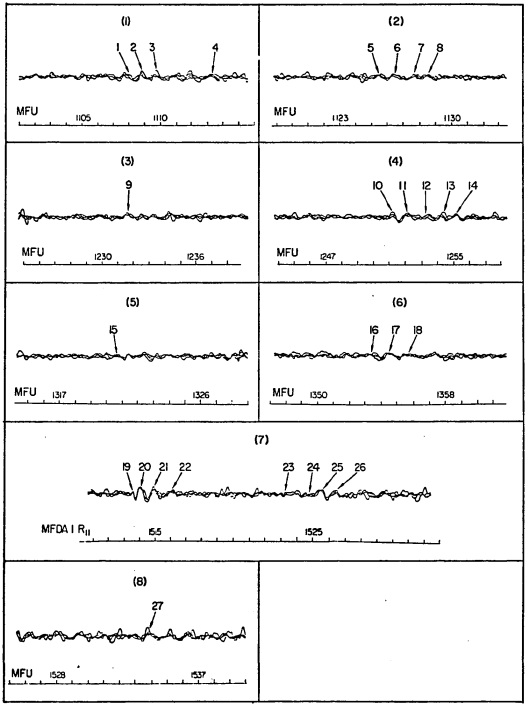

Fig. 5.6. Samples of the superimposed pressure records from College for 25 June 1969 showing the wave packets scaled for study. Numbers show location of attempting scalings.

single event the dynamics of which result in the production of AIW.

5.3 Correlation of AIW to the Geomagnetic Disturbance

The association of AIW with the geomagnetic disturbance is well established in literature (Wilson and Nichparenko, 1967; Campbell and Young, 1963, etc). An interesting question which has been pondered at the College observatory is the possibility that the geomagnetic disturbance not only contributes coherent wave energy into the pressure records, but also incoherent background noise which might be enhanced at the onset of the polar magnetic substorm. To investigate this possibility, the histogram shown in Figure 5.7 was constructed. The upper curve depicts the mean variation in pressure amplitude of the peak-peak background noise of infrasound at the College observatory. Shading on this histrogram shows the times when coherent and vague-coherent energy occurred. The middle distribution shows the mean range of the total magnetic disturbance vector measured in gammas at all of the magnetometer stations in Alaska, Canada, northern U.S. and Greenland whose data were available for use in this study. The lower trace shows magnitude of the mean intensity for this vector at College. The scale for the two lower histograms is on the right of the figure.

The histogram representing the plot of the College AIW data is identical to the one shown in Figure 5.4. It was constructed by visually inspecting the superimposed traces representing the four College microbarograph stations, and dividing the record into successive 10-minute groups covering the period of interest. Noise at a single station was taken to be on non-thermospheric origin and

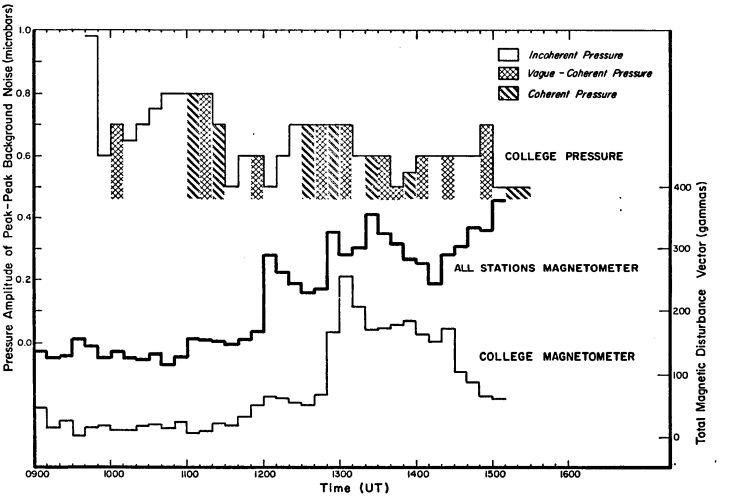

Fig. 5.7. Correlation of background infrasonic noise with geomagnetic disturbances at College and the general environs of the North American continent.

TABLE I Scalings of AIW for the night of 25 June 1969

Time	Wave Label	Azimuth (degrees) Ave.	Δφ	Trace Velocity (m/sec)	Period (sec)
1107:40-1115	1,2,3,4	07°	7	453	44
1124:40-1129:30	5,6,7,8	77°	3	951	64
1231- 1233	9	326°	7	414	58
1250-50:40	10	12°	2	565	38
1250:40-51:40	11	11°	2	414	56
1251:40-55	12,13,14	11°	5	553	50
1320-23	15	353°	8	353	34
1353-57	16,17,18	119°	5	359	71
1513:30-14	14	13°	3	386	20
1514-14:30	20	10°	2	430	44
1514:30-15:30	21	22°	5	351	50
1515:20-16:20	22	17°	5	479	60
1524-26:30	23,24,25,25	10°	2	406	56
1523-36	27	34°	4	835	50

eliminated from consideration as was likewise the amplitude peak-peak during times when a signal was present. During signal passage the background noise was taken to be at the mean level of the noise immediately before and after the passage of the signal.

The magnetic disturbance histogram for College in this figure was constructed by digitizing the College magnetogram at 10-minute intervals for the three components, computing ΔF, and assuming that the changes occuring between the intervals happened with step-function-like changes.

The "all stations" histogram of the figure was plotted by taking the value of the maximum-minimum in the numerical distribution of ΔF vectors among all the stations of Alaska, Canada, Greenland and northern USA and plotting them in similar 10-minute groupings as for the College histogram.

If there is an association between the level of background noise of infrasound with the level of geomagnetic activity, one might expect that an increase in the latter would give rise to an enhancement of the former. Allowing up to 3 1/2 hours acoustic propagation time from the parts of the ionosphere even as far away as southern Greenland, the histograms do not bear out such a correlation. In fact, there is a general diminution in level of background noise of infrasound across the entire analysis span while there was an overall increase in the level of geomagnetic activity.

On the other hand, when comparing the number of periods when coherent or vague-coherent activity occurs, there does seem to be an association between the rise in the overall ambient geomagnetic activity and the

occurrence of infrasonic pressure disturbances of this type. An interesting way to display this lack of correlation is shown in Figure 5.8 where the "all stations" histogram is time-shifted by 1.2 hour with respect to the College pressure histogram. Then in the preponderance of instances, rises in geomagnetic activity associate themselves with the onset of coherent waves in the pressure record. Vague-coherences and incoherent seem to occur at times of waning geomagnetic activity.

The geomagnetic activity as shown by the College histogram does not bear any such relationship to the AIW record since it must be accepted in the real time frame in which it sits (see again Figure 5.7) or time-shifted by at most about 10 minutes. This appears to point toward the conclusion that for the most part, the magnetic disturbance as seen as College had little or no relationship to the AIW received at that observatory on the night of 25 June 1969.

(a) The Problem of Relating Auroral Infrasound to Contours of Geomagnetic Disturbance

Probably the first and most obvious question which arises in the mind of an observer on initially pondering the presence of an AIW disturbance on the pressure records is the one querying where the signal came from to begin with. This question is studied in this report and the effort is directed toward answering the more pointed question as to where within the Polar magnetic substorm the infrasound emissions originate.

The problem is not a simple one and if one is confronted with a complex AIW record having hours of continuous coherence and a polar

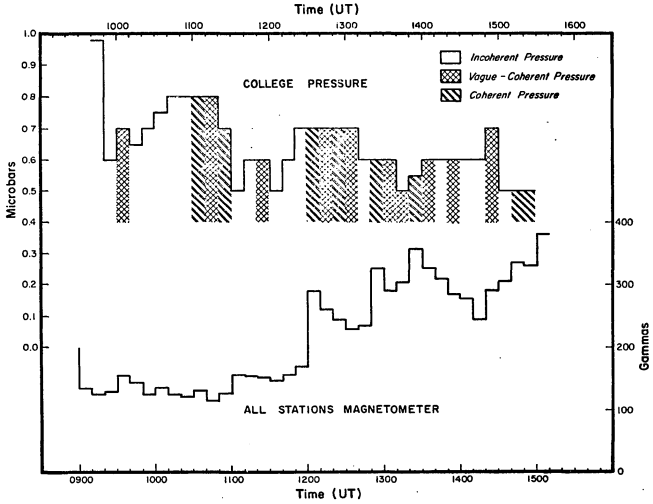

Fig. 5.8. Relationship of geomagnetic disturbances over North American continent to incoherent background noise of infrasound at College, Alaska.

magnetic substorm spread around the auroral oval and across 30° of geomagnetic latitude say, it is even more complicated. Though the problem is still challenging in the case of relatively simple AIW records as this night of 25 June 1969, the simpler geomagnetic disturbance of such a night having limited temporal and areal extent allows for the elimination of many areas of uncertainty.

As an example of the types of uncertainty with which one is faced, consider the representation in Figure 5.9. The ray drawn northeasterly from College, Alaska represents the great-circle path of wave #12 scaled on this night (effect of horizontal wind fields neglected). The numbers to the left and above the ray show assumed propagation times based upon a mean transit speed of 270 m/sec., and the numbers on the right show possible origin times of the signal at 10-minute intervals. This mean transit speed was selected from data based upon infrasonic waves from nuclear explosions in transit from Novaya Zemlya, their point of origin, to Resolute Bay where the detectors were located (Donn and Ewing, 1962). The 10-minute time interval along the ray path in Figure 5.9 is based upon the times when there was an actual contour mapping of the progress of the geomagnetic activity at that particular time.

What this diagram attempts to show is that for each contour mapping made of the magnetic substorm, if that time is taken to be the origin time of the signal, there exists a unique point along the ray from which the signal could have come--the arrival time and an assumed transit speed being considered known. In fact, if one does not actually know the origin time, each point designated along this ray will

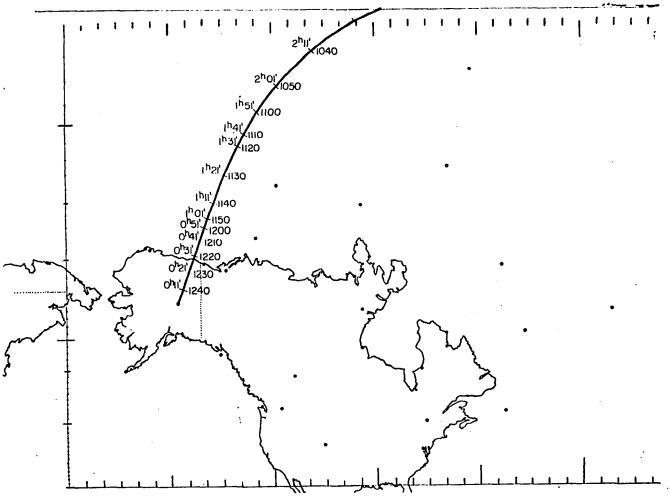

Fig. 5.9. A plot of wave #12 ray path showing possible origin times (right-hand or lower numbers) and possible propagation times (left-hand or upper numbers) based upon 10-minute intervals prior to its arrival time.

be a possible solution as one assumes the origin time at earlier intervals and correspondingly slides the epicenter further along the ray at the assumed transit speed. So reasonably then, since there is nothing significant about an arbitrary selection of a 10-minute interval to sample the progress of the substorm, the signal origin could come at any time and thus there are an infinite number of solutions for location from which the signal could have emanated.

In an effort to eliminate the number of possible solutions, a few features of AIW morphology were taken to be known and mean transit speed was assumed. Then an effort was made here to correlate the received signal to the most intense areas of geomagnetic disturbance in the hope of finding some consistent or systematic relationship between the propagation distance and visual signal characteristics on the one hand, or a better value of mean transit speed if a reasonable location of signal generation can be found. The major feature of AIW morphology that is taken to be known in this determination is the idea that AIW generation is associated with geomagnetic disturbances, and that magnetic disturbances of level 50 gammas or less produce no detectable infrasound.

The method of eliminating some of the possible solutions for origin time and location of AIW tumbled logically out of the formulation of the Polar magnetic substorm by contours. The total disturbance vector $\Delta F^2 = (\Delta X^2 + \Delta Y^2 + \Delta 2^2)$ was contoured thereby providing an areal location for the geomagnetic disturbance: areas within the contoured system were considered likely source regions of AIW and those outside

the system, i.e., less than 50 gammas, were considered unlikely. This one consideration eliminated many possible solutions of the signal origin along a given ray.

Further considerations leading to the selection of a likely origin time and place from the myriad of available solutions along a given ray were: the absence of the minimal level of geomagnetic disturbance along portions of the azimuth; or the presence of the disturbance along the azimuth at a time which would give a ridiculous value for the deduced speed of sound based upon the origin time in question. As it happened in this study, these considerations typically lead to a fairly localized region of space and a small range of times from which to select the best available value. Throughout this procedure, due to the unavailability of real-time wind data along the entire propagation path, the effect of wind was ignored.

5.5 Correlation of AIW with Geomagnetic Disturbance Contours

In the effort to localize likely areas within the substorm from which AIW originate and at the same time deduce a mean transit speed for the propagation of the AIW, there follows a sequence of figures showing mapped representation of the substorm. These maps showing the stage of development of the polar magnetic substorm to the particular instant were taken to encompass the likely range of times during which a particular AIW was generated. Since it seemed reasonable that the maximally-disturbed region is a very likely source location for AIW generation, the attempts at correlating a location within the substorm is centered around this region. The reasonableness of this assumption will be borne out by

the data and conclusions of Chapter 4.

Waves #1-4

This small noisy wave packet appears as a signal which is poorly correlated between the four channels of the infrasonic array. It was received between 1107-1114 UT and a picture of it may be seen by referring to Figure 3.6 and to Table I for the particulars of the scaling. The mappings of the substorm over the correlation period for this wave packet are shown in Figure 5.10. The arrow on the maps point to the likely origin point of the AIW. A general overview of the substorm shows that there were no rapid or drastic alterations of the basic structure of the disturbance system during this time span. There appears to be an overall southerly motion of the auroral electrojet (AEJ) center with no attendant sudden increase of decrease in goemagnetic disturbance. Prior to 1000 UT the magnetic disturbance was similar to that immediately afterward, but when the arrival time of the AIW is considered, there results a computed mean transit speed less than 159 m/sec for the areal correlation to hold. Such a low transit speed is considered unlikely and earlier times than 1000 UT are thus eliminated from the correlation. Following 1050 UT the geometry of the substorm is again similar, but the deduced mean transit speed would have to be greater than 417 m/sec., which is quite high. The most likely generation time giving a reasonable transit speed is near 1030 UT. The method of arriving at this and other times will be discussed in a succeeding section "Mean Hoizontal Transit Speed".

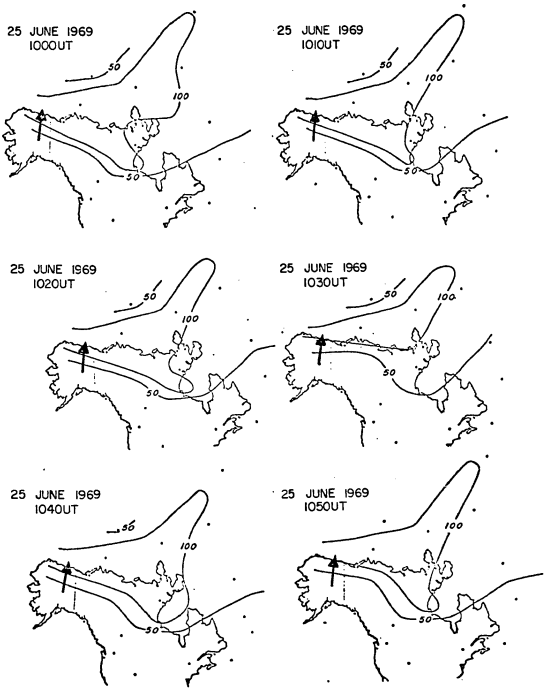

Fig. 5.10. Development of the magnetic disturbance during the inferred generation time of the AIW packet # 1-4. The arrow points to a likely source region of the wave packet from the particular time of the amp.

Waves #5-8

Here again we have a poorly coherent wave packet of low amplitude AIW which merges slowly from the background noise of nearly the same level. Reference again to Figure 5.6 and Table I gives the picture and scalings for the waves. The maps showing the progress of the geomagnetic disturbance correlating with the genesis period of the signal are displayed in Figure 5.11. The magnetic disturbance first reaches the level of 100 gammas near 0930 UT along the scaled azimuth of 77° for this wave train. Earlier the system lay north of this bearing, but a slow southward increase in geomagnetic disturbance extended it well within the azimuthal range of the signal. Near 0950 UT, the nearest map time for correlation of mean transit speed (MTS), there is a slight increase to 150 gammas within the system and then it returns to the former level between 100 and 150 gammas. A southerly branch of the AEJ appears to be fairly stationary during this time period as is also the northerly branch.

Wave #9

Correlation with the contoured substorm by this ill-defined wave packet in addition to its poor coherence is limited by the station-spacing of the geomagnetic data since its origin is along an azimuth which quickly extends into a region of no data. This situation is depicted in Figure 5.12. A slight extension of the open contours seems reasonable, however, since the gradient along a geomagnetic parallel is small compared to that along a meridian.

The meaningful interval of correlation with the substorm for an

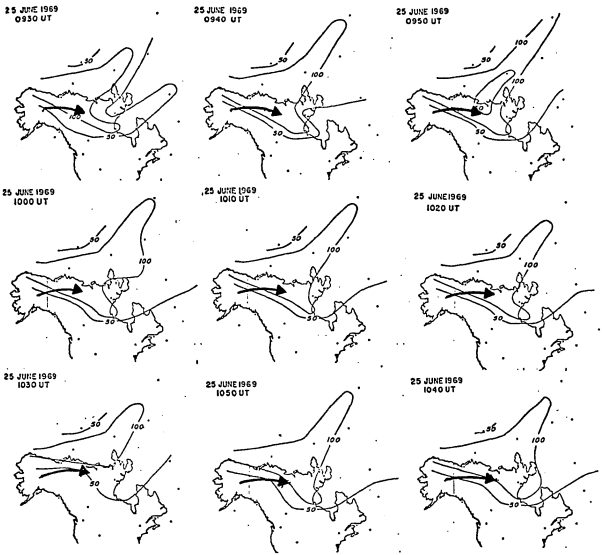

Fig. 5.11. Development of the magnetic disturbance during the inferred generation time of the AIW packet # 5-8. The arrow on each map, oriented along the direction from which the waves were received, point to a possible source region for the signal.

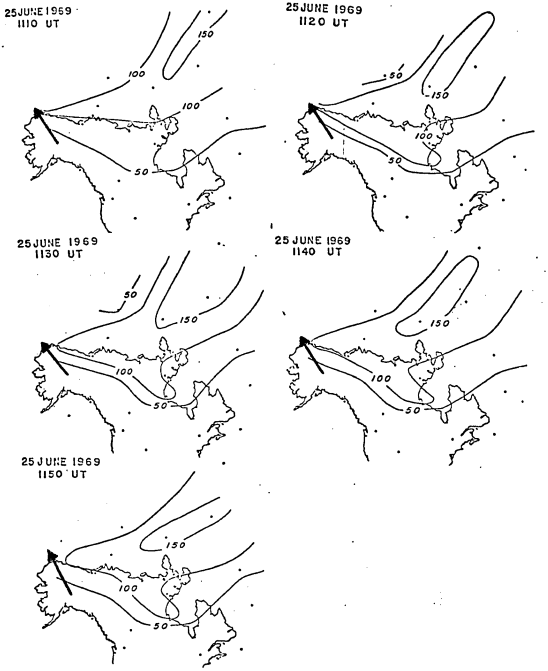

Fig. 5.12. Development of the magnetic disturbance during the inferred generation time of AIW wave #9. Arrows point to possible origin points for the signal.

origin time, as the maps show, is the span 1110-1150 UT. Prior to this time the AEJ is too close to College and afterwards too far away to give a good value of MTS. Following 1150 UT the disturbance system withdraws well east of Alaska and does not expand westward again to include this azimuth until well after the 1232 UT arrival time of the AIW. The best correlation for origin time based on MTS appears to be near 1130 UT.

Waves #10-14

This wave packet as the others studied in this section is also depicted in Figure 5.6 and Table 1. The similarity in separate scalings of azimuth and horizontal trace velocity for the various components of the wave train and their close arrival time seems to point toward a single event by the AIW generator. As the maps show in Figure 5.13, the best origin time correlation is in the range 1210-1230 UT. Prior to these times the disturbance is not located along the azimuth scaled for the waves; after these times the arrival-time/propagation-distance colution suggest a supersonic MTS greater than 500 m/sec.. During this time span the substorm appears to be slowly expanding along the oval. Despite the broadening of the area included in this disturbance, there was no overall increase in intensity of the magnetic substorm during this time. The time which gives the most likely emission time shown by these maps is near 1210 UT, which corresponds to an MTS near 295 m/sec. and propagation distance co near 740 km.

Wave #15

Reference is made again to Figure 5.6 and Table 1 which depicts this wave as almost a single cycle of coherence near 1321 UT vaguely

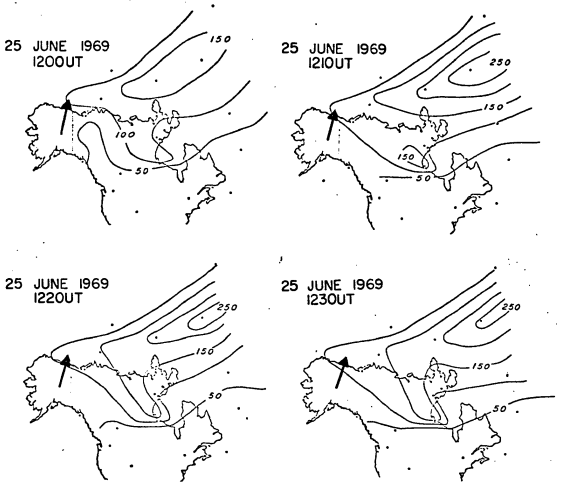

Fig. 5.13. Development of the magnetic disturbance during the inferred generation time of AlW wave #10-14. Arrows point to possible origin points for the signal.

coherent before and after. Such an event could be strongly argued as a chance correlation among the four microphone stations and no effort will be made to defend against such a stand. The attempt is made here only to account for its presence and to merely assert the possibility of there being and equal chance that it is an AIW degraded by propagation in the atmosphere. It scales poorly showing an error range in azimuth ($\Delta\phi$) of 8° among the various stations. It correlates with the onset time of the substorm between 1300-1310 UT, and appears to be of nearby Alaskan origin.

The maps in Figure 5.14 depict the likely origin times. During this period the expansive phase of the substorm is in progress and the system has expanded rapidly along the auroral oval and there has occurred southerly motion of the AEJ. It is interesting to note that only negligible infrasound is now being received at College despite the rapid onset locally of one of the largest inputs of geomagnetic energy that night which reached the disturbance level of 300 gammas at the center of the system. Propagation times from the most disturbed central region within and just north of northern Alaska should vary between 20-40 minutes, but there are significant AIW occurring in the record between 1320-1340 UT other than the one discussed here.

Waves #16-18

This wave group, pictured in Figure 5.6 and whose scalings are shown in Table I, arrives from a direction which is statistically insignificant insofar as the morphology of AIW is concerned. Scaling of signals from this direction are uncommon and in this case, the wave group does not

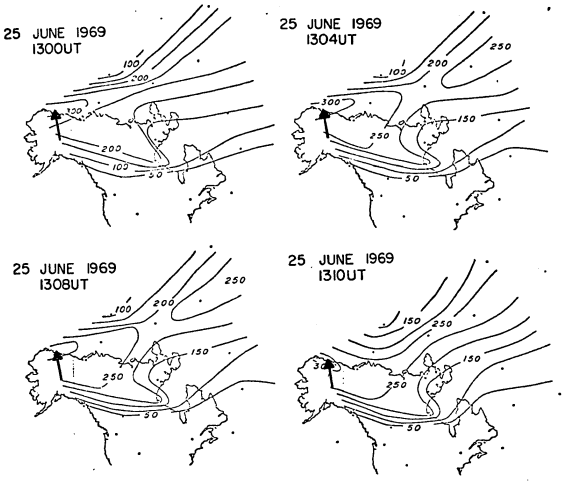

Fig. 5.14. Development of the magnetic disturbance during the inferred generation time of AIW wave #15. Arrows point to a possible origin location for the signal.

correlate very well with any of the maps presented earlier. Possible times of correlation with the maximally disturbed portion of the substorm along its azimuth of 119° would place the ray in such a broad area of disturbance that little accuracy could be expected from its almost arbitrary possible origin point. The possible range of times referred to here occurs between 1300-1310 UT (see map sequence Figure 5.14) when the disturbance greater than 250 gammas broadened and extended itself well southeast of College. Since the location of any line-current type source in this area would be unreasonable, no attempt is made to correlate this wave group with an electrojet.

Waves #19-22

Compared to the other wave packets received on the night of 25 June 1969, this group whose arrival time spanned from about 1513:40 to 1517 UT was the most coherent and largest amplitude signal. Maximum peak-peak pressure was 1.8 microbars which placed it above the background noise by a factor of slightly more than three. The display of this packet in Figure 5.6 shows it to be a dispersed wave train followed by a few cycles of noisier, larger period waves which appear about 11 minutes later. This classifies it as a repeated pulse event ($MFDA_{I}R_{II}$, see Appendix I) of the type discussed in Chapter 2, Section 2.3 (b).

Possible emission times of this wave packet are shown by the maps spanning 1150-1250 UT as shown in Figure 5.15. An interesting feature of this wave packet is the azimuthal spread of the various components as depicted by the rays representing the azimuths along which the waves

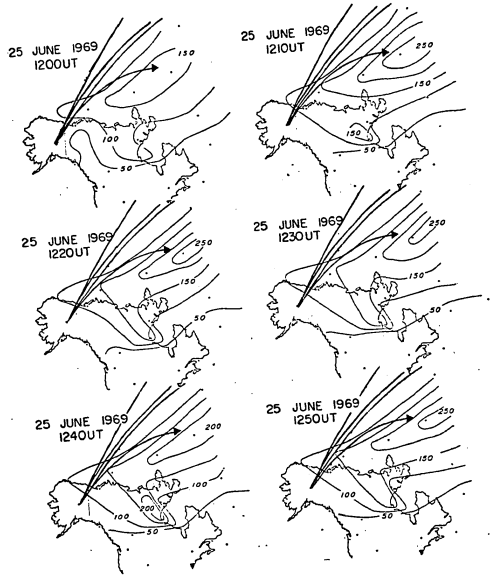

Fig 5.15. Development of the magnetic disturbance during the inferred generation time of the AIW packet # 19-22. The arrows point to to likely source regions for the signal. Other rays show true azimuths of arrival of wave packet.

propagated. The rays appear to spread in a somewhat erratic fashion north of the most disturbed region of the system over western Greenland. If the AIW are to correlate with this AEJ region, then since these maps represent the most likely time-span over which emission occurred, there must be other factors operating which could have deflected the waves. Such a factor is the winds between the ground and the E-region as well as the neutral winds above that level. Pocket observation of wind at Thule, Greenland (WDC-A, June 1969) showed it to be blowing toward northwest from 65 km. down to earths surface during the propagation time of the signal. This would likely shift the azimuth of the signal northwardly thereby causing a ray drawn from the receiving station to not intersect with the original source location of the AIW.

Reasonable values of MTS can be attained if one associates the origin of the signal to have occurred near the time of 1210-1220 UT. This association fits the largest, most coherent wave packet of the night with the first onset of the 250 gamma disturbance which happened over northwestern Greenland. Considerable deflection of the waves due to wind had to be considered in order to make this association.

Wave #27

This wave packet of about 3 cycles is a barely detectable group whose picture and scaling may be viewed in Figure 5.6 and Table 1. It is correlatable with the electrojet over an interval from 1210-1300 UT. It represents the final wave packet scaled for the night of 25 June 1969, and a map sequence showing its proposed place of origin is presented in Figure 5.16. As in the case of the previous packet, waves 19-22, the

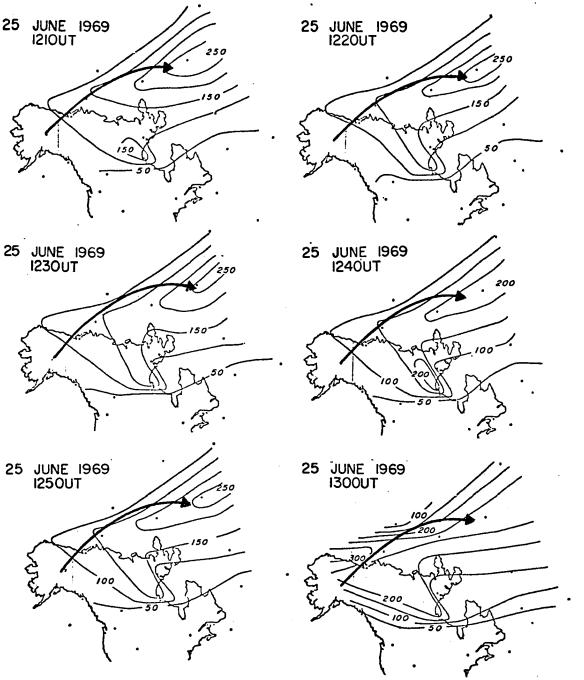

Fig. 5.16. Development of the magnetic disturbance during the inferred generation time of AIW packet #27. The arrows point to a likely source region of the wave packet for the particular time of the map.

level of geomagnetic disturbance which corresponds with the generation time is 250 gammas.

5.6 Mean Transit Speed

In the search for the area of the Polar magnetic substorm in which AIW are generated, the need for a mean propagation speed for AIW arises. Since temperature varies strongly in the vertical direction and probably slower in the horizontal directions, sound speed must also vary accordingly. This means that in propagating from source to receiver, a given AIW packet must travel in different speed zones governed both by the structure of the atmosphere and the frequency structure of the dispersed wave packet. Ignorance of the sound speed structure of the atmosphere from the ground to the ionosphere as well as the absence of real-time knowledge of this quantity along the entire propagation path leaves the researcher with only the most generalized approach that can be improvised in order to make an educated guess. One attempt at such a guess is to use a fictitious speed - a mean transit speed, as it were. This speed may be defined simply as the propagation distance divided by the total propagation time between source and receiver.

Now as it happens in the study of AIW and in correlating them with contoured substorm maps, the source location is an unknown. For this reason an assumed location was specified and an effort was made to correlate the knowledge deductible for this "known source" to see if systematic results are obtained. If consistent results follow, then perhaps this may lend credence to both the MTS thus-derived, as well as the reality of the trial source.

More specifically then, for this contoured study of the polar magnetic substorm, it was assumed that the regions of space that were most geomagnetically disturbed are the likely areas generating AIW. This region is always the central portion of the cells of contours which, if they were topographic contours, would represent hills. Most likely, this region is the locus of the AEJ to apply a name to it, but were this not the case, if the region correlates with AIW generation any other name could serve as well.

In attempting to find a MTS for AIW, it is assumed that across the course of a substorm, this value remains relatively fixed over a small range of values varying not more than ±15 m/sec. say. The reasonableness of this assumption is based on the data by Donn and Ewing (1967) which shows that nuclear bomb waves received by various stations in various seasons of the year for the period range 0.4-1.0 min varied from 272-297 m/sec or less that ±15 m/sec. about a median value.

Furthermore, waves from separate explosions 9 days apart from the same source to receivers at Shionomisaki were received with a difference in MTS of 0.1 m/sec. for a case of waves of 1 min. period. In another case, nuclear bomb waves in the range 0.8 min. were received at the station in Kyoto from epicenters 1 min. of latitude apart 3955 km away. The variation in MTS for the two explosion 7 days apart was 3.2 m/sec.. In a third case, waves received at Resolute Bay 12 October 1958, from one location 3375 km distant and on 24 October, 1958 for an epicenter 3416 km away differed in MTS by 7.0 m/sec. for 1.1 min period waves. The period range of interest for AIW studied at College and in

this report is from 0.1 min to slightly less than 1.2 min.

With the assumption that the MTS remains relatively invariant over a small range of values over the course of a polar magnetic substorm, it follows that within this small time span, signals received from various points within the substorm will have MTS's that are quite similar. If this is true, then one need only take a large number of waves for a given night, associate them with having originated in a particular location, figure their origin time by whatever method, and compute transit speeds which should range over a small group of values. Or if one had a good value of MTS, then the problem of locating the time of origin may be inferred if the source is known, or possibly the location of the source may be inferred if one knows the origin time and the MTS.

(a) Derivation Method of MTS

In attempting to arrive at a value of MTS for the night of 25 June 1969, it was assumed that the location of the AIW source was known; i.e., at the intersection of the azimuthal ray and the center of the disturbance system--the AEJ. The origin time and MTS were obtained together utilizing the assumption of invariance of MTS as explained earlier.

Procedurally, a given azimuthal ray was selected as scaled from the pressure records and its plotted intersection with the AEJ or the contoured substorm maps was recorded for a series of maps at the 10-minute mapping interval. The number of maps chosen for the correlation period was selected from those which, when calculated using an initially-

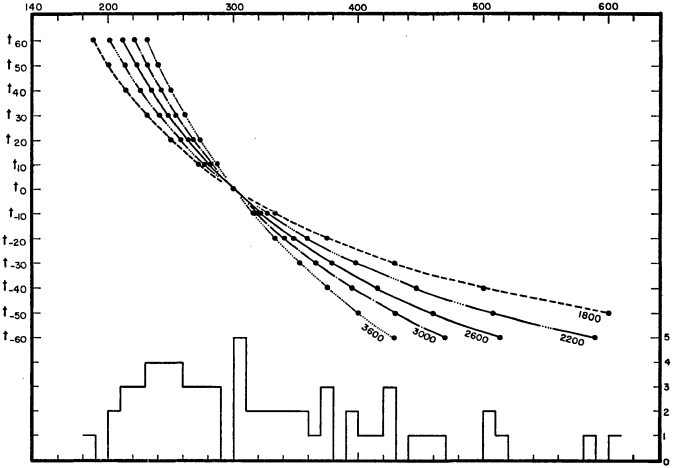

Fig. 5.17. Variation in mean transit speed with time for fixed distances and assumed theoretical value of 300 m/sec. at origin time.

The result of knowing the actual distance of the sound generator, and computing a MTS from times +60 and -60 minutes about the time T_0 is to obtain a new value of MTS each time. Now since we know that the proper value of MTS for this hypothetical situation is 300 m/sec., the effect of varying the time by 10-minute increments from T_0 at the fixed distance represented by each separate curve is to cause the newly derived value of MTS to differ even increasingly above and below the proper value of 300 m/sec. assumed for this example. The result carrying out this procedure for a number of distances gives the family of curves depicted in Figure 5.17. The proper value of MTS is located at the point which is common to all of the curves, whereas the other spurious points cause the curves to diverge from each other away from the proper point. The proper point is located at the area of maximum density of the family of curves, or the maximum number of data points probably. A histogram constructed below the graph shows that the one bar containing the 5 points which the curves depict at 300 m/sec. stands above - though only slightly - the rest of the group.

It is very simple to show that the same distribution would result if, for another MTS assumed known, the travel time is held stationary and the source allowed to move uniformly, or the case that both the time varies uniformly and the source moves uniformly. That is to say that the assumed proper value of MTS will still appear at the location where the curve density per unit area is a maximum, or simply where the 'squeezing' effect of the curves is greatest. Moreover, if the MTS is allowed itself to vary over a small range of 15 m/sec. say, and

similar effects as fixed source and time variable by 10-minute increments is assumed, the similar effect is observed, where the proper MTS range appears where the family of curves squeeze together, though somewhat less dramatic than the example shown here, and the proper range can be picked from a histogram, which will show a slightly higher distribution at the proper range. Each of the cases mentioned above was actually computed, but are not presented here because of the redundance.

With the foregoing hypothetical examples establishing the likelihood of the procedure being useful for obtaining a reasonable, though possibly not exact result, the graph and histogram in Figure 5.18 for the waves of 25 June 1969 is shown.

The points along each curve represents separate computations of MTS derived over the correlation period for each map shown in Figures 5.10 thru 5.16 for the individual waves assuming it to be an origin of time of AIW. The vertical axis of the plot of Figure 5.18 is the correlation time of a given map of the 10-minute intervals referenced to the earliest time in the correlation period as zero. For example, Wave #32 was correlatable over the period of 1210-1350 UT. The time 1210 UT was chosen as the zero reference for this particular case and each succeeding 10-minute map represents a point along the curve up to 1 hour 40 min. later corresponding to 1350 UT--the end of the correlation period based on 272 m/sec.. Each curve was constructed in like manner. The curves begin and end at a particular point for either or both of two reasons:

1. There were no longer intersection with the AEJ at that azimuth, or

2. The deduced MTS became unreasonably subsonic or supersonic.

As the plotted curves show, there is a concentration of points in the vicinity of 240 m/sec. and as MTS increases, the points become fewer and diverge. This observation is better shown as a histogram in the upper part of Figure 5.16. Here the distribution of MTS's have been broken into equal intervals of 20 m/sec. length as shown.

After having located the MTS for the AIW of 25 June 1969 to occur in the range 240-260 m/sec. as shown by the histogram, the actual data points were extracted from this part of the distribution, and a numerical average of 243 m/sec. was obtained. In all problems involving the need for a MTS in this investigation, the value derived here was used.

An interesting comparison can be made between the MTS just derived and values of a transit velocity derived from ray-tracing. If one considers for purposes of analysis the distance between two successive bounces off the ground of an AIW signal while it is refracted back to the ground between hops, a different value of transit speed may be computed for each ray angle considered. If one then calculated the trace velocity at the apogee of each ray; $V_{\dagger}$ = C Sec. as used earlier in this report, then a curve may be plotted for the trace velocity vs transit velocity for each ray. A resulting curve for numerous such rays for a series of source heights of the infrasound is given in Figure. 5.19. The ray-tracing used here was based upon a non-arctic atmosphere compiled by T. Georges (private communication). The curve shows a pronounced

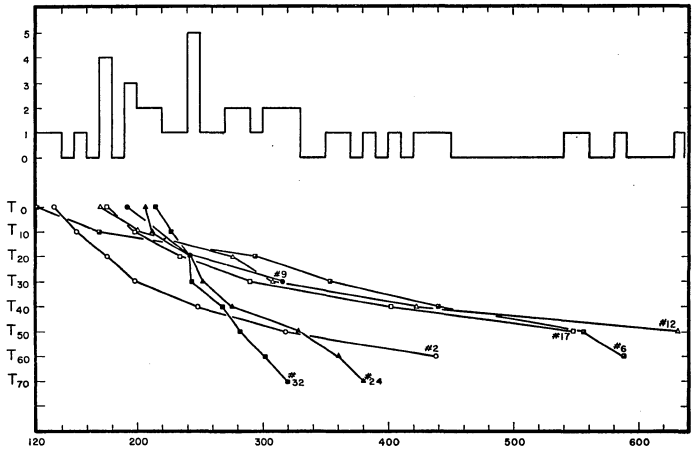

Fig. 5.18. Calculation of mean horizontal transit speed for the AIW of 25 June 1969.

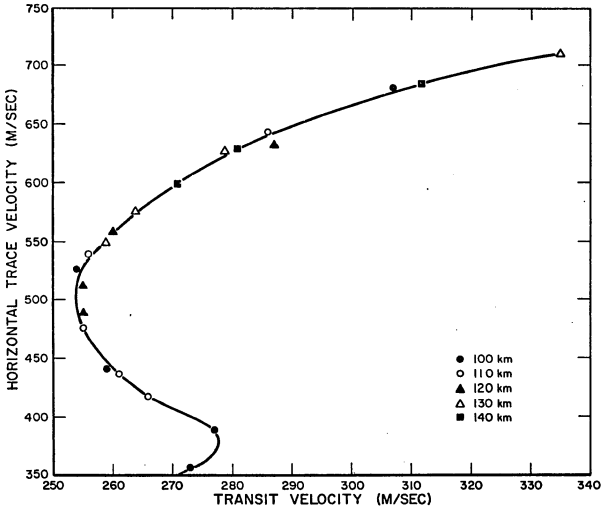

Fig. 5.19. Variation of trace velocity of AIW with transit speed between two surface bounces separated by a refraction path in the upper atmosphere.

minumum near the trace velocity of 500 m/sec. and a transit velocity of 255 m/sec.. Reference again to the distribution of the occurrence frequency of AIW in trace velocity groupings as shown in Figure 2.4 of Chapter 2 reveals that AIW in the 500 m/sec. range are the most frequently occurring group. This trace velocity group corresponds fairly closely to an angle of inclination to the horizontal of about 50°. The correspondence of transit speed of this most frequently occurring group of signals is quite close in transit velocity shown by the ray-tracing to the one derived independently here.

As it is used in this report, the MTS is mainly applicable to sources which are in excess of 100 km distance from the receiver, because for closer distances, ray tracing shows that much lower MTS's are applicable.

5.7 Discussion

The major purpose for studying the AIW data for the night of 25 June 1969 was to elicit an approximate value of mean horizontal transit speed which would be useful for interpreting the arrivals of AIW correlated with contour maps of geomagnetic disturbance. Since large substorms develop quite complexly in space and time, and a complex AIW record would also confuse correlation, it was decided to select a night in which only a single AIW event was recorded in the records. Yet as a closer inspection of the AIW records showed, and as displayed and discussed in this chapter, numerous low amplitude waves were present having the same general amplitude of the background noise. This led to the correlation of more waves than initially anticipated, and from the

effort to interpret these emissions in terms of observable features on the magnetic disturbance maps, the procedure of deriving the MTS evolved.

The correlation of the AIW with a region of space had to be based upon some assumptions concerning a likely origin, and for this purpose, the inferred position of the auroral electrojet was invoked. The reasonableness of this assumption was based upon the earlier associations of AIW with the auroral oval (Wilson, 1972) as discussed in Chapter 2 of this study, and the association of the auroral electrojet with the auroral oval (Akasofu et al. 1965). Using the intersection of the ray drawn along the arrival angle of the AIW with the inferred electrojet positions, it was seen that only a limited number of such intersections occurred during the magnetic disturbance, and these could be used for the determination.

In the course of the study an attempt was made to notice changes in the level of background noise with the rises in geomagnetic activity, but no significant result was noted for the 10-100 sec. passband used here.

The major errors made in the correlation of the AIW with the magnetic disturbance was doubtless those associated with the actual location of the position of the electrojet. This correlation was nevertheless attempted even though most of the AIW came from areas poorly distributed with magnetic observatories. As was done in other parts of this report, map distances were measured from the Lambert Conformal Conic projection of scale 1:1,000,000. Distance measure-

ments in the vicinity of Alaska were probably not off by more than 5 km due to map error. Extending this baseline to the western coast of Greenland should not have produced more than three times that amount, say, due to map inaccuracies. For a given measurement of transit speed used in this study, an error in measured distance to the inferred position of the jet of 100 km led to a difference in the measured MTS of 10 m/sec.. It was felt throughout this determination that a number within 10 m/sec., or even 20 m/sec. of the proper value, or values, would be very useful for this study.

The fact that the final curves constructed from the data agreed with the form of the hypothetical curves and plausibility argument given in the earlier part of the discussion gave some feeling of confindence in the derived result. The final test must come, of course, if using this value, or even others constructed from similar arguments, consistent results can be achieved during the analysis of the records of auroral infrasound correlated with the magnetic disturbance.

CHAPTER 6

DATA NIGHT 9 NOVEMBER 1969

6.0 Introduction

The morphology of the geomagnetic disturbances and related phenomena associated with the production of auroral infrasound on the night of 9 November 1969 are studied in this chapter. A very detailed description of it near the onset time of the infrasonic pressure disturbances is presented. In attacking the problem of locating the generator of AIW within the substorm, both ray-tracing and the mean horizontal transit speed are invoked to derive a picture of AIW production which includes the earlier morphological features of the auroral infrasound as established at the Geophysical Institute, as well as extending the morphology into newer regions. In pursuit of the location of the AIW generator within the substorm, the use of the aforementioned techniques applied to the contoured magnetic disturbance maps justify the use of all three from the consistent picture which evolves.

6.1 Geomagnetic Activity 9 November 1969

The period 8-10 Nov. 1969 was the occassion of a geomagnetic storm of not especially great intensity according to the report of World Data Center A (Lincoln and Bucknam, etc). Yet the intervening day of 9 Nov. 1969 was important to this investigation because of the incidence of large, well-defined infrasonic pressure disturbance signals which were received at the recording sites of both College, Alaska, and Inuvik, N.W.T., Canada. One of the intriguing aspects of this period, as will be discussed later, is that the infrasound was

associated mainly with one of the smaller substorms rather than the largest one in the sequence.

The magnetic data utilized for this night was obtained from the 31 observatories shown on the location chart in Figure 6.1. Scaling of the magnetograms was done by hand. Quiet day curves based upon the days 6, 14, 15, 17 and 20 November 1969 were used for the zero levels. A composite trace of the level for these days was plotted for five observatories and the center of the resulting distribution was found to coincide closely with the level of the magnetogram for 15 Nov. 1969. For the remaining magnetograms then, the level of the quiet day 15 Nov. 1969 was taken to be the quiet day level and the scalings were referenced thereto. The K_p indices for the quiet day 15 Nov. 1969 are 0, 0, 0+, 0+, 0+, 0+, 0+, 0+, and the sum $K_p = 2$.

Based upon the digitization of the magnetograms for 9 Nov. 1969, 56 hand-drawn contour maps of the total magnetic disturbance vector, $\Delta\vec{F} = \delta H^2 + \delta D^2 + \delta Z^2$ were constructed, where δH, $\delta D \alpha \delta Z$ are the difference between the quiet day curve and the components H, D and Z. The maps were drawn for each 10-minute interval between 0230-0730 UT and at 2-minute intervals for points of interest in between. The purpose of the maps is to locate both temporally and spatially those centers of geomagnetic activity which may be related to the production of infrasonic disturbances in the atmosphere.

The following five pages display the maps of the five hours of geomagnetic disturbances which were studied. They are presented as Figure 6.2 A thru E. The time of each map is displayed in the upper

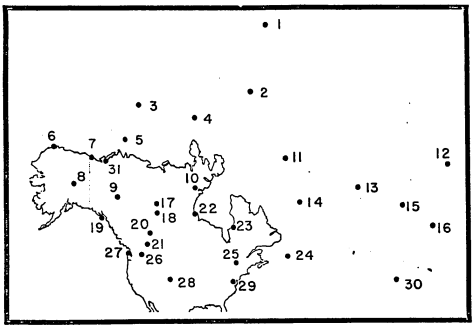

1. Alert
2. Thule
3. Mould Bay
4. Resolute Bay
5. Sachs Harbor
6. Barrow
7. Bar-1
8. College
9. Tungsten
10. Baker Lake
11. Godhavn
12. Tromso
13. Leirvogur
14. Narsarssuak
15. Lerwick
16. Rude Skov
17. Fort Smith
18. Fort Chipewyan
19. Sitka
20. Meanook
21. Calgary
22. Fort Churchill
23. Great Whale River
24. St. Johns
25. Ottawa
26. Newport
27. Victoria
28. Boulder
29. Fredricksburg
30. Toledo
31. Inuvik

Fig. 6.1. Location chart of magnetic observatories whose magnetograms were used for the geomagnetic study 9 Nov. 1969.

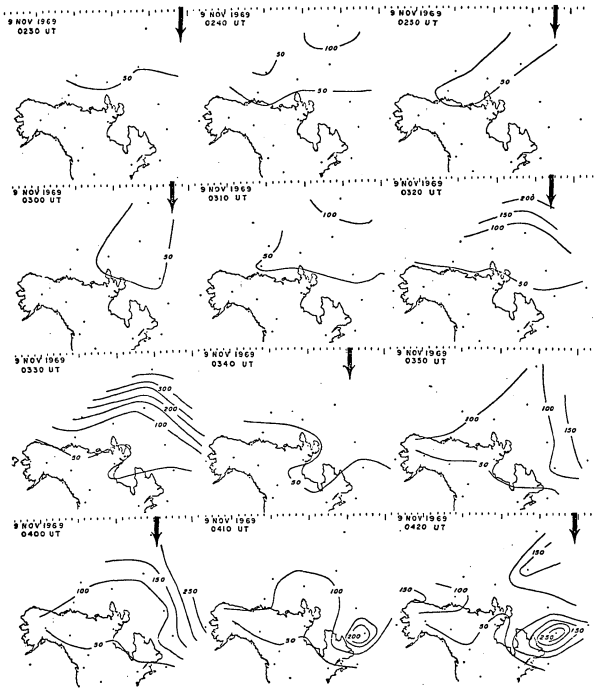

Fig. 6.2. (A) Contours of the total magnetic disturbance vector at an interval of 50 gammas. Arrow shows position of local midnight.

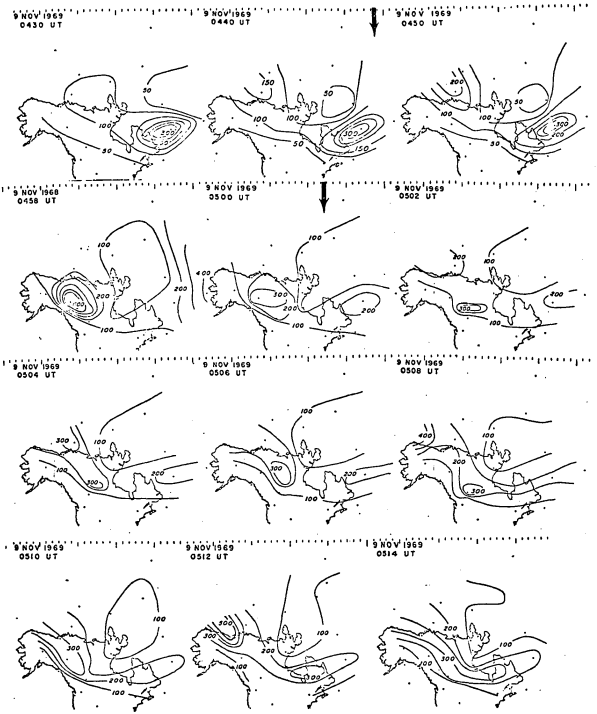

Fig. 6.2. (B) Contours of total magnetic disturbance-vector at interval of 50 gammas until 0450; 100 gamma interval thereafter.

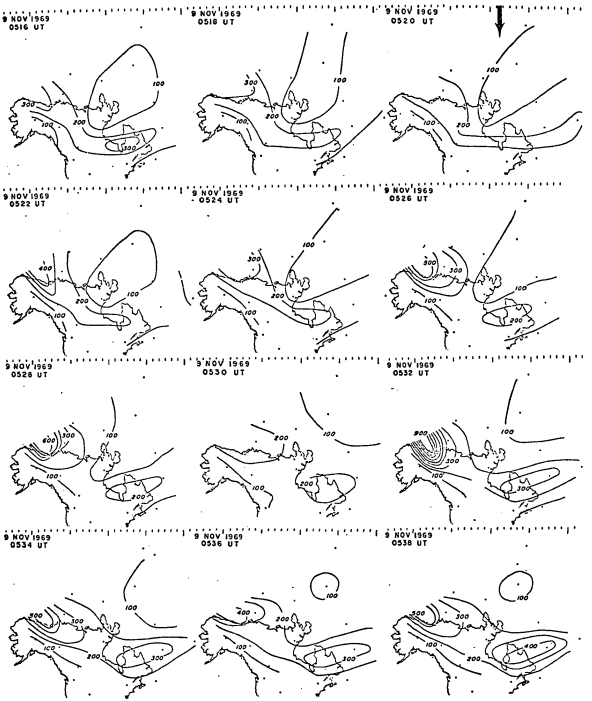

Fig. 6.2. (C) Contours of total magnetic disturbance vector at interval of 100 gammas.

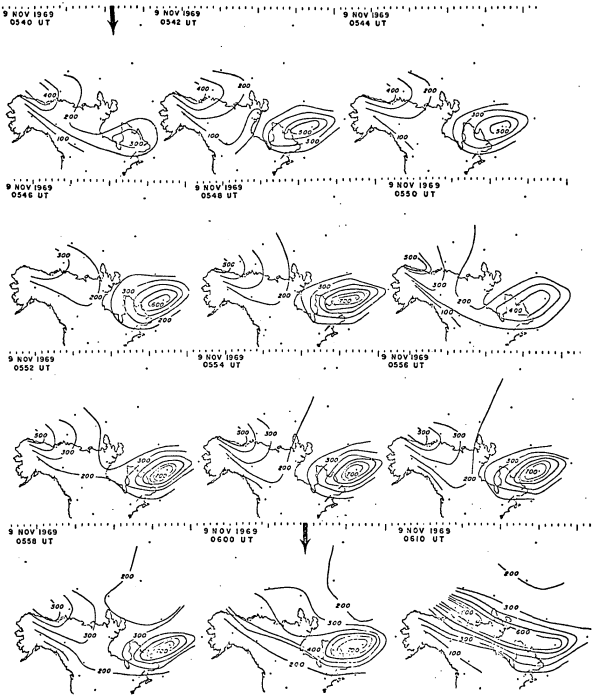

Fig. 6.2. (D) Contours of total magnetic disturbance vector at interval of 100 gammas.

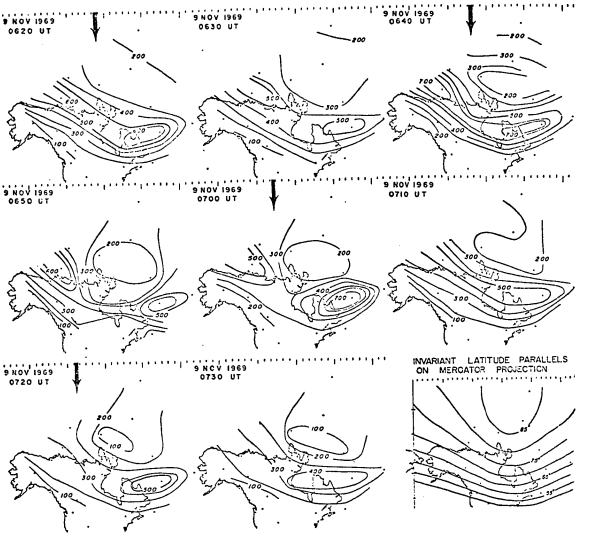

Fig. 6.2. (E) Contours of total magnetic disturbance vector at interval of 100 gammas. The final chart shows the Mercator map used in this study with superimposed parallels of invariant latitude.

border every 20 minutes to show the position of local midnight. Dots distributed throughout the diagrams show the location of the magnetic observatories whose data were used to construct the maps.

The contour interval is 50 gammas from 0230 to 0450 UT; thereafter a contour interval of 100 gammas is used for the more intense disturbances which followed. All points along the earth within the SSR which were equally geomagnetically disturbed at the particular time are connected by a contour. Thus a contour represents the amount by which the magnetic field has departed from the quiet day level at the time and location in question. The maps are all drawn in geographic coordinates on a Mercator projection of scale 1:58,500,000 at the equator; consequently, great circles on this projection will be curved lines.

Inspection of the maps (Figure 6.2A) shows that geomagnetic disturbances had already begun at high latitudes at the beginning of the analysis period at 0230 UT. This activity preceded by more than an hour of subsequent substorm activity in the night-midnight sector of the mid-latitude and auroral zone stations. Certainly this is by no means an unusual development since other workers have reported such disturbances to be rather a commonplace precursor of the polar magnetic substorm (Khorosheva and Darchiyeva, 1970; Ivliyev et al., 1970; Pudovkin et al., 1970).

A closer look at this effect may be afforded by an examination of the display of magnetograms in Figure 6.3. The central map in this figure is selected from the ensemble of maps presented in the earlier figure but shows the level of geomagnetic disturbance at 0330 UT.

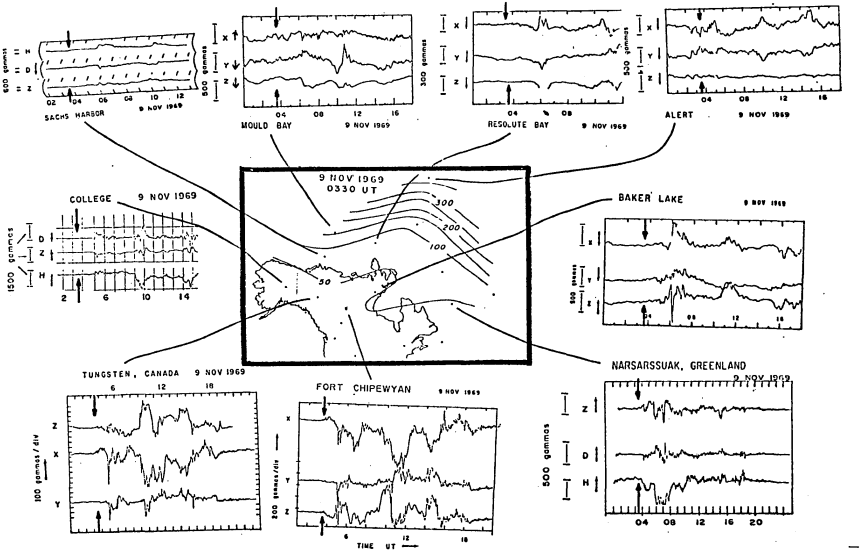

Fig. 6.3. Display of magnetograms for 9 Nov. 1969. Center chart shows station locations as well as contours of magnetic disturbance in high latitudes at the peak of its development prior to the substorm onset. Arrows on 'grams show time of chart at 0330 UT.

Arrows placed in the body of the magnetograms indicate the time for which the map was drawn and lines drawn from the name of the observatory show its location on the map.

As the figure shows, the stations at Alert and Mould Bay were having significant levels of disturbance while the lower latitude observatories were just beginning to depart from the quiet-day level. Comparing Figures 6.3 and 6.2, one will notice that within the next hour, the magnetic perturbation grows more intense in the midnight sector culminating in a sharp onset of the expansive phase of the substorm near 0500 UT. This period of time from near 0330 UT to the 0500 UT substorm onset seems to fit the "growth phase" description as discussed by McPherron (1970). Or again, if one follows the progression of the 50 gamma contour on the map sequence, one gets the feeling of a disturbance propagating from higher to lower latitudes. Such an equatorward motion of magnetic disturbance prior to the expansive phase of the substorm has been described as the growth of a "mini-jet" field which grows at the high latiude part of the oval and then moves southward (Iijima, 1972). It is not the purpose of this discussion to evaluate the appropriateness of the term "growth phase" to the pre-substorm portion of the magnetic disturbances seen on this night, or to examine the cautions of other observers of the phenomenon (Akasofu and Snyder, 1972). It is only important in this study to show, as will be done later, what meaning, if any, that this part of the magnetic disturbance had insofar as the production of detectable infrasound is concerned. As it will turn out, on 9 Nov. 1969 the AIW in the 10-100 sec. passband from this phase

are inconsequential if they exist at all.

Returning to the ensemble of maps (Figure 6.2) showing the development of the magnetic activity on this night, one can see that a sharp onset of the expansive phase of the substorm commenced near 0500 UT after the intensity of the disturbance grew stronger in the midnight sector. As one would expect, the magnetic perturbations which followed became both intense and moved rapidly. The substorm extended itself from the midnight sector westwardly into the evening sector. The developments following 0500 UT were, in fact, so rapid that a loss of continuity is experienced between maps even at the expanded two-minute interval.

Because of their importance to the onset of infrasonic pressure disturbances at Inuvik and College, the ensuing minutes following the onset of the expansive phase of the substorm were examined more closely. The onset of the expansive phase of the polar magnetic substorm was characterized by sharp decreases of the H-component in the night sector near western Canada, and by an increase in this component at College in the late evening. At the same time, near 0458 UT, there was a brightening of auroral arcs apparent through clouds at College and Ft. Yukon, and a poleward expansion which was visible at Inuvik in a cloudless sky. A more detailed inspection will be made of the electrojet and auroral phenomena associated with the poleward expansion in a subsequent section; however, a view of the magnetograms from some of the stations near the oval is shown in Figure 6.4. The onset of the expansive phase is depicted by an arrow(s) along the border(s) of the

magnetograms. Reference may be made to the magnetograms of some of the other observatories by simply referring back to the other figure depicting the substorm in its earlier stage at 0330 UT (Figure 6.3).

Returning again to the map ensemble in Figure 6.2, after the onset of the expansive phase of the substorm which suddenly intensified in the evening sector in western Canada near 0458 UT, there was a general northward motion of the disturbance doubtlessly in conjunction with the poleward expansion. The intense central portion of the disturbance was distributed unevenly along the oval but remained situated above 70° invariant latitude (see the map of coordinated invariant latitude in Figure 6.2e) for the remainder of the substorm. This places the most disturbed portion of the substorm geomagnetically west of Inuvik (geographically northwest) and from north to northwest of College in both systems during most of the substorm. Near 0532 UT there occured a brief intensification of the substorm north of western Canada and Alaska, and following intense activity in the midnight sector after 0540 UT, the disturbance began to distribute itself more evenly along the zone close to the 75° invariant latitude parallel.

A quick summary of the magnetic disturbances then would reveal a presubstorm period at about 1 1/2 hours duration in which high latitude (about 80° invariant latitude) perturbations appeared and progressed southward. There followed an increase of activity in the midnight sector, a greater-than-600-gamma sharp onset of the expansive phase in the late evening sector, brightening and poleward motion of the auroras near this same time, and more intensive geomagnetic activity

extending to the end of the analysis period at 0730 UT. A review of the magnetograms presented in the two earlier figures (6.3 and 6.4) will show that there were at least three substorm which occurred in the SSR for College and Inuvik on 9 Nov. 1969. Although it was not the most intense of the substorm periods of the night, the period from 0500-0730 UT was the most productive of infrasonic pressure disturbances, as will be discussed later. For the day 9 Nov. 1969 the K_p indices were 3, 5, 5, 5+, 5+, 6-, 4, and 2. The sum of K_p was 35+.

6.2 Presubstorm Pressure Disturbances, Inuvik

The infrasonic pressure records at Inuvik for the night of 9 Nov. 1969 were studied for the hours 0200-1600 UT. The traces from the four stations were searched for coherent wave forms photographed, scaled at points of interest, and analyzed for amplitude of noise level. A sample of the superimposed traces from the four channels taken from the beginning of the analysis interval to a time just prior to the onset of a substorm is shown in Figure 6.5. A summary of the analysis of this record follows.

Characterized by a fairly low noise level, this span of the record seems to be devoid of any coherent infrasound related to the ambient geomagnetism as depicted for the environs of the North American continent in the maps shown earlier. Of the vague coherences which are apparent at a few points in this part of the record, only the wave train between 0320-0340 UT could be scaled to any type of sensible solution, and even here the results were very poor, ($\Delta\phi > 10°$) so the results were discarded.

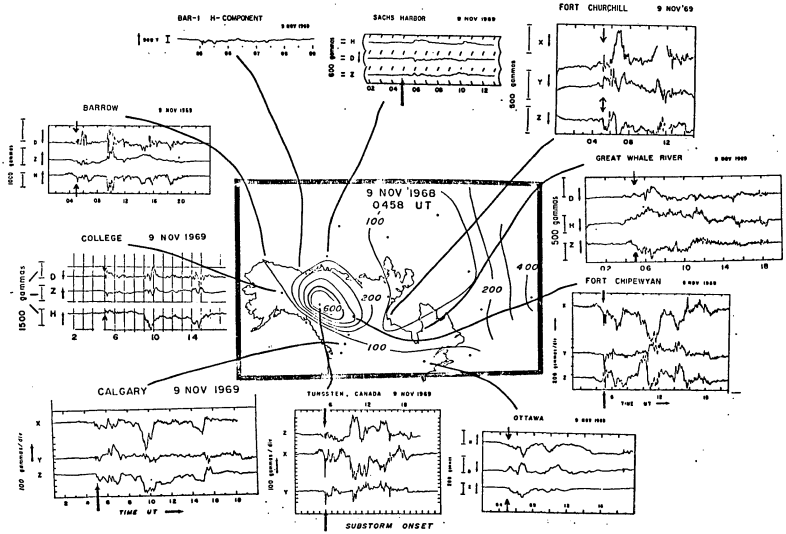

Fig. 6.4. Examples of magnetograms depicting the onset time (0458) of the substorm. Center chart shows observatory locations as well as the disturbance contours at the onset. Arrows on 'grams show onset time.

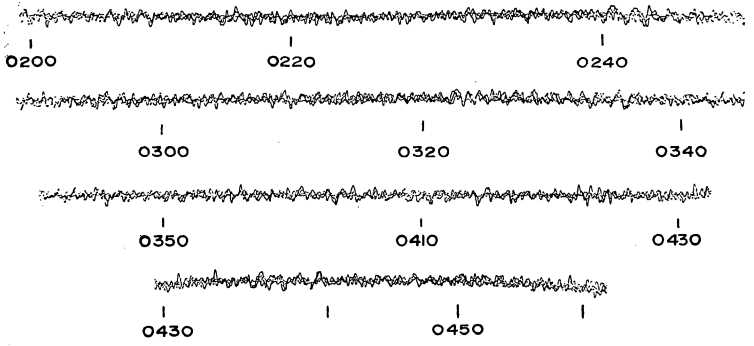

Fig. 6.5 Pre-substorm pressure records at Inuvik, N.W.T. on 9 Nov. 1969

The Inuvik pressure records were then scanned for the average noise level by noting the pressure amplitude of two parallel lines of ten minutes length placed peak-peak about the traces in such a way as to represent a median value as determined by visual inspection. This method of analysis was meant to give an approximate and quick indication of the quantity measured rather than being statistically valid computation. The results were quite uniform except during periods when coherent signals were present. At those times, since the procedure was meant to give some idea of background noise, the amplitudes measured corresponded closer to the levels before and after the signal period independent of the signal amplitude. And in the case of the 10-minute interval containing only coherent waves of both small and large amplitude, a median level was visually selected between the two extremes favoring the dominant amplitude present.

A histogram showing the results of this analysis is presented in Figure 6.6. The arrow in the figure indicates the onset time of the auroral substorm at Inuvik. This figure is intended to show the level of background noise before, during and after the substorms of night. Since the onset of coherent signals tends to override lower-level background noise, a period of large amplitude signals tends to dilute the meaning of "background noise" when they occur. Such a period appears in the record immediately after the onset of the substorm. As the histogram shows, the presence of larger amplitude dominate the post-substorm period until near 0800 UT. During this time span the histogram does not accurately describe background noise, nor does

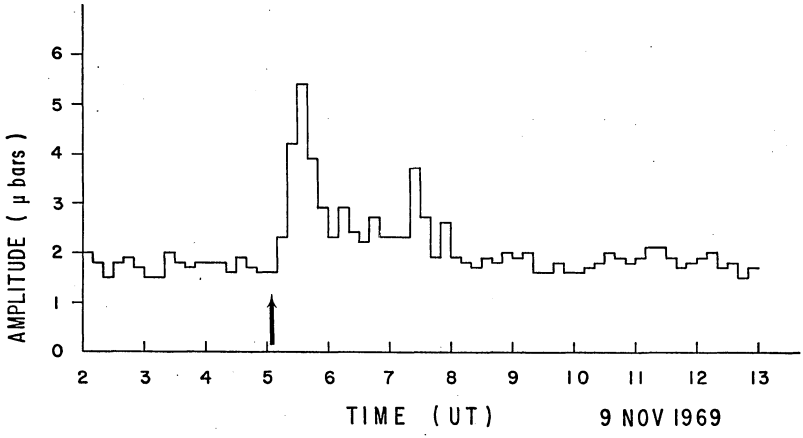

Fig. 6.6 Variation in amplitude of background noise at Inuvik, N.W.T.

it give the actual amplitude of the signals, but rather a median level for the 10-minute period indicated. Despite these short-comings however, the figure does show some of the features for which it was intended, that is, an indication of the ambient noise level before and after the substorm. This pressure level as used in this report is taken to be representative of the ambient background noise at the times in question.

The important question pursued in constructing this figure is whether or not the ambient geomagnetism temporally and spatially near a polar magnetic substorm contributes to the level of the incoherent background noise at a given station. The figure shows no significant change before or after the substorm period.

A good illustration of this point is to compare the pressure noise background to the total range of geomagnetic activity as observed at Alaska, Greenland, Canada, and Iceland. The histogram in Figure 6.7 depicts the total geomagnetic activity in the upper half, and the pressure noise background discussed in the previous figure in the lower part. The upper diagram was constructed using the data from only those observatories mentioned by subtracting the largest value of the total magnetic disturbance vector from the smallest for a sequence of 10-minute intervals. This procedure was mentioned in the earlier section concerning the data night of 25 June 1969. For this determination, access was not available to any of the geomagnetic indices in current use because of their inclusion of observatories from Europe, eastern Russia, or in some cases, the southern hemisphere. A good

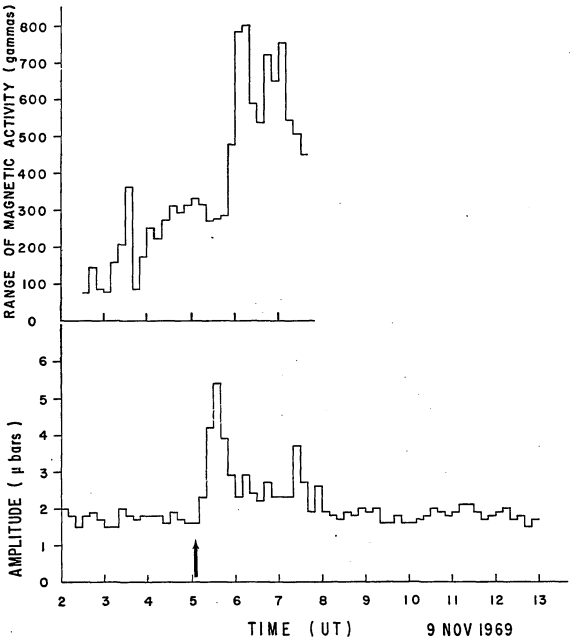

Fig.6.7 Comparison of total range of magnetic activity in the environs of N. America (above) to the amplitude of infrasonic pressure disturbance background noise (below).

review article on the popular geomagnetic indices (Rostoker, 1972) discusses the strengths and weaknesses of the various types from the point of view of the student of geomagnetism. From the viewpoint of the researcher in geomagnetically-related pressure disturbance, however, there is no evidence thus far to relate infrasonic disturbances in Alaska to magnetic perturbations in the aforementioned areas.

Returning to the figure, the upper diagram shows an overall increase in geomagnetic activity as seen by the observatories in Alaska, Canada, Greenland, and Iceland - the infrasonic pressure disturbance signal source region for Alaska (hereinafter referred to as the SSR). The dominant features of these histograms are the continual increase in geomagnetic activity in the SSR over almost the entire geomagnetic analysis span from 0230-0730 UT while excepting the substorm period from near 0500-0800 UT, the infrasonic background noise remains relatively stable. It is also interesting to note that the largest pressure amplitudes occur before the largest magnetic perturbation thus revealing the lack of correlation between the two. This reflects the fact that there were no disturbances locally during this span of time whose effects would appear to be nearly concurrent enough to be noticed on the two histograms. This does not exclude the possibility that some infrasound energy from the farther reaches of the magnetic disturbance perhaps 2-3 hours propagation time away, say, could have arrived coincident with the pressure disturbances associated with the substorm onset. So without closer inspection of the azimuthal arrival pattern of the infrasound between 0500-0600 UT, one could not definitely state

whether or not the growth phase of the substorm played any or what role in the production of infrasound on 9 Nov. 1969.

6.3 Onset of Substorm and Associated Effects

(a) Auroral Substorm

As mentioned in the previous section, the onset of the expansive phase of the magnetic substorm was accompanied by a brightening of auroral arcs and an ensuing poleward expansion. On 9 Nov. 1969, it was clear at Inuvik, and overcast at College and Ft. Yukon at the principle times of interest.

Despite the presence of a thin overcast at College, arcs were discernible overhead through the clouds. A brightening of the aurora to the point of overexposure of the film commenced about 0458 UT. Since the clouds were thick enough to make the motion of the arcs uncertain, no attempt was made to reproduce the College all-sky camera data here.

Clearer pictures of the poleward expansion were obtained at Inuvik, however, and a reproduction of the principle positions of the polewardly-moving arc are shown in Figure 6.8. In the last picture of the sequence (0507:30 UT) a second arc may be seen south of the first polewardly-progressing arc. This gives the impression of a more complex situation than the case of a single arc and current filament moving northward. Overexposure of the film in the following frame due to the intense auroral luminosity does not give another view of this arc, however.

The lower part of Figure 6.8 shows two maps of the geomagnetic disturbance in the SSR during the poleward expansion. A small line segment superimposed in the disturbance shows the position of the

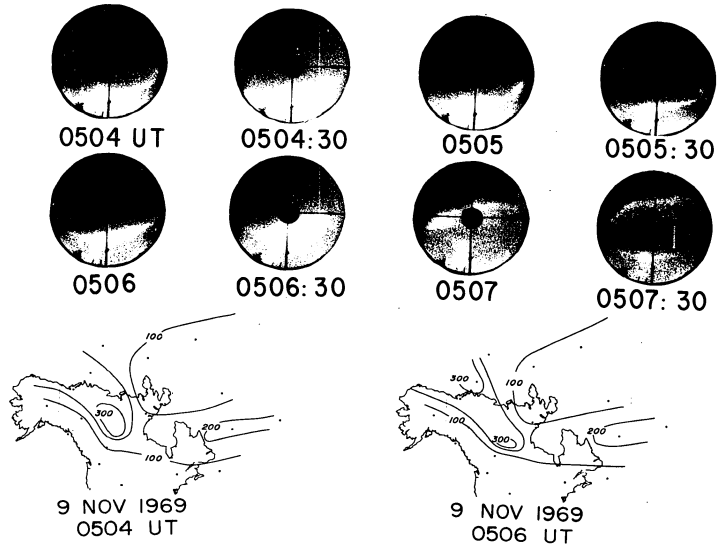

Fig. 6.8. All-Sky Camera photographs of the poleward expansion at Inuvik, N.W.T. on 9 Nov. 1969. The two maps taken from the map ensemble presented earlier show superposed line segments representing the ground-projection of the auroral arc at the time indicated.

northernmost poleward-moving arc at the time in question. It might be interesting to note that the position of the arc within the magnetic disturbance contours is near the centrally-located, most disturbed part of the system. Due to the poor placement of the magnetic observatories in this region for contouring purposes, the position of this arc with respect to the contours is not precise.

In order to afford a closer view of the poleward expansion, Figure 6.9 is presented to give quantitative information concerning the northernmost polewardly-propagating form. Part A of the figure is a sequence of traces representing the projection on the ground of the successive positions of the arc as seen by the all-sky camera. Part B of the figure shows these same traces approximated by one or two line segments. Dashed-line rays are drawn normal to these segments to give an indication of the direction of motion of the arc at the time indicated. Both diagrams are superposed upon a reference frame showing the direction of true north (TN) and magnetic north (MN) which lies 38°42' east of north at Inuvik. The accompanying table shows measured details concerning the arc: the time in UT, the horizontal distance along the earth's surface from Inuvik to the ground-projection of the arc (kilometers); the speed in m/sec., and the angle of travel measured with respect to true north. The bottom diagram in Figure 6.9, part D, shows the cosmic noise absorption associated with the expansion.

As Figure 6.9 shows, the arc moves rapidly northward toward some direction between true and magnetic north varying only slightly in azimuth as it propagates. In fact, as the table in Figure 6.9

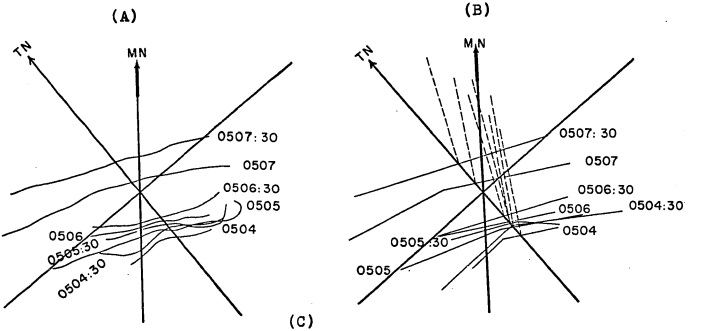

(C)

TIME	0504	0504:30	0505	0505:30	0506	0506:30	0507	0507:30
DISTANCE	-165	-155	-131	-115	-97	-85	34	105
SPEED	-	333	800	533	600	400	3967	2366
ANGLE	29	31	32	30	30	25	29	24

AVERAGE ANGLE = 28 TOTAL ANGULAR RANGE = 8 AVERAGE SEED = 1286 m/sec

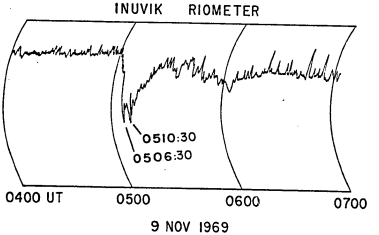

Fig. 6.9. Quantitative information concerning the poleward expansion and associated cosmic noise absorption. (A) Diagram of the sequential positions of the ground-projection of the arc. (B) The same arc approximated by straight lines with dashed normals to show direction of motion. (C) Table showing time of arc position (UT), distance from Inuvik (Km.), speed (m/sec.) and azimuth of motion with respect to true north; (D) Associated absorption.

shows, the arc appears to vary from an average angle of travel (28°) only by plus-or-minus four degrees. Thus the total angular range in direction of motion of this polewardly-moving arc is about eight degrees during the 3 1/2 minute interval reproduced here from the Inuvik all-sky camera. The speeds were quite erratic doubtlessly reflecting inaccuracies in scaling, possible imprecision owing to the effect of perspective not being totally removed (note the rapid increase in speed after the arc passes the zenith and the less rapid decrease). No attempt was made to asses the amount of inaccuracy encountered in the scaling of the film.

The cosmic noise associated with the zenith arc is shown in Figure 6.9 by the peak at 0506:30 UT. A subsequent peak of equal magnitude follows at 0510:30 showing most likely that the second arc seen in the all-sky camera (ASC) photograph at 0507:30 shown in Figure 6.8 also crossed the Inuvik zenith four minutes later.

(b) Polar Magnetic Substorm

The onset of the polar magnetic disturbance was discussed in the preceding section of this chapter. At this point it might be significant to consider a few inferences concerning the auroral electrojets in a very superficial way. As was discussed in the earlier chapter concerning the auroral electrojet, the current system(s) seem to become well developed following the expansive phase of the polar substorm. Accepting this viewpoint as fact, this investigation further maintains that he likely spatial location of such a system is most intensely developed within the most intensely-disturbed part of the

magnetic disturbance contours as presented in this report. This is not to rule out the possibility or even likelihood that currents of lesser magnitude are not flowing elsewhere within the system; their presence is simply less well-defined by this procedure of contouring $|\Delta F|$. Nevertheless, it is important to bear in mind that the contoured system of magnetic disturbance ΔF as presented here smears over many details concerning localized geomagnetic activity which other types of presentation of the magnetic substorm might lucidly portray.

In order to gain an insight into the possible implications of more complex features of the electrojet system for this data night of 9 Nov. 1969, Figure 6.10 was constructed to show a display of an enlarged section of the Z-component of the magnetograms for a selection of observatories for the hours 0400-0600 UT. The map in the center of the figure was chosen mainly for defining the location of the observatories. It also gives another look at the substorm during the poleward expansion. Earlier workers (Kamide et al., 1969) have cited reversals of the Z-component to be indicative of localized current concentrations which are manifestations of the existence of a microstructure within the auroral electrojet. As the figure shows, within the span of 10-minutes or so either side of 0500 UT, the stations within and immediately south of the main electrojet disturbance show numerous reversals of the Z-component. This implies both finer-scale structure within the main jet as well as within the nearby one. This may also imply that there are erratic motions or temporal changes of at least two oppositely-directed electrojets.

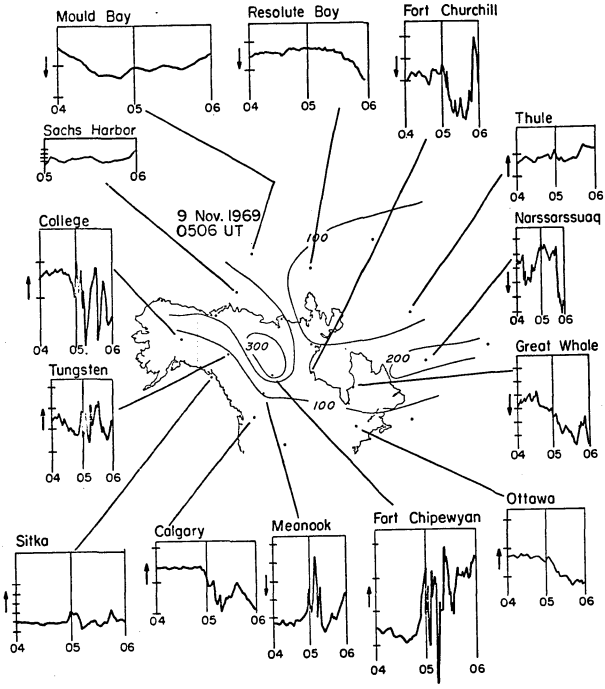

Fig. 6.10. Enlarged portions of the Z-components of a selection of magnetograms in and around the auroral oval (unspecified). The map in the center references station positions and the magnetic disturbance at an instant during the poleward expansion.

To explore this possibility a bit further, Figure 6.11 is given which shows the rapid-run magnetogram for College for the period 0455-0510 UT for 9 Nov. 1969. If one considers a simple line current model of the electrojets independent of induction effects, a westward electrojet would be indicated by a Z-reversal accompanied by a negative H maximum at the time of zenith passage (Z = 0) of the poleward moving electrojet. Likewise an eastward electrojet would be inferred for the case of a Z-reversal followed by a positive H maximum at the zenith crossing. In light of such a simple model, it seems reasonable to assume that both the Z-reversal and the displaced H maximum conjoin to manifest motion of the current system, whereas a simple temporal change in current strength would not displace the Z and H extreme with respect to each other, nor cause a change in sign of the Z-component relative to the zero level. Returning to the rapid-run magnetogram in Figure 6.11, four points are enumerated along the two curves which represent times when the conditions are met, according to the simple line current model just described, when electrojet motions are implied. In the case (1) the maximum in H preceded by the Z maximum and its subsequent reversal describe an eastward electrojet which was north of College near 0456 UT which proceeded to move southward just within a couple of minutes of the onset of the expansive phase of the polar magnetic substorm at College. (Already some brightening of the auroral arcs was apparent through the cloudy overcast.) By 0501:30, the situation (2) indicates a westward electrojet moving north since the Z maximum precedes an H minimum. Likewise (3) indicates an eastward electrojet moving north and

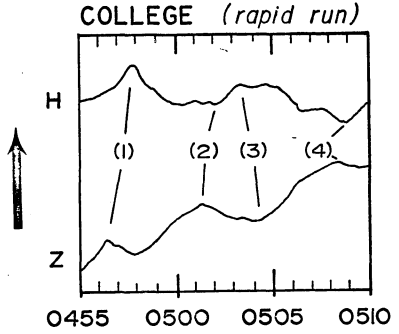

Fig. 6.11. Electrojet phenomena near College just prior to and following the onset of the expansove phase of the auroral substorm. (1) Eastward jet moves southward. (2) Westward jet moves north; (3) east jet moves northward; (4) west jet moves northward.

(4) a westward electrojet moving north. Whereas these simple considerations seem to lead to a very complex arrangement of electrojets moving in various directions, some semblance of order may be inferred from it. The only southward motion occurred near the onset of the expansive phase of the substorm, whereas northward motion ensued immediately after 0500 UT by which time the poleward expansion of arcs was well under way. The presence of the eastward electrojet seems reasonable in light of the model of the polar jets as seen by Akasofu, Chapman, and Meng (1965) if one considers it the eastward return current as in their model. A glance at the magnetograms shown in the earlier figure shows that while most of the other stations near the auroral zone were experiencing negative bays in H, College and Sitka (not shown) were having a positive excursion in H.

Other interpretations of the situation depicted in the foregoing figures are, of course, possible. One interpretation might be a simple westward electrojet and its return current moving back and forth across College (Akasofu, private communication). Some form of this motion seems likely except in this instance, the west ward electrojet was not observed to be moving southward. Possibly there was a double westward electrojet as Figure 6.11 seems to imply, but an eastward electrojet also is interspersed between the two. Whatever the correct interpretation, the important point that is being made here is that a simple uni-directional current does not seem to be the case; instead there were multiple currents involved during the early part of the substorm expansion. One manifestation of this in addition to the situation depicted

by College rapid run magnetogram or even the Z-reversals shown on the Z-component magnetograms in Figure 6.10 is afforded by the riometers in Figure 6.12. Here an indication of a second electrojet passage is shown by the double peak in absorption at Inuvik, Bar-1, Ft. Yukon, but less definitely at College.

6.4 Post-Poleward Expansion Period and Production of Infrasound

(a) Inuvik

The choice of Inuvik as the starting point of the discussion on infrasound is based upon the fact that the most well-defined pressure disturbance on 9 Nov. 1969 was first observed at this station rather than at College, and the all-sky camera at Inuvik could see auroras thru clear sky. The discussion which follows emphasizes the observable phenomena noted by the ASC and riometer, and due to the unfortunate absence of more than the H component of the Inuvik magnetometer, relies on the general picture of the magnetic disturbance which is afforded by the contoured maps as presented earlier. These maps are supported in the Inuvik area by the H-component from Bar-1, and the three-component magnetograms from Sachs Harbor, Tungsten, College, and Barrow. This distribution of observatories surrounding Inuvik aided greatly in the better placement of the disturbance contours near Inuvik.

Following the auroral poleward expansion which passes overhead at Inuvik there ensued within three minutes an equatorward-travelling arc which was seen by the Inuvik all-sky camera. Such a phenomenon has been reported by Johnson (1972) and Wilson (1972) as an associated effect with the generation of infrasound. The latter investigator

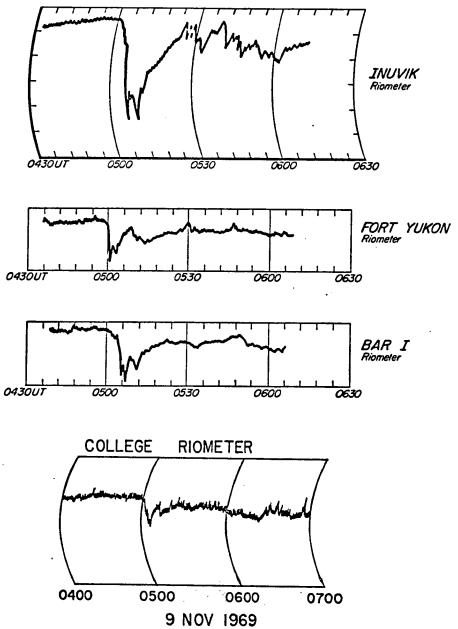

Fig. 6.12. Cosmic noise absorption at four stations in and near Alaska showing two peaks near the poleward expansion time just before and after 0500 UT. (This effect is present but of small amplitude at College.)

has, in fact, researched the particular equatorward-moving arc studied here and concluded that this arc was the generator of a large infrasonic pressure pulse observed a few moments after zenith passage of the arc.

Figure 6.13 shows a view of this equatorward-moving arc (c) and the ambient geomagnetic disturbances in the vicinity of North America (a) and an enlarged portion of the map near Inuvik (b). The upper part of the diagram shows a line segment representing the ground projection of the arc northeast of Inuvik at three instants during its motion. It appears to have originated near the most intense part of the geomagnetic disturbance toward the geomagnetic eastern end of it. Moreover, as a subsequent figure will show, this arc is not simply propagating uniformly outward from the disturbance, but is actually rotating around within the region related to the locus of the most intense electrojet. Part (b) of the present figure shows an enlargement of the Inuvik area portion of the maps just above them. (The final position at 0516 UT is uncertain as to whether it is the same arc or an ensuing one which may be seen in the picture frames at 0514 and 0515 UT in part (c) of the figure.) It is quite apparent in the first two enlarged sections that the eastern edge of the arc is moving faster than the western edge in the rapidly-changing geomagnetic disturbance. The photographs in part (c) of the figure show four minutes of the equatorward motion as seen by the ASC.

To look at some of the quantitative factors scaled from the film, a diagram of the successive positions of the motion, a table of measured values and a view of cosmic noise absorption is associated with the arc is shown in Figure 6.14. Part (A) of the figure shows a diagram of the

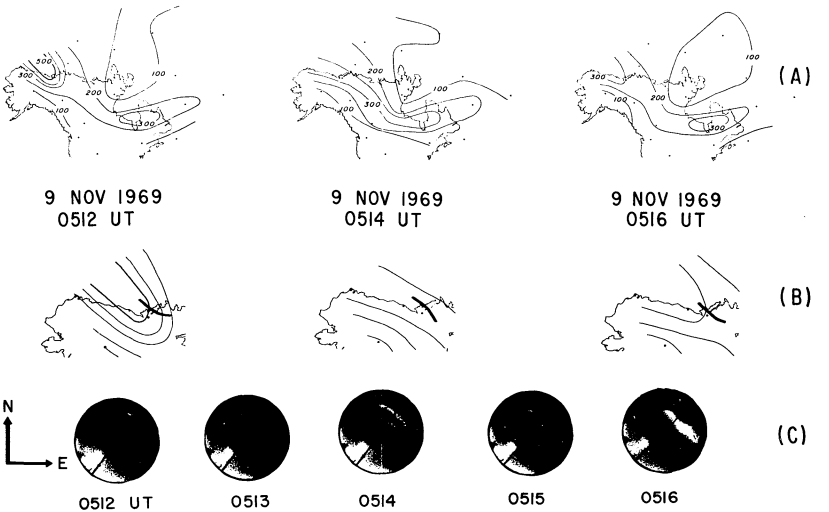

Fig. 6.13. Motion of a supersonic equatorward-moving arc after the poleward expansion at Inuvik. (A) Ambient geomagnetic disturbances during passage of arc. (B) Enlarged view of (A) near Inuvik. (C) All-Sky Camera photographs of arc.

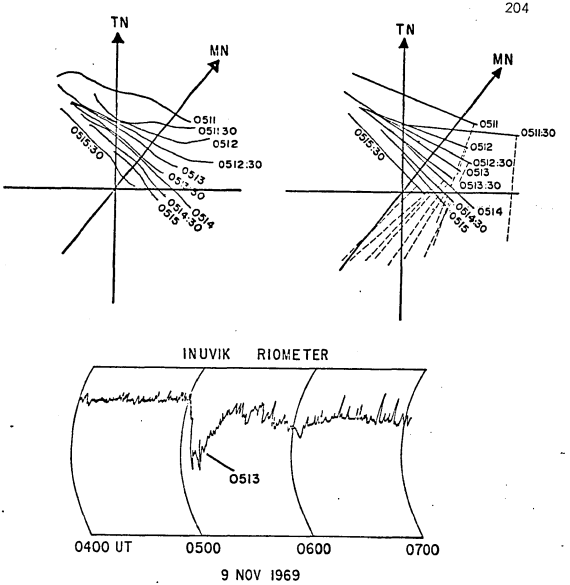

Time	0511	0511:30	0512	0512:33	0513	0513:30	0514	0514:30	0515	0515:30
Distance	269	235		192	160	145	119	109	94	79	38
Speed		1133		1433	1087	500	867	333	500	500	1366
Angle	201	184		199	205	210	216	221	223	228	225

Total angular range= 41° ; Average speed= 855 m/sec.

Fig. 6.14. Quantitative details of equatorward-moving arc of Figure 6.13. (A) Ground projection of successive positions of arc as mapped from ADC frame (left) and approximated by straight lines (right). (B) Enhancement of cosmic noise absorption during passage. (C) Quantitative details of the motion.

actual ground projection of the successive positions of the arc in equatorward motion as viewed from 0511-0515:30 UT. On the right side of part (a) is a representation of these arc positions by straight lines along which dashed lines were constructed normal to their length to give an indication of the direction of motion of the arc at the instant designated. Both of these diagrams are referenced to true geographic north (TN) and magnetic north (MN) which is situated at an angle of 38°42' E of north. As these two diagrams show, the arc was turning erratically in a counterclockwise direction as viewed from above the arc. Part (b) of the figure shows that as the arc approached the zenith, there occurred an enhancement in cosmic noise absorption as one would expect; however, the enhancement peaked at 0513 UT when the portion of the arc along 40°, say, was some 145 km horizontally from Inuvik. Further approach of the arc toward the Inuvik zenith was characterized by a diminution in absorption. Part (c) of the figure is a table showing the UT time of each arc position illustrated above in the figure, the distance of the ground projection of the arc in km along as azimuth of 40°; the horizontal travel speed of the arc in m/sec. based on the distances given herein, and the azimuthal angle along which the arc was travelling at the instants in question.

One can see from both the diagrams and the table in this figure that the arc was involved in both translational and rotational motion simultaneously, while moving erratically in both. (In the actual situation the arc did not engage in rigid-body rotation, but obviously moved non-uniformly throughout its length. Only the largest scale

motion is approximated here.) In the 4 1/2 minute period over which the arc was mapped here, its direction of motion covered an angular range of 41°, and its average speed over the entire interval was 855 m/sec. Compare this motion of the arc within the most intense part of the electrojet with the arc in poleward expansion which averaged an angular range of direction of only 8° in 3 1/2 minutes.

Considerable details have been presented concerning the poleward expansion and equatorward motion and the immediate ensuing minutes because the initial infrasonic pressure disturbances of the lower atmosphere commenced near that time at Inuvik and afterwards at College. The contrast between the two separate phenomena are interesting and important because the poleward expansion does not itself seem to be the direct cause of the resulting pressure disturbance, but the circumstances surrounding the equatorwardly-moving arc does.

At this point we view a reproduction of the pressure signal received at Inuvik close to 0521 UT. Figure 6.15 shows the large amplitude pressure pulse which was received within 10 minutes after the first ASC photograph of the equatorward motion was observable. The trace represents the super position of the four microphone pressure records at Inuvik to show the phase coherence in the wave. The measured and computed values relating to the essentials concerning the wave are shown in tabular form just beneath the pressure recording. This signal is classed $MFDA_1$ (see Appendix I) since the highest frequency component arrived first as a positive cycle.

The pressure signal shown in this figure were aligned by the usual

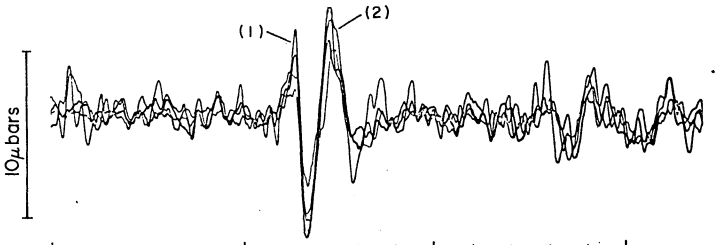

	azimuth	speed	error in azimuth
(1)	37°	314 m/sec	4°
(2)	47°	289m/sec	2°

Fig. 6.15. A large amplitude infrasonic pressure pulse received at Inuvik following the observation of an equatorward-moving arc.

hand-scaling methods (see Nichparenko, 1967) and scaled for the two separate peaks of the large M-shaped signal. The azimuth, speed, error in azimuth, which is an expression of the total range of error in degrees by which the five available solutions of azimuth disagree were computed for both peaks. The shape of this wave is a fairly commonly occurring feature of large pressure pulses in the system in use, and there is some evidence that the second peak in the pulse may contain largely the ringing effect due to the transient response characteristics of the electronics. Such a situation has been suspected as a result of noting and comparing the different wave shape resulting from a similar signal which was passed thru the separate electronics of a digital data aquisition system which has been described by Herrin and McDonald (1971).

One of the most puzzling features of this signal is the fact that the scaling of either peak results in a trace velocity which is less than the local speed of sound (321 m/sec.). Since a measure of the tilt of the wave normal to the horizontal is given by the expression a - Sec^{-1} V/c, where V is the trace velocity measured from the records, and c is the local speed of sound, no inclination angle (a) can be computed for a value which makes the argument of the Sec^{-1} less than one. Aside from interference effects which might result in a new wave propagating in a different direction and speed as a consequence of the super-position of two wave pulses from different directions clashing, it is very difficult to account for this type of thing. On the other hand, one might consider the difference between the group and phase velocity near the acoustic cutoff, with the former being possibly less

than the local sound speed, and the latter slightly more. This is also a difficult correlation to make insofar as the current ideas of dispersion pertain to an isothermal atmosphere (see discussion of dispersion Chapter 2). Nevertheless, a calculation for an isothermal atmosphere shows the cutoff period to be 293 sec., the Brunt period to be 330 sec., and the period of the AIW's in question to be 50 and 72 sec. - well above the cutoff period.

One possibility for the scaling of a speed lower than the local acoustic speed is that of a scaling error. Since the least accurate of the measured values from the infrasound chart records concerns those related to trace velocity, it is quite possible that the true trace velocity of the signal was close to the speed of sound, and the scaling results yielded a lower value. In any case, the small number of signals which are found in this category attest to a certain uniqueness to their nature which is an exception to the common experience.

I. All-sky Camera Analysis

Following the poleward expansion at Inuvik which crossed the Inuvik zenith near 0506 UT on 9 Nov. 1969, there followed not simply a single equatorward-moving arc as discussed previously, but a general equatorward drift of a sequence of arcs and forms until near 0545 UT at which time the motions became quite complex. A number of well-defined arcs of supersonic speeds approached the station at Inuvik during this period. A discussion of their motions and an attempt to correlate them with the auroral infrasonic waves recorded at that station follows.

During the time period 0516-0519 UT, an arc appeared to the north

of Inuvik passing overhead in the Inuvik zenith near 0519 UT. The ASC mapping of the ground projection of this arc and related data are shown in Figure 6.16. Part (a) of the figure shows the successive positions of the ground projection of the arc (left), and the approximation of the arc by straight lines whose normals show the direction of motion (right). Part (b) of the figure is a tabulation of the time (UT), the horizontal distance of the ground projection of the arc from Inuvik in km; the speed (m/sec.) and the azimuthal angle from which the arc progressed. For all the auroral maps the height of the aurora was assumed to be 110 km.

Figure 6.16c contains the maps of the geomagnetic disturbance during the period in question, and a line to show the position of the auroral form within the disturbance for the times examined in the earlier parts of the figure. Where motions of the aurora became indistinct, no data is listed for the particular arc for that particular time.

Figure 6.17 (a, b, and c) presents a view of the auroral luminosity of the form following the one studied in the previous figure. This figure contains the pertinent data concerning the arc which was also drifting equatorward from 0520-0524 UT, immediately following the arc of the preceeding figure, Figure 6.16.

Figure 6.18 (a, b, and c) again follows the same format of the two previous figures to illustrate the next arc from 0526:30 - 0529:30 UT. The final arc sequence in this portion of the study is shown in Figure 6.19 (a, b, and c), which again follows the identical format as the three preceeding figures. It should be pointed out in the case of this arc, however, that the geometry of the outline of this arc was quite

(A)

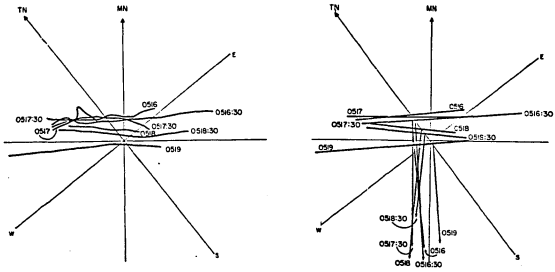

(B)

TIME	0516	0516:30	0517	0517:30	0518	0518:30	0519
DISTANCE	68	64	?	66	32	13	-9
SPEED	-	13	-	0.33	1133	633	733
ANGLE	32	34	-	38	43	48	33

AVERAGE ANGLE = 38 , TOTAL ANGULAR RANGE = 16 , AVERAGESPEED = 425 m/sec

Fig. 6.16. Equatorward motion of a supersonic arc observed at Inuvik about 10 minutes after the zenith crossing of the polewardly expanding arc.

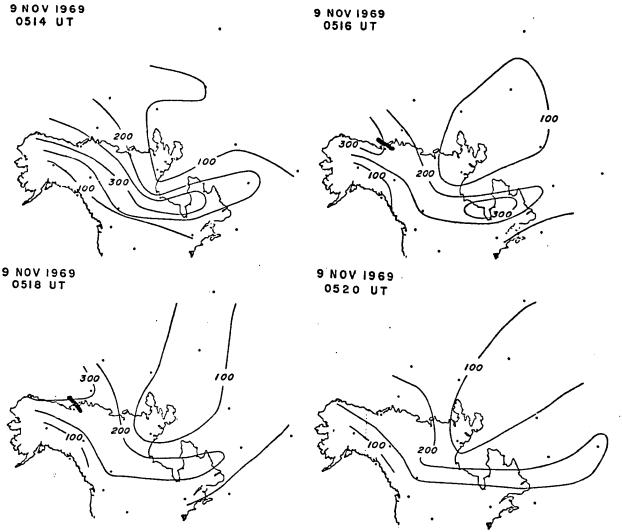

Fig. 6.16C. Equatorward motion of a supersonic arc observed at Inuvik about 10 minutes after the zenith crossing of the polewardly expanding arc.

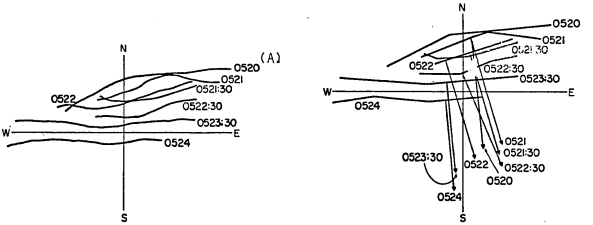

(B)

TIME	0520	0521	0521:30	0522	0522:30	0523:30	0524
DISTANCE	149	107	88	77	41	20	-26
SPEED	-	700	633	367	1200	350	1533
ANGLE	355	343	344	344	344	355	356

AVERAGE ANGLE = 348 . TOTAL ANGULAR RANGE = 13 . AVERAGESPEED = 729 m/sec.

Fig. 6.17. Equatorward mation of a supersonic arc observed at Inuvik about 14 minutes after zenith crossing of poleward expansion. Part (a) shows the mapped arc after transferrance from all-sky camera photograph (left, and the straight line approximation of the arc with dashed normals depicing its motion direction. Part (b) shows the measured and calculated valued pertaining to it.

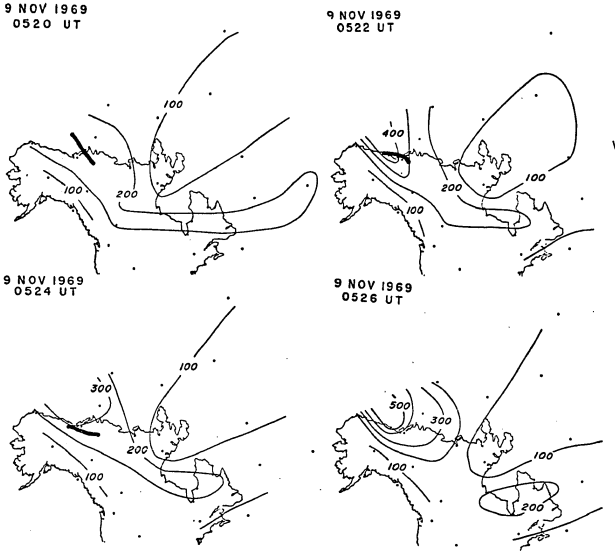

Fig. 6.17 c. Maps of geomagnetic disturbance during equatorward motion of a supersonic arc.

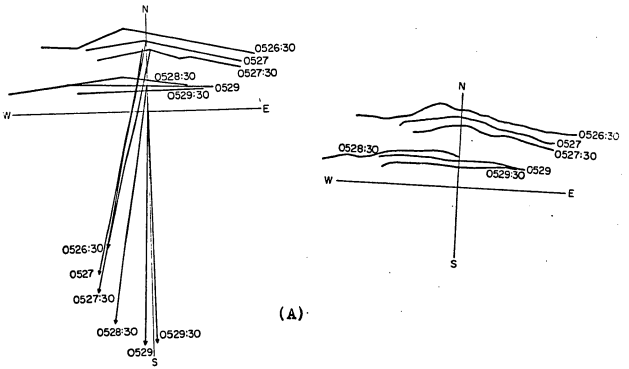

(B)

TIME	0526:30	0527	0527:30	0528:30	0529	0529:30
DISTANCE	212	179	165	91	77	53
SPEED	-	1100	467	1233	467	800
ANGLE	12	13	14	9	2	359

AVERAGE ANGLE = 08 , TOTAL ANGULR RNGE = 15 , AVERAGE SPEED = 883 m/sec

Fig. 6.18. Equator motion of a supersonic arc observed at Inuvik about 20 minutes after the zenith crossing of the poleward expansion. Parts (a) and (b) show the same format as that of the other two figures preceding.

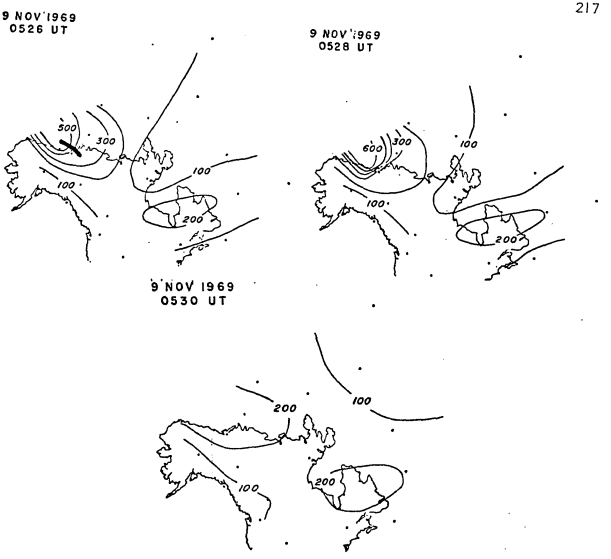

Fig. 6.18 c. Maps of geomagntic disturbance showing position of auroral form.

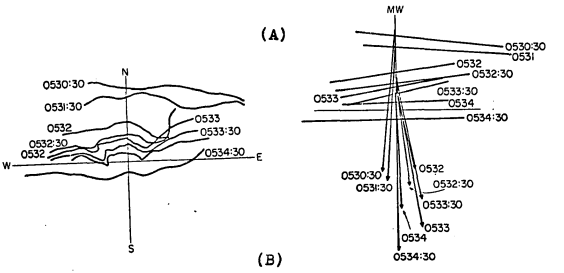

TIME	0530:30	0531:30	0532	0532:30	0533	0533:30	0534	0534:30
DISTANCE	-	200	125	97	73	36	30	42
SPEED	-	-	2500	933	800	1233	200	2400
ANGLE	07	05	352	354	350	347	358	00

AVERAGE ANGLE = 357 . TOTAL ANGULAR RANGE = 20 . AVERAGE SPEED = 1344 m/sec.

Fig. 6.19. Equatorward motion of a supersonic arc observed at Inuvik about 24 minutes after zenith crossing of the poleward expansion. Parts (b) and (a) show the same format as before.

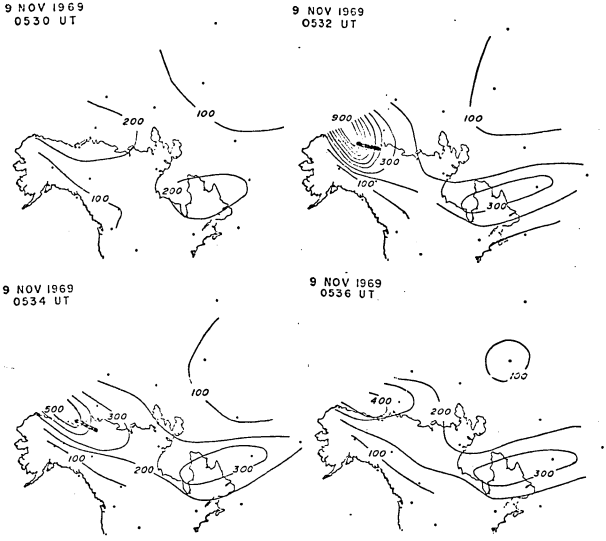

Fig. 6.19 c. Maps of geomagnetic disturbance showing position of auroral arc.

complicated, and the representation of its deeply indented configuration by a single straight line is misleading. What was done in this case was to adhere fairly closely to that portion of the arc which was fairly straight near the geomagnetic meridian.

Concerning all four of the figures (6.16-6.19), a very interesting and outstanding feature of the four is that in the both numerical order and chronological sequence in which they appear, there is an overall increase in average speed of the auroral forms. This value was computed for each case by dividing the total distance covered by the arc during the time period of observation by the total time of that same interval. It also happens that there is an overall increase in the local intensity of the geomagnetic disturbance in step with the increases. The peak speed in individual cases occur during the peak magnetic disturbance of the interval (0518, 0532 UT), or after the peak (0524, 0534:30 UT), and other cases are indeterminate due to improper matching of the map and camera frame times. One reason for this is that the maps over this period were preselected at a time interval of two minutes, whereas the camera photographed every 30 seconds. Obviously, an even finer time sequence of maps is necessary across some periods of interest in order to maximize correlations.

A summary of some of the data concerning the four arcs studied in the four previous figures is shown in Table 2. The columns represent: the time interval of the arc sequence, the time of the first observed supersonic motions of the arc, the horizontal distance of the arc from Inuvik, and the inclination angle to the horizontal that the form made

TABLE 2: Comparison of the distances from Inuvik fo the times of first supersonic motion of four arcs with the distances computed by ray-tracing and also the predicted AIW (see text)

Time Interval	Supersonic time	Dist at SS time	Inclination angle	Projected Distance	Travel Time	Zenith crossing	Average azimuthal	Predicted AIW time
0516-0519	0518	32 km	73°	32 km 34 km	5.6 6.3	0519	38°	SS-0523,24 Z_p-0525
0520-0524	0521	107 km	45°	106 km 100 km	7.9 8.0	0524	348°	SS-0529 Z_p-0530
0526:30-0529:30	0527	179 km	31°	186 km 152 km	11.0 10.2	stopped near 0529	08°	SS-0537,38 Z_p-0535
0530:30-0534:30	0532	125 km	41°	120 km 111 km	8.5 8.5	0534:30	357°	SS-0540:30 Z_p-0540:30

at Inuvik. In the following column I attempt to compare the horizontal distance of travel for an acoustic pulse, inferred from a ray tracing program for a source height at 110 km and 100 km (top), with the distance of the auroral form (column 3) assumed to be emitting a pulse at the angle given in column four. The next column (6) shows the travel time for an acoustic ray at the arrival angle of the amount given in column 4 for each of the source height mentioned. Column 7 shows the approximate zenith crossing time of the auroral arc. The final two columns show the average direction of motion of the auroral form, and the predicted time when an infrasonic pulse would be generated either from the earliest supersonic motion (SS), or after the zenith passage (Z_p) of closest approach of the arc to Inuvik, based on travel time due to ray tracing.

The strikingly interesting points contained in this table are, first of all, the fairly close estimate of the horizontal distance of an acoustical pulse emitted at the known distance of the aurora (column 3) compared to that given by ray-tracing (column 5). The closest estimate of that distance is given by the ray-tracing whose source height is at 100 km (see Appendix II). The predicted arrival time of an infrasonic pulse as shown in the last column of the table was obtained by using the travel time obtained from both of the ray tracings mentioned for the distance given in column 3 and applying it to the time of first supersonic motion. Then a simple 6-minute delay was added to the zenith crossing time to compare it also. Following the computation of predicted time of an acoustic pulse, the pressure records were searched near the time in question to see if indeed, a pulse was really there and from

what its direction was.

Reference to the sample of the pressure record of Inuvik presented in 6.16 (a) indicates that the first arc (0516-0519 UT) does not correlate with a disturbance at the predicted times. There is coherence in the record at the predicted times for the next arc, but the signals could not be scaled to an azimuthal error range of less than 10°, so they were omitted from the study. The predicted times of signal arrival for the next two arcs pertain strongly to the group of large amplitude pulses which arrived between approximately 0536-0543 UT. The arc sequence 0526:30-0529:30 UT correlate with a reasonable delay time from the earliest time of supersonic motion to predict an arrival time of 0537,38 UT depending on which source height for the ray tracing is used. The predicted arrival times are nearly perfect. However, the entire range of direction of motion of the auroral form is between 14°-359°, whereas the closest wave in this wave train was from 48° ($\Delta\phi$ - 2°) at that time, and next closest was at 55° ($\Delta\phi$ = 1°).

The predictions of the final form is very striking, by contrast, because its prediction of a pulse at 0540:30 UT from both the earliest time of supersonic motion as well as the zenith crossing time are precise! As it happens, the form in question was the very complex form mentioned earlier, and the direction of travel of the portion of the arc near the geomagnetic meridian did range over the azimuth of 354° scaled for the actual infrasonic wave. Moreover, because the agreement of the ray tracing for the source at 100 km with the distances mentioned earlier, this tracing was used to compute the horizontal distance of

the source of an acoustic pulse received at the arrival angle of the correlated signal. For the 0540:30 signal, the trace velocity was 494 m/sec. and inclination of its wave normal was computed to be 49°. The ray tracing travel time for a ray of ground angle 49° would be about 7 1/2 minutes from a horizontal distance of 84 km and would result in a signal origin time of 0532 UT. This time, as a glance at Figure 6.19 will show, corresponds to the time of fastest motion of the auroral arc, and also corresponds to the largest magnetic perturbation of the entire substorm. A slight extension of the azimuths over which this complex auroral arc travelled would doubtlessly include those covered by the rest of the waves in this wave train with reasonable delay time, thus the association of this wave group with the dynamic processes related to this rapidly moving auroral form seem quiet definite. The correlation made here is quite consistent with many features of the model of Wilson (1969).

(b) Correlation of AlW at both Stations

In section 6.4(a) of this chapter, the reception of large amplitude pressure pulse scaled at a trace speed lower than local acoustic velocity was discussed. The occurrence of this event closely following the poleward expansion and an equatorward-moving supersonic arc was also noted. It should be pointed out at this time that other less-coherent signals were noted spasmodically in the pressure records at both College and Inuvik prior to the poleward expansion, but owing to scaling difficulties of the noisy signals, only a few were actually listed among the infrasonic observations for this night.

In order to give an overview of the pressure disturbances at the two stations, the superposed traces for the four stations at College and the four stations at Inuvik are presented in Figure 6.20 (a) and (b). They cover the time period from 0510-0730 UT which represents the post-expansive phase periods of the polar magnetic and auroral substorms. The numbers shown above the traces display the measured azimuth and error range in azimuth (parens) for the wave pointed to by the arrow. These scalings represent the outermost azimuths centered about the grouping of the other signals scaled for the night which are discussed later in this section. As this figure shows, the earlier large amplitude pressure signals were recorded at Inuvik near 0521 UT, while the most coherent large amplitude signals were not recorded at College until near 0604 UT. At both stations, the AIW events can be classified mostly as Mmi (see Appendix I). Ignoring for the moment the noisier, lesser coherent and lower amplitude signals in the College record prior to 0604 UT, it would appear from looking at the 'best' signals alone that the disturbance source was located to the north of both stations. Inuvik receives the disturbances, in this view, about 43 minutes prior to the reception at College, which represents a reasonable propagation time between the two stations.

Looking closer at the signals scaled at the two stations for 9 Nov. 1969, attention is now directed to Figure 6.21 a and b. Part (a) of the figure shows the total signals scaled at the College observatory between the hours 0354-0638 UT inclusive; Part (b) of the figure shows similar rays which represent the azimuths from which the

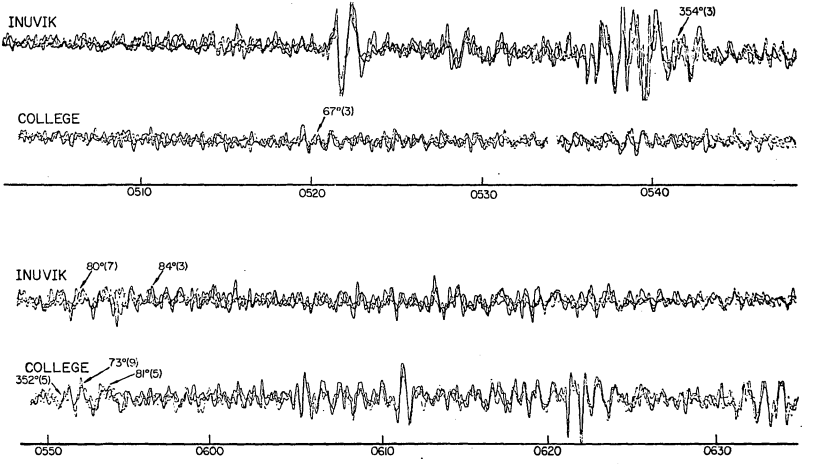

Figure 6.20(A) Superposed pressure records of the four channels at College and Inuvik to show the coherent waves received following the expansive phase of the auroral and polar magnetic substorms. Numbers show azimuths and azimuthal error range (parens) of waves differing in direction of travel from the average of the others.

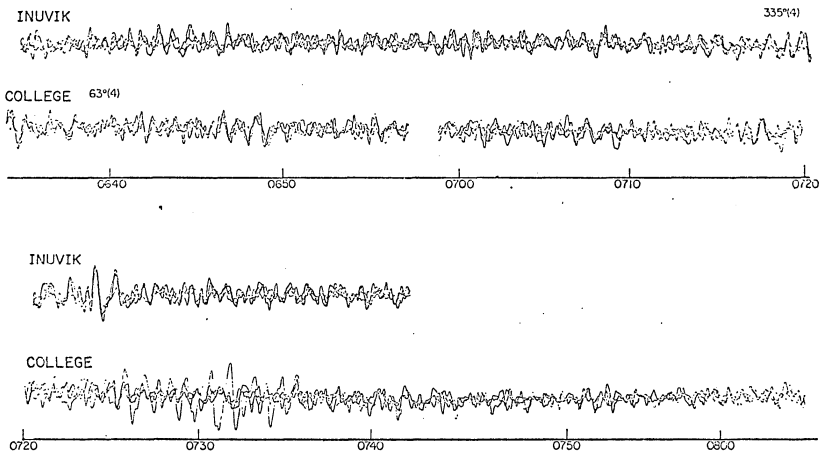

Fig. 6.20 b. Continuation of the pressure traces of part (a) of this figure.

pressure disturbances were received from 0317-0720 UT inclusive. Both diagrams represent sketches to show the relative positions of the scalings of azimuth, but are uncorrected for great-circle curvature which would render them slightly concave towards the equator.

As the Figure 6.21 shows, there is a tendency for most of the signals to cluster about the northeast direction centered closely to 40° at College and slightly greater than that value at Inuvik. The azimuths of the signals which are apart from the clusters are labelled to correspond to the waves specified in the pressure traces shown earlier in Figure 4.16 (a) and (b). Returning to this former figure, one will note that the waves which are specified as not belonging to the central clusters (all others on the pressure records to) are in each case the noisier, longer period, and less-coherent waves. Note also that with the exception of the AIW from 65° which was received at College at 0413 UT, all of the remaining signals in the diagrams of Figure 6.21 (a) and (b) occurred during the time-span of the pressure record in Figure 6.20 (a) and (b).

A further tendency for the signals received at College and Inuvik to cluster about 40° is shown by the graph of number of signals vs angle of arrival in Figure 6.22. Here the total number of signals observed for nearly 6 1/2 years at College, 1 1/2 years at Inuvik, and 5 months at Stevens Village, Alaska, show a strong tendency to peak about 40° at both College and Inuvik, but less so at Stevens Village for the much smaller data sample.

Inasmuch as the data for the night 9 Nov. 1969 reflects the overall morphological tendency for largest number of signals to conjoin near the northeast direction of 40°, it would appear that there must be some fairly

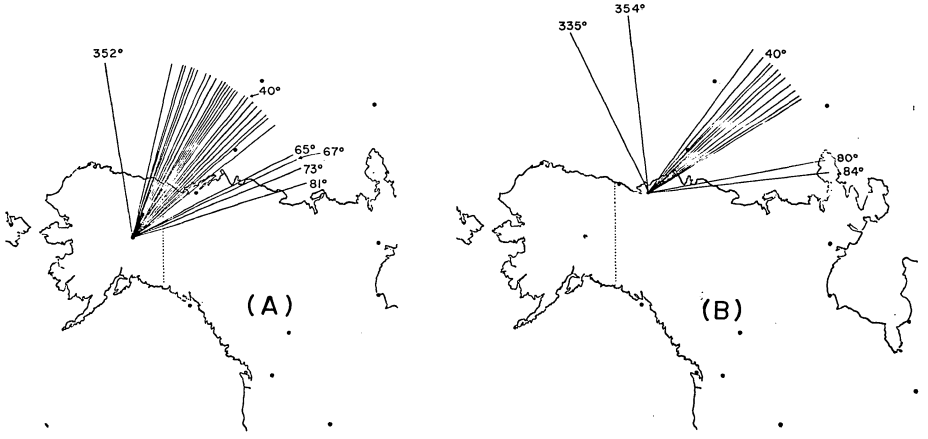

Fig. 6.21. Diagrams showing rays from the station at College (a) and Inuvik (b). The rays represent the directions from which pressure disturbances were received at the two stations on the night of 9 Nov. 1969. Numbers on the rays display the actual azimuths of the perturbations which are shwon in Fig. 4.16.

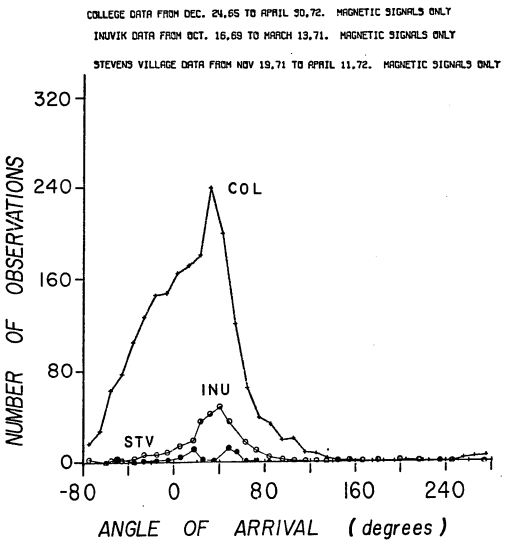

Fig. 6.22. Distribution of the total number of signals recorded at College, Inuvik and Stevens Village for the dated indicated, versus the azimuth from which the signal was received.

permanent feature of either the upper atmosphere or the generator of the AIW which results in a preferred direction for the propagation of infrasound. An argument for the latter choice will be presented in the discussion section of this chapter.

(c) Source Region for College AIW

The association of the most outstanding wave packets of AIW received at Inuvik with equatorward drifting arcs was shown in sections 6.4 (a) and 6.4 (a) 1 of this chapter. It remains now to specify the inferred generation regions of AIW for College bearing in mind that clouds at College excluded any reliable ASC coverage during this period.

The location of the source regions for the AIW received at College was ascertained by use of the contoured geomagnetic disturbance maps as depicted earlier in Figure 6.2, and invoking the mean horizontal transit speed of 243 m/sec. (MTS) deduced in the 25 June 1969 study of chapter 3. Procedurally, the arrival azimuths of the College signals were correlated to the locations of the AEJ portions of the geomagnetic disturbance and the resulting location and time recorded from the map in question. From these two quantities and the arrival time of the signal and the geographic location of College, both a projected propagation time and great circle travel distance could be computed. Having affixed these quantities, the MTS was then used to predict an arrival time of a signal from the inferred location selected from the maps. The resulting time as predicted by this procedure was then compared to the actual AIW record at the predicted time to see if there was really a signal

present, and if there was, to observe whether its azimuth correlated with the location of the disturbance area previously located on the maps. The results of this procedure are shown in Figure 6.23 (a) and (b).

The arrows in some of the maps in Figure 6.23 show the azimuths along which the AIW travelled, and their terminus shows the inferred location of the origin of the signal. Insert times show the arrival times of signals whose origins are correlated on the particular map. Maps not containing arrows show times of interest which did not correlate with the received AIW at College. Reference to the map sequence in Figure 6.2 is recommended in conjunction with this figure so as to retain the continuity omitted in the present figure. Moreover, further reference will be needed to Figure 6.20 in order to review the AIW studied here. In all of the correlations entered in the present figure, the times predicted by the aforementioned procedure agreed with the actual arrival time within one minute or less.

Part (a) of Figure 6.23 shows the source location of two of the earlier signals received at College and the time of the map indicates the onset time of the substorm as discussed earlier in this chapter. The presubstorm 200 gamma disturbance north of Inuvik at 0450 UT and the 400 gamma disturbance near Barrow at 0508 UT - during the auroral poleward expansion - do not correlate with AIW received at College. The intensification of the geomagnetic disturbance northwest of Inuvik at 0512 UT correlates with a sequence of signals received at College which represent the onset of equatorward auroral drift from the location of the AEJ near Inuvik. The decrease in the disturbance level of geomagnetic

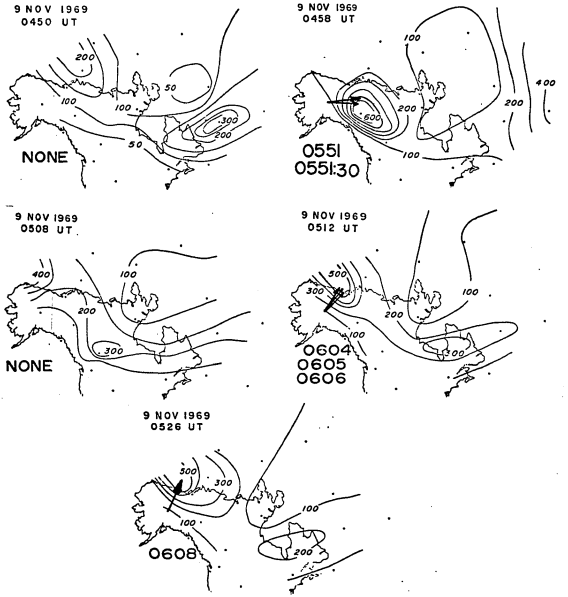

Fig. 6.23 a. Location of source regions for the AIW received at College on 9 Nov. 1969. Arrows show azimuth and location from which AIW arrived. Arrival time of AIW shown in inset.

activity which followed as evidenced by the map at 0522 UT, did not correlate with the reception of AIW at College, but the increase at 0526 UT did. Again, this time correlates with the time of equatorward motion of arcs at Inuvik which were studied in section 6.4 (a) I of this chapter.

Part (b) of Figure 6.23 continues the correlation of the AIW received at College with inferred source regions on the maps of geomagnetic disturbance. The signals, as they arrived in sequence at College, corresponded to the maps indicated, while the intervening waves all fell closely in time and azimuth to the ones presented here. From 0538-0544 UT, (the maps for interim period not shown in this figure) there appeared to have been continuous emission of infrasound which correlated with reception at College, and quite sharply near 0546 UT, the correlation ceased, and no further disturbances were received at College. Despite the onset of an intensification near Barrow of 500 gammas, no further AIW could be successfully scaled in the College records, and no correlation with this sudden increase in disturbance could be made. Near 0646 UT, there appeared three cycles of noisy coherence in the College AIW records which could not be scaled within the acceptance criteria established for this study. Following this period (see Figure 6.20 (b)) there appeared only unscalable vague coherence in the College record which lapses to completely incoherent by 0720 UT. Thus it would appear for all practical purposes, that the period following 0544 UT resulted in no further infrasound detected at either College or Inuvik for the remainder of the study period, despite subsequent intensification of

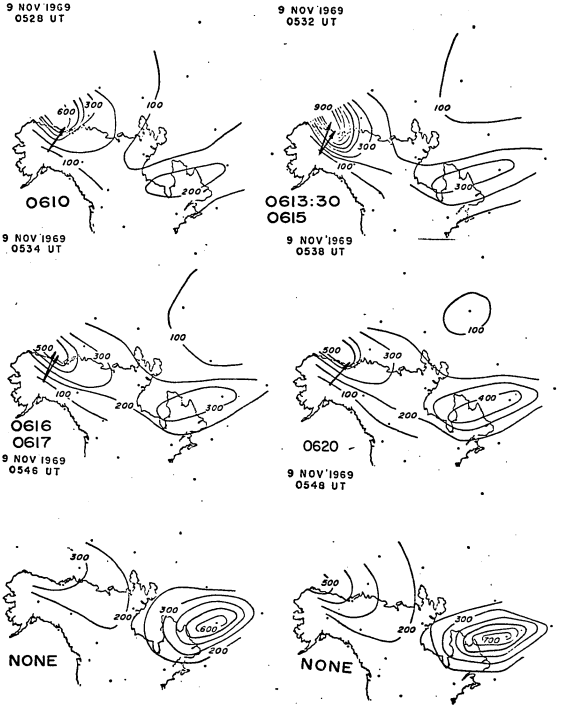

Fig. 6.23 b. Location of source regions of AIW received at College on 9 Nov. 1969. Arrows etc. as per previous figure.

the electrojet north of Inuvik following 0610 UT.

To ascribe a morphological pattern to the correlations of AIW to the substorm as learned from Figure 6.23, the onset of the substorm generated AIW westward as detected at College at 0551 UT, but not northward as detected at Inuvik (the latter point not illustrated in the figure). Intensifications of the substorm west - in invariant longitude - of Inuvik led to no AIW there with the possible exception of a single cycle at that station at 0720 UT. On the other hand, while the substorm intensified west of Inuvik many times, as the figure shows, many AIW were received at College until the substorm waned somewhat. Then the substorm intensified west and north of College at 0548 UT with the same result: no further AIW was received at College. The period of time productive for AIW for both stations from 0512-0544 UT was characterized mainly by equatorward auroral drift.

A review of the maps of Figure 6.23 shows that there seemed to have been a preferred geometry of AIW reception with the magnetic disturbance in order for a given station to detect AIW on the night of 9 Nov. 1969. The maps containing arrows which point to the inferred location of origin of the AIW are taken to be the instantaneous picture of the magnetic disturbance at the time of AIW genesis. Those containing no arrows are the maps from which no signals were detected. When the disturbance cell was oriented south of the station (0458 UT); no signals were detected (Inuvik).

The elongation of the electrojet depicted by the maps is roughly parallel to an invariant latitude line. If one imagined meridians to

such a system, they would roughly coincide to the general direction of the equatorward auroral drift. If one then imagined such a meridian line segment placed at the end of the contoured magnetic disturbance cells as depicted at 0508 UT at the location of the part of the 300 gamma contour north of Alaska, it would be directed toward the west of Alaska. This would also be the case at 0548 UT for the 500 gamma intensification near Barrow. These were times which did not correlate with the reception of AIW at College or Inuvik.

On the other hand, if one similarly noticed the direction of the invariant geomagnetic meridian near the eastern ends of the intensified disturbance at 0512, 0526, 0528, 0532, 0534 and 0538 UT, one sees that an extended auroral form as depicted earlier on the maps (Figures 6.16c, 6.17c, 6.18c and 6.19c) would indeed be heading in the general direction of the College station. This observation correlates very strongly with the original morphological features associated with the generation of an AIW pulse by Wilson (1967), and also contains some implications of a finite beam width of the outgoing signal. Thus the meridional auroral drift about the eastern edges of the magnetic disturbance of the auroral electrojet explains both the onset and cessation of AIW signals at both College and Inuvik in the post-expansion phase. During the pre-expansive phase, no AIW were detected at College, and Inuvik. The onset of the substorm in western Canada (map 0458 UT, Figure 6.23a) did generate infrasound detectable at College, and in this case, the western edge of the intense disturbance appeared to be the probable location of origin.

To relate the observed AlW emissions and their inferred genesis regions to auroral morphology, the AlW observed at College which were associated with the substorm onset in western Canada at 0458 UT were likely related to westward travelling surges which propagate into the evening sector. The fact that the subsequent motion of the intense portions of the electrojet situated it west of Inuvik, the latter was still situated in the evening sector - or early night - which is a time that is not favorable for eastwardly drifting auroras. These auroral motions in conjunction with local time are features of the model of Akasofu (1964).

6.5 Discussion

The study of the infrasonic pressure disturbances generated during the polar magnetic substorm of the night of 9 Nov. 1969 has been pursued here with the view of maximizing the use of supplementary data needed to study the subject successfully. Many details were given concerning the general features of the auroral and magnetic substorms in progress during the arrival time of the signals, and special attention was given to portions of these substorms that bear a closer look. Rather than proceeding with the view that the phenomena concerning the generation are well known and understood, this investigation has attempted to observe the subject from many viewpoints, hoping that at some point within this investigation or in subsequent research by others, a consistent picture will emerge.

What was not brought out explicitly in the main text was that the pressure disturbances studied across the time period followed in this

chapter comprised the large portion of the coherent infrasound received at both station during the course of the night. Despite this fact, the more intense substorms of the UT date 9 Nov. 1969, proceeded with very little detection of infrasound even though the observing conditions were not hampered by wind noise. Since this is not an unusual situation, the subject is still open to investigation and remains unanswered here. At this point, only conjectures can be made. The question is still open as to whether the infrasound is not being generated or simply not being received, the latter choice implying many unknown facets of the propagation conditions.

A very interesting and potentially significant association was made in this chapter concerning the generation regions within the substorm which are important for infrasound production. It refers to the association of the eastern and western ends of the auroral electrojet as being prolific centers of AIW generation. This includes the case in which the electrojet is unevenly distributed along its own longitudinal axis, and in which a new intensification is observed within the belt along which the electrojet is flowing. The cases studied in this chapter showed that these eastern ends of the jet were the locations in which supersonic aurora were observed moving meridionally.

An extension of this association may be made by returning to the original map sequence in the beginning of the chapter, Figure 6.2 (d) and 6.2 (e). Here it can be observed that following the correlation to the preceeding maps after 0458 UT with AIW production, a period begins after 0600 UT when the substorm becomes more intense and spreads

continuously along a wide belt from the very early morning sector through the evening sector (note arrow depicting local midnight meridian). During this intensive and extensive areal development of the auroral electrojet, there was little or no detectable infrasound at either College or Inuvik. The uneven intensities in the electrojet shown by the 700 gamma disturbance at 0640 UT, the 500 and 600 gamma contours at 0650 UT, and the 400 and 500 gamma contours at 0700 UT, all have their eastern edges well east of the two observatories at College and Inuvik. In conjunction with the associations made in this chapter, these locations would be unlikely to be effective producers of AIW at the stations mentioned.

Another interesting outgrowth of this chapter is the use of the ray tracing technique and mean horizontal transit speed derived in chapter 5. Ray-tracing was used for the correlation of a wave packet received at Inuvik which appeared to have been generated within 125 km of that station. For greater distances, the MTS was used in order to account for the AIW which appeared in the College record. The usefulness of the latter number (243 m/sec.) for these correlations cannot be overemphasized, because by simply intersecting the arrival azimuth of the AIW with the axis of the auroral electrojet, and applying the MTS, the arrival time of a given AIW could be predicted within the minute or less of its actual arrival. If, on the other hand, a speed of 255 m/sec. were used over the average of roughly 700 km baseline, an error by as much as 2 minutes would have been predicted for the arrival time of the AIW. In no case was such a wide margin of error experienced

using the 243 m/sec. value.

In addition to using the MTS as an indispensable tool, the procedure of contouring was also justified in that the combination of these two creations gave a consistent picture of the location of AIW generation. The lesson learned from the analysis of the 31 October 1968 data in chapter 4 was that a large number of maps would be needed to get closer to the configuration of the magnetic disturbance at the time of generation of the signal. It was seen in this chapter that across certain critical time periods during the substorm, the 2-minute mapping interval was not always sufficient to show the continuity. The procedure itself is quite cumbersome to apply, however, and the most effective use of it for AIW studies should only be those occasions where the most complete coverage of magnetometer and other supplementary instrumentation is available.

CHAPTER 7

DATA NIGHT 12 NOVEMBER 1969

7.0 Introduction

The night of 12 Nov. 1969 was selected for study for three reasons: (1) there were no AIW signals received at either of the two infrasonic observatories, College and Inuvik; (2) there were polar magnetic disturbances present; and (3) there was All-Sky Camera coverage available from six stations in and around Alaska. The main effort in this chapter is to study the motions of aurorae about the contours of geomagnetic disturbance on the one hand, and to attempt to observe any noticeable contrasts with the other nights studied in this report in which there was reception of auroral infrasound.

7.1 Geomagnetic Activity

The geomagnetic disturbances studied in this chapter were based upon hand-scaling of magnetograms from 21 magnetic observatories on and around the North American continent. The location of these observatories is shown on the chart in Fig. 7.1. Also shown on the chart are circles around the stations which had All-Sky Camera data available. There was no magnetic data available from Kotzebue and Ft. Yukon, however.

The period of time selected for analysis was the relatively geomagnetically active period between 0810-1200 UT. A selection of magnetograms from some of the observatories is shown in Fig. 7.2.

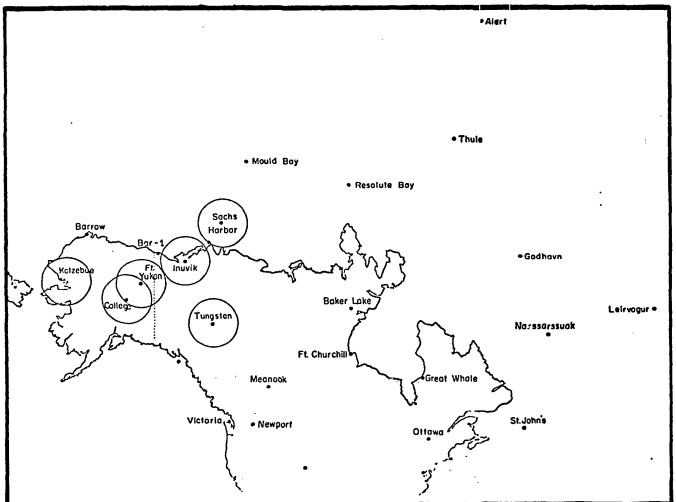

Fig. 7.1. Station location chart of magnetometer stations (dots) and All-Sky Camera stations (circles).

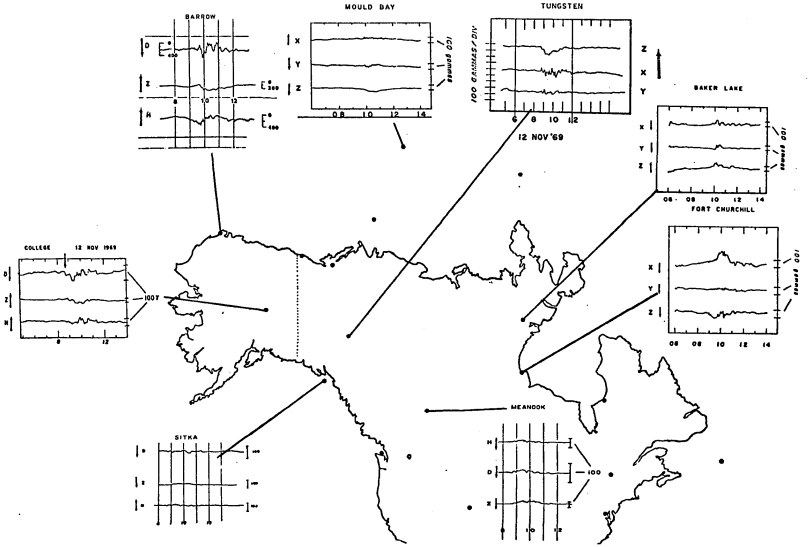

Fig. 7.2 Selection of magnetograms from some of the stations whose data are used in this report for the night of 12 Nov. 1969.

Each component of the magnetograms was scaled generally at an interval of 10 minutes throughout the study period. The reference level used was the quiet day curve generated for the same quiet days as discussed for the data of 9 Nov. 1969 in chapter 6 of this report. Following the digitization of the magnetograms, the three components were reduced to the total magnetic disturbance vector $\Delta F^2 = \delta X^2+\delta Y^2+\delta Z^2 = \delta H^2+\delta D^2+\delta Z^2$, where the quantities on the right hand side are the difference between the quiet day level and the perturbed level of the particular component.

As in the previous chapters of this report, the magnetic disturbance activity is studied from the vantage point of contours of the total disturbance vector. The contour interval selected was 50 gammas. The display of the magnetic disturbance maps for the study period of 0810-1200 UT is shown in Fig. 7.3 (a,b, & c). The arrows drawn at the location of the All-Sky Camera stations indicate the general direction of motion of the visual aurora as inferred from cinematic projection of the All-Sky Camera film. In the cases where no arrow is present, the interpretation to be given is that either no aurora was visible, or the visible aurora did not have a detectable motion at the particular instant timed by the map. No attempt was made to distinguish between these two cases because only the features significant to the generation of infrasound are of interest here. The location of the auroral electrojet is taken to be in the most disturbed part of the magnetic disturbance contours as was indicated in the earlier chapters.

At the beginning of the study period as shown by the maps in Fig. 7.3, the oval is situated in high latitudes around Sachs Harbor from

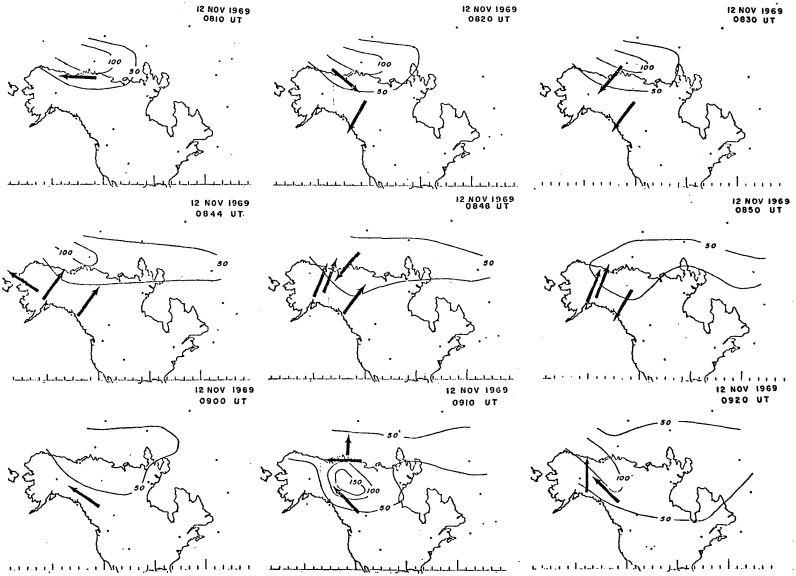

Fig. 7.3. Contoured maps of geomagnetic disturbance for 12 Nov. 1969. Contour interval is 50 gammas.

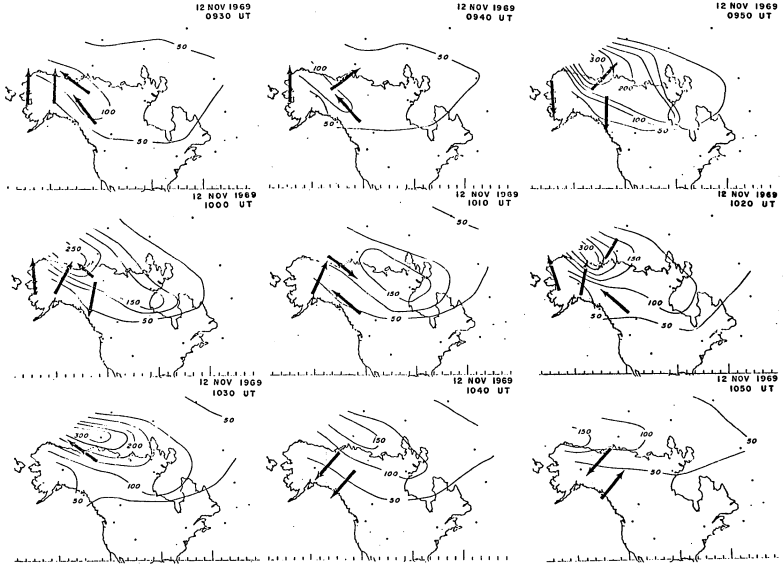

Fig. 7.3 b.

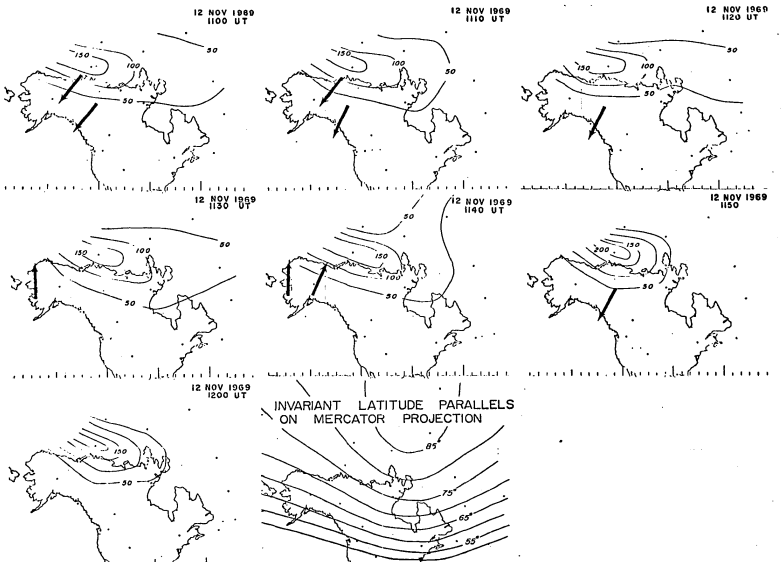

Fig. 7.3 c.

0810-0844 UT. At 0840 UT, the onset of an auroral substorm is indicated by the brightening of an auroral arc over Tungsten Canada. Subsequent brightening begins at College about 4 minutes later. Following this brightening of the arcs at the two stations, the arcs then commence to drift poleward. The most brightening and motion takes place at Tugsten where the polewardly moving arc averaged a speed of more than 2700 m/sec. contrasting to All-Sky Camera frames at the onset are shown in Fig. 7.4. It can be seen in this figure that the auroral electrojet is well north of the area in which the arcs brighten, and the arcs then commence motion toward it. Arrows in the body of the magnetograms show the time of substorm onset, and the arrows on the maps show the motion of the aurorae. It is obvious from the maps that the disturbance level near the substorm onset is less than 50 gammas.

Returning again to the contour maps in Fig. 7.3, it can be seen that there was a general northerly drift of auroral forms at College, Ft. Yukon and Tungsten after the substorm onset. A reversal in direction was seen at Tugnsten near 0850, and then there was a return to north to northwesterly drift at these stations. No aurora was visible at Kotzebue until near 0843, which was close to the brightening of aurorae near College. Near 0950 UT, the magnetic disturbance reached the peak value for the period, and the motion of the auroral forms became somewhat erratic at the various stations. At times between 0950-1030 UT, the general drift is toward the electrojet, and at other times, it is away from it. By 1030 UT the electrojet is well north of the Alaskan border, and the aurorae (not shown) have disappeared at Kotzebue,

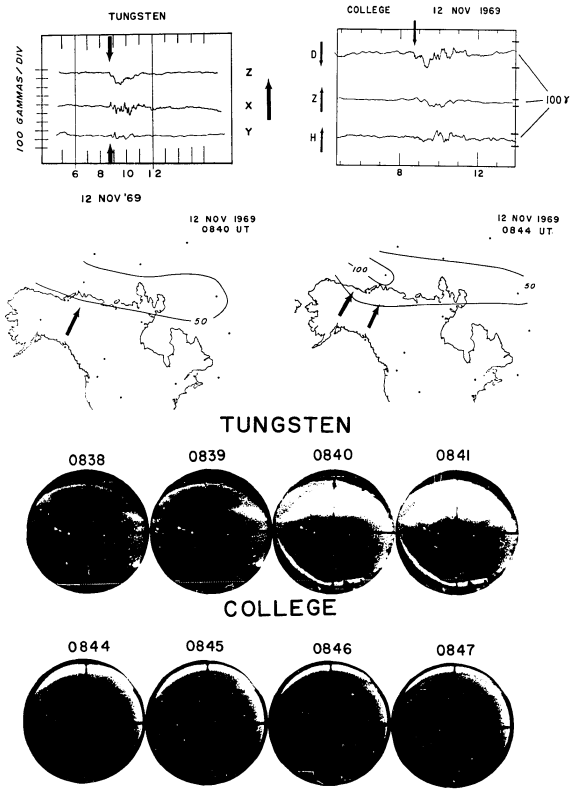

Fig. 7.4. Onset of the auroral substorm as seen at College and Tungsten as viewed by arrows on magnetograms (upper) showing times, arrows on maps showing direction of motion (middle), and by ASC frames.

are very faint at Tungsten, College and Ft. Yukon, but show up brightly in the northernmost parts of the Inuvik sky. At this time, it was cloudy at Sachs Harbor. Faint forms or no aurora dominated most stations after 1030 UT, although Tungsten and Inuvik had detectable motions of aurorae, and even some aurorae could be seen through the clouds at Sachs Harbor near 1100 UT.

7.1 Significant Features for AIW

Viewing the information contained on the maps in Fig. 7.3 from the point of view of the known morphological characteristics of AIW generation, little infrasound would be expected near the pre-substorm times before 0840 as the drift was subsonic. The supersonic poleward expansions would not be expected to produce infrasound (Wilson, 1971), and drift near College is mainly northerly until 0950 UT. At that time there was an increase on the level of the magnetic disturbance north of Alaska, accompanied by a brightening of auroral forms at Inuvik (not shown). Again the conditions taken to be necessary for AIW generation are not met because the aurora at Inuvik is moving northward, and little motion is discernible of the aurora visible at College and Ft. Yukon at 0950. Auroral drift is still in an unfavorable direction at both stations at 1000, and 1010 UT, but at 1020 UT, the conditions look promising for detection of an AIW pulse. The aurora is moving toward Inuvik, and there has been an intensification in the level of geomagnetic disturbance.

A measurement of the speed of the auroral form moving across the

Inuvik zenith at 1020 showed it to be a diffuse form travelling more than an average of 2100 m/sec.. Though the auroral form is not pictured here, from 1038-1040:30 UT, an arc passed through the zenith at Inuvik moving in the general direction of College. The arc was travelling at supersonic speeds, and averaged about 820 m/sec. over the period mentioned above. These two arcs above all others met the apparent criteria for AIW generation and led to a search of the pressure records for the signal.

A sample of the pressure records from College and Inuvik is shown in Fig. 7.5 for the critical times in question. If the 1020 UT arc at Inuvik had produced a signal detectable at College, using the mean horizontal transit speed of 243 m/sec., the arrival time of the AIW would be expected near 1111 UT. For the auroral form studied from 1038-1040:30 UT at Inuvik, the signal arrival time at College for an AIW generated by it would be near 1128 UT. Arrows placed on the College record at these times show that no coherent infrasound appears in the record at that or any other time for the period shown. A vaguely coherent pulse near 1122 UT does not scale within an acceptable range to merit being called a recognizable wave.

At Inuvik, the 1020 aurora would have produced a pulse expected from 7-10 minutes after the zenith passage of the arc, or near 1027-1030 UT. Only a transient power failure on a single channel stands out in the interval for an expected acoustic pulse from the aurora. For the 1038-1040:30 arc at Inuvik, the expected arrival time of an AIW would be near 1045, approximately. Again there is no detectable

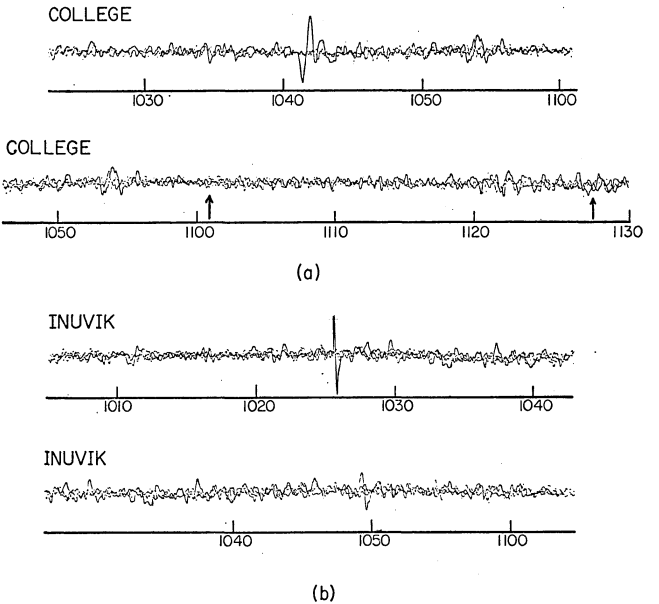

Fig. 7.5. Pressure records from College and Inuvik showing absence of AIW coherence throughout selected span and at times indicated by arrows. (see Text)

coherence in the record near that time.

7.3 Discussion

From the point of view of AIW morphology, it was quite understandable why no AIW emissions were observed at the ground for the two observing sites for most of the study period. The motions of the auroral drift was either mainly subsonic, or away from the observing station. Viewing the maps alone, the time at 1020 UT looked very favorable for signal generation because the location and orientation of the contours were very similar to the 0526 UT map of the 9 Nov. 1969 data studied in chapter 6, and the latter case correlated with AIW production. There was one noticeable difference between the two cases however: the 9 Nov. 1969 disturbance was 200 gammas greater at the time. Both had supersonic auroral motion associated with them, but the one studied here had an average speed of more than 2100 m/sec., whereas the 9 Nov. arc had an average speed of 833 m/sec.. This latter contrast in speeds is consistent with the theoretical findings of Fedder and Banks (1972), Swift (1973) and is implied in the early shock wave mechanism of Wilson (1967). All these researchers findings show that the higher the Mach numbers above Mach 1 produce lower amplitude pulses.

On the other hand, the equatorward arc commencing at 1038 UT at Inuvik was rather thin in visual width and low luminosity. It was in the 800 m/sec. speed range, so one is left to invoke numerous other reasons why no AIW was detected at either station for this event.

CHAPTER 8

Conclusion

The central purpose of this investigation has been to study the morphology of auroral infrasonic waves within the framework of the auroral and polar magnetic substorms. The main thrust of the study was to attempt to locate those areas within the magnetic substorm which were possibly significant insofar as the production of AIW is concerned. It was also an intent of this study to specify the time periods during the development and decay of the substorm when the production of infrasound was likely.

In keeping with these overall aims, the most general statement concerning the location and times of AIW production within the polar magnetic substorm relates the AIW to the auroral electrojet at times of onset, expansion and recovery phases. The poleward expansion of the auroral arc does not, in itself, seem to be associated with AIW, but some AIW emission westward of the area undergoing magnetic intensification at the time of onset has been detected. Following the time of the auroral poleward expansion, there is frequently observed an equatorward motion of aurora within 10 minutes or less which did correlate with AIW production on two of the four nights studied here.

The latter conclusions are based upon the observations of the data nights 31 Oct. 1968 and 9 Nov. 1969. Further conclusions based upon these two nights lead to the finding that the geometry of the station with respect to the electrojet is important. A station located

near the central meridian of an intense electrojet with little, if any, auroral infrasound detection. This is adequately borne out during the 1000 UT substorm of the 31 Oct. 1968 data where it was shown that after the auroral reversal in direction following the poleward expansion observed at College, the jet expanded rapidly east- and westwardly. From 1047 UT through 1121 UT (see maps Fig. 4.3, chapter 4) College was situated well away from the ends of an intense (greater than 1000 gammas) magnetic perturbation due to the electrojet. During the entire span of time, only a few cycles of coherent AIW were recorded at College.

It is further concluded from the 31 Oct. 1968 and 9 Nov. 1969 data that the eastern end of the electrojet system is a prolific source region for the production of infrasound. In the case of the 31 Oct. 1968 data, the best correlation by triangulation from the stations at Pullman and Boulder for the 1000 UT substorm showed the origin point of the infrasound to be at the eastern end of the jet. In the subsequent substorm at 1337 UT when the College station was near the eastern end of the electrojet disturbance, coherent AIW was received at College for many hours. For the 9 Nov. 1969 data, it was shown that the intense onsets of magnetic disturbance within the electrojet produced AIW at College when the eastern end of the disturbance was situated in a general meridional direction from the station. The association with supersonic aurora during the generation time was also shown.

Despite the association of the generation of the AIW with supersonic arcs for many years at College, there are still features of the

generation of AIW which bear further study. For example, if the association of AIW with generation near the ends of a current system holds as a persistent feature in future data, the relationship of the locale and the supersonic aurora observed there bear further study. Whether or not the ends of the electrojet are more likely the place to find the supersonic motions is not covered by this study, but one might reasonably ponder the question. It would also be reasonable to question the role of Birkeland currents and the relationship to the supersonic aurora and associated infrasound in the vicinity of the ends of the ionospheric portions of the current system. In the case of the 1337 substorm of the 31 Oct. 1969 data, despite the general auroral drift to the east and southeast throughout the substorm, many AIW were scaled from the direction east of north. In one case (Fig. 4.12, chapter 4) there was a fairly smooth succession of azimuths ranging from northwest to northeast which correlated with the passage of a rayed arc from west to east, after a propagation delay time. Fitting the latter association into a simple bow wave model requires rather complex motional geometry.

A conclusion arising out of the 9 Nov. 1969 and 25 June 1969 data is that increases in the level of geomagnetic disturbance in the region of N. America and Greenland specified as the signal source region (SSR) does not correlate with rises in amplitude of background noise in the 10-100 sec. period range. Increases in vague coherence and coherence in the records were correlated with increasing magnetic activity in the 25 June 1969 data, however.

It is further concluded that the mean horizontal transit speed derived in this study has significant potentialities in locating the source of AIW, but its applicability to all seasons and years is still open to question.

The application of ray-tracing was found to be helpful for sources within 125 Km., but the best correlations came with the profile which assumed a source height of 100 Km.. Considering the fact that the profile used was a composite of lower atmosphere observations, a standard model upper atmosphere up to the mesopause, and an assumed computation of sound speed based upon a standard model thermosphere, ignoring winds, the good results achieved could have been a fortuitous occurrence.

Inasmuch as consistent and interesting findings were noted by utilizing the method of contouring the magnetic disturbance, it is also concluded here that the procedure is a justifiable one in order to achieve a spatial and temporal representation of the substorm.

The final conclusions of this study relate to the types of infrasound observed on the 10-100 sec. passband. First of all, many different types of AIW are found to occur on the chart records when they are viewed from their physical appearance. For the case of single and repeated impulse events, a distinct seasonal preference appeared which left open the question as to whether their origin was mainly due to:

1. AIW generator effects
2. equipmental effects
3. atmospheric effects.

If subsequent research finds the true cause to be the atmospheric effects, then both these and possibly other types of AIW as well as

the many other types of naturally-occurring infrasound seen on the passband might be useful indicators of particular features of atmospheric structure. The fact that the lower and upper atmosphere is frequently probed by any one of the many types of natural infrasound, each signal of which must contain some tiny signature of the propagation path, the understanding of these phenomena may lead to a better understanding of the atmosphere itself. Thus it is a final conclusion of this study that auroral infrasonic waves and the other types of natural infrasound, aside from the interest inherent in their own intricate nature, may well prove useful as a probe for the upper and middle parts of the atmosphere.

APPENDIX

The fact that a large diversity exists among the signal types which have been tentatively identified as AIW at the Alaskan arrays, a system of classification is proposed in order to systematize further research. Underlying the motivation behind this scheme is the possibility that recognition of these signals as specific types might lead to a better understanding of their generation, propagation, and thereby the potentiality of this naturally occurring source of infrasound as an upper atmospheric probe. The mechanics of the system are simple, and coded abbreviations are used which suggest as closely as practical, without too many re-occurring letters, the features for which they stand. The whole system is intended to describe the physical appearance of the signals on the 10-100 sec. passband, with no concern as to how they are produced or propagated.

The first breakdown of the signal types is dichotomous based on the number of cycles present in the signal: S, which means a single half cycle or full cycle impulse, and M, which means more than one cycle. It is obvious that this grouping is all-encompassing to this point, and a large number of sub-categories are now added which attempt to retain enough generality to cover possible wave types which have not as yet been observed. The entire system was based upon the examination of photographs of all the observed signals at the Alaskan arrays, and covers the classification of AIW signals only. Reference to page of this appendix will show an outline of the scheme with their appropriate codes in order to follow better the explanation which now continues.

The single impulse group is subdivided according to the sense (positive or negative) the initial impulse P or N of only a half cycle, or B, of a complete cycle, which is then subdivided in terms of which half cycle arrives first as shown on page . A repeated pulse group, R_3, R_6, and R_{11}, is entered under the single impulse category to account for the case in which a second impulse is found following the initial one. The characteristics of this group are described on the classification chart of AIW found in this appendix.

The multiple impulse events are divided into two types: F type, which have 5 or less cycles, and the m type which have more than five. Both of these subgroups are divided symmetrically based upon whether or not the waves show dispersive effects in successive cycles, how the frequency components are distributed sequentially, if it can be determined, and the repeated pulse category is used in both. The exception is the case of the MFW category, which refers to the presence of tiny high frequency waves whose description is given in chapter 3. The remaining parts of the sub-groups should be self explanatory, but some additional information concerning their recognition can be given.

Pictures of many of these AIW types are presented in chapter 2 Fig. 2.2. Since the major types are represented there and some of the groups may actually constitute a null set, no further attempt is made to search the records for an example of each sub-type. An example of a possible category with no members is the case of the set MFDB and also possibly MmDB. These sub-categories describe the usual dispersive

characteristics of wave trains of other kinds in that the low frequency components arrive first. When dispersive effects are recognizable among AlW, the situation is opposite, because the high frequency components seem to arrive first.

The sets MFl and Mml occur with such frequency in the records, that a few more words concerning them are in place. Frequently the waves in these two categories appear gradually out of the noise background and render their onset and cessation times indeterminate. For this reason, if one cannot determine when the wave begins or ends, then it follows that its dispersion features are indeterminate. On the other hand, it need not be noise which obscures the onset time of the signal, but the presence of other signals-see frame (13), chapter 2, Fig. 2.2 for a picture of this case.

Repeated pulses are of such a nature that they can be treated as a separate grouping altogether, but since a given component of the repeated pulse may have the characteristics of any of the other signal classes, the repeated pulses are included as a subgroup of the other classes. A given repeated pulse group may then be described first by the other classifications describing it followed by the proper subscripted R, i.e., R_3, R_6, or R_{11}.

Classification of auroral infrasonic Waves

S...Single impulse event
- P... Positive pulse SP
- N... Negative pulse SN
- B... Both positive and negative SB
  - 1. positive phase first SB_1
  - 2. negative phase first SB_2
- R_3...Repeated pulse 2 1/2 minutes later SR_3
- R_6... " " 4-7 " " SR_6
- R_{11}.. " " 8-12 " " SR_{11}

M...Multiple impulse event
- F...few cycles present only (less than 5) MF
  - U...nondispersed MFU
    1. positive phase first MFU_1
    2. negative phase first MFU_2
    3. Indeterminate MFU_3
    4. repeated pulse R_3, R_6, R_{11}
  - D...dispersed MFD
    - A...high frequency first MFDA
      1. positive phase first $MFDA_1$
      2. negative phase first $MFDA_2$
      3. Indeterminate $MFDA_3$
      4. Repeated pulse R_3, R_6, R_{11}
    - B...low frequency first MFDB
      1. positive phase first $MFDB_1$
      2. negative phase first $MFDB_2$
      3. Indeterminate $MFDB_3$
      4. repeated pulse R_3, R_6, R_{11}
    - I...Indeterminate dispersion MFI
    - W...wavelet MFW
    - R_3...repeated pulses 2 1/2-4 minutes later MFR_3
    - R_6... " " 4-7 " " MFR
    - R_{11}.. " " 8-11 " " MFR_{11}
- m...many cycles present (more than 5)
  - U...nondispersed MmU
    1. positive phase first MmU_1
    2. negative phase first MmU_2
    3. Indeterminate MmU_3
    4. repeated pulse R_3, R_6, R_{11}
  - D...dispersed MmD
    - A...high frequency first MmDA
      1. positive phase first $MmDA_1$
      2. negative phase first $MmDA_2$
      3. Indeterminate $MmDA_3$
      4. repeated pulse R_3, R_6, R_{11}
    - B...low frequency first MmDB
      1. positive phase first $MmDB_1$
      2. negative phase first $MmDB_2$
      3. Indeterminate $MmDB_3$
      4. repeated pulse R_3, R_6, R_{11}
    - I...Indeterminate dispersion MmI
    - R_3...repeated waves follow 2 1/2-4 minutes after MmR_3
    - R_6... " " " 4-7 " " MmR_6
    - R_{11}.. " " " 8-12 " " MmR_{11}

The classification system proposed here is both new and unresearched. The task of patiently searching through the signals, now numbering in excess of 2500 in order to classify, record, and do statistical analyses on the total grouping is enormous. A step in this direction was made for the 1970 observations at College, as was discussed in chapter 2. It remains here to complete the picture of percentages of signal types in each observed large category for that year. The percentages of occurrence of the AIW signal types observed at College for 1970 are shown in the table below.

TABLE AI-1

Signal Type	Number of Obs	Percentage Occurrence
SP	1	0.2
SN	0	0.0
SB	7	1.8
MFU	10	2.5
MFDA	31	7.9
MFDB	0	0.0
MFI	73	18.5
MmU	4	1.0
MmDA	12	3.0
MmDB	0	0.0
MmI	246	62.4
MmR_6	7	1.8
MmR_{11}	3	0.8

APPENDIX II

Ray-Tracing

In order to assist in locating the likely range from Inuvik at which an AIW was generated, a ray-tracing program was written. The input data to the sound speed profile was balloon-sounding data of temperature from which computed sound speed was undertaken up to approximately 30 Km.. From that point up to 118 Km., a standard atmospheric sound speed profile for 60 degrees north in January from USSA Supplements, 1966 was attached to the previous profile. For 120-250 Km. a standard profile of temperature for exospheric temperature 1100 degrees Kelvin was employed. The sound speed was computed assuming the relationship $C_s = 20.06\ (T)^{1/2}$ holds. The latter assumption is invalid, of course, but the need for the ray-tracing approach justified its use albeit sparingly. The fact that the ray-tracing arguement for AIW in a medium which might be only two or three wavelengths long also was a consideration for cautious and limited application of the ray-tracing procedure.

The program itself computed Snell's law of refraction for a series of 99 iso-velocity layers. It computed the refraction law by using a cosine format so as to reference the angles to inclination to the horizontal for quicker comparison to AIW. The equation for the refraction was $\phi_n = \mathrm{Cos}^{-1}\ C_n/C_{n-1}\ \mathrm{Cos}\phi_{n-1}$, where the ϕ_n's were the emergence angles into a new layer, and the ϕ_{n-1}'s were the entrance angles of the layer.

Travel time was also computed for each layer given by $T_n = Y_n/C_n \ CSC \ \phi_n$ summing for each layer so as to give a cumulative output of travel time.

Range was computed and cumulatively summed for each layer using $X_n = Y_n \ Cot \ \phi_n$.

The program neglects winds, earth curvature and horizontal sound speed gradients. Diagrams of the rays and sound speed profiles for a source at 100 and 110 Km. are shown if Figs. A-2.1 and A-2.2 respectively.

Since the sound speed profile was digitized at 100 points, care was taken to place one of these points at each major transition region of the model and real parts of the compiled atmosphere. Based upon these locations, the time spent by each ray in a given atmospheric layer could be computed as a percentage of the total travel time from the source height to the ground. The following average values apply to the angles which initially start downwards (negative).

Mesosphere..... 32%
Stratosphere..... 42%
Troposphere..... 7%
Thermosphere..... 18%

For positive angles, the average percentage of the total travel time spent in the same layer was

Mesosphere..... 18%
Stratosphere..... 27%
Troposphere..... 4%
Thermosphere..... 51% .

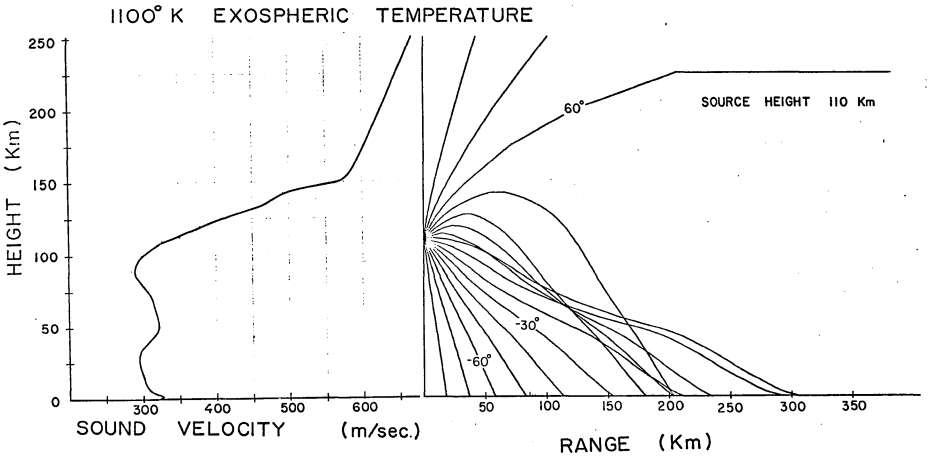

Fig. A-2.1. Compilped sound speed profile and resulting ray diagram for a source height of 110 Km.. Rays are at 10° interval.

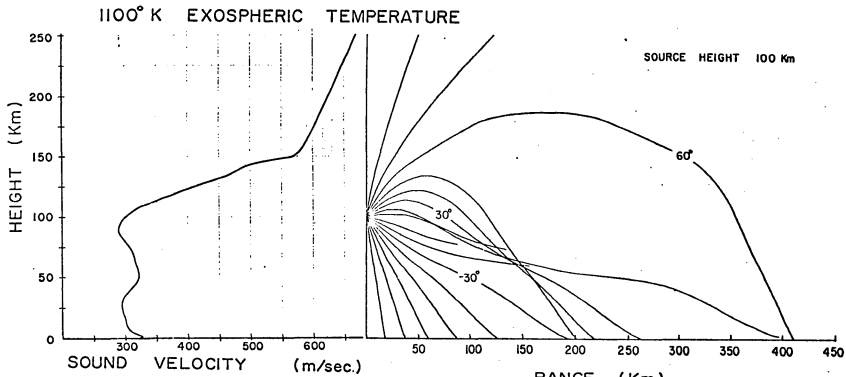

Fig. A-2.2. Compiled sound speed profile and resulting ray diagram for a source height of 100 Km.. Rays are at 10° interval.

BIBLIOGRAPHY

Akasofu, Syun-Ichi, Large-scale Auroral Motions and Polar Magnetic Disturbances-I, Journal of Atmospheric and Terrestrial Physics, 19, 1960, 10-25.

_____, The Development of the Auroral Substorm, Planetary and Space Science, 12, 1964, 273-282.

_____, Chapman, S., & Meng, C.-I. The Polar Electrojet, Journal of Atmospheric and Terrestrial Physics, 27, 1965, 1275-1305.

_____, et.al., Dynamics of the Aurora-IV. Polar Magnetic Substorms and Westward Travelling Surges, Journal of Atmospheric and Terrestrial Physics, 1966a,28

_____, et.al., Dynamics of the Aurora-V. Poleward Motions., Journal of Atmospheric and Terrestrial Physics, 28, 1966b, 497-503.

_____, et.al., Dynamics of the Aurora-VII. Equatorward Motions and the Multiplicity of Auroral Arcs, Journal of Atmospheric and Terrestrial Physics, 28, 1966c, 627-635.

_____, & Meng, C.-I., Polar Magnetic Substorm in the Evening Sector, Journal of Atmospheric and Terrestrial Physics, 29, 1967, 1135-1137.

_____, Polar and Magnetospheric Substorms, Dordrecht- Holland : D. Reidel Publishing Company, 1968, 208 pages.

_____, and Chapman, S., Solar-Terrestrial Physics., Oxford: Oxford University Press, 1972, 901 pages.

_____, and Snyder, A.L., Comments on the Growth Phase of Magnetospheric Substorms, Journal of Geophysical Research, 77, 1972.

Atkinson, G., Theory of Polar Substorms, Journal of Geophysical Research, 71, 1966, 5157-5168.

_____, The Current System of Geomagnetic Bays, Journal of Geophysical Research, 72, 1967, 6063-6067.

Axford, W.I., Magnetospheric Convection, Reviews of Geophysics, 7, 1969, 421-459.

Barry, G., Ray Tracings of Acoustic Waves in the Upper Atmosphere, Journal of Atmospheric and Terrestrial Physics, 25, 1963, 621-629.

Bhattacharyya, B.K., A Study of Auroral Motions from All-Sky Camera Records, Canadian Journal of Physics, 38, 1960.

Bonnevier, Bjorn, et.al., A Three Dimensional Model Current System for Polar Magnetic Substorms, Journal of Geophysical Research, 75, 1970, 107-122.

Bostrom, Rolf, A Model of the Auroral Electrojets, Journal of Geophysical Research, 69, 1964, 4983-4999.

Brown, R.F., An Automatic Multichannel Correlator, Journal of Research of the National Bureau of Standards, 67c, 1963, 33-38.

Bucknam, Dale B., and Lincoln, J. Virginia, Data on the Solar Proton Event of November 2, 1969 through the Geomagnetic Storm of November 8-10, 1969, Upper Atmosphere Geophysics, Rpt. # UAG-13, Boulder, Colorado: U.S. Dept. of Commerce, May, 1971.

Campbell, W.H., and Young, J.M., Auroral Zone Observations of Infrasonic Pressure Waves Related to Ionospheric Disturbances and Geomagnetic Activity, Journal of Geophysical Research, 68, 1963, 5909-5916.

Chapman, S., The Electric Current Systems of Magnetic Storms, Terrestrial Magnetism and Electricity and Magnetism, 40, 1935, 349-370.

Chapman, S., & Bartels, J., Geomagnetism, I, London: Oxford University Press, Amen House, 1962 ed. 338-354.

Chimonas, G., Infrasonic Waves Generated by Auroral Currents, Planetary and Space Science, 18, 1970, 591-598.

_____, & Peltier, W.R., The Bow Wave Generated by an Auroral Arc in Supersonic Motion, Planetary and Space Science, 15, 1970, 599-612.

Chrzanowski, P., et.al., Traveling Pressure Waves Associated with Geomagnetic Activity, Journal of Geophysical Research, 66, 1961, 3727-33.

_____, et.al., Infrasonic Pressure Waves Associated with Magnetic Storms, Journal of the Physical Society of Japan, 17, 1962, 9-13.

Cook, Richard K., Atmospheric Sound Propagation, Atmospheric Exploration by Remote Probes, 2, Washington, D.C.: National Academy of Sciences, National Research Council, 1969, 633-669.

Cook, Richard K., Infrasound Radiated during the Montana Earthquake of 1959 August 18, The Geophysical Journal of the Royal Astronomical Society, 26, 1971, 191-198.

_____, and Bedard, Alfred J., On the Measurement of Infrasound, The Geophysical Journal of the Royal Astronomical Society, 26, 1971, 5-11.

Cummings, W.D., and Dessler, A.J., Field-Aligned Currents in the Magnetosphere, Journal of Geophysical Research, 72, 1967, 1007-1013.

_____, and Coleman, P.J., Simultaneous Magnetic Field Variations at the Earth's Surface and at Synchronous, Equatorial Distance. Part I. Bay-Associated Events., Radio Science 3, 1968, 758-761.

Davis, T.N., and Kimball, D.S., Incidence of auroras and their north-south motions in the northern auroral zone, Geophysical Institute Report, UAG R100, University of Alaska, 1960.

Donn, William L., and Ewing, Maurice, Atmospheric Waves from Nuclear Explosions, Journal of Geophysical Research, 67, 1962, 1855-1866.

_____, and Posmentier, E.S., Infrasonic waves from the marine storm of April 7, 1966, Journal of Geophysical Research, 72, 1967, 2053-61.

ESSA, NASA, USAF, U.S. Standard Atmosphere Supplements, 1966, Washington, D.C.: Government Printing Office, 1966.

Evans, J.E., North Polar, South Polar, World Maps and Tables of Invariant Magnetic Coordinates for Six Altitudes: 0, 100, 300, 600, 1000, and 3000 Km., Palo Alto, California: Lockheed Palo Alto Reseach Laboratory, 1969.

Fahl, Charles, Internal Atmospheric Gravity Waves at Fairbanks, Alaska, Master's thesis, Geophysical Institute, University of Alaska, Fairbanks, Alaska, 1969, unpublished.

Fejer, J.A., Theory of Auroral Electrojets, Journal of Geophysical Research, 68, 1963, 2147-2157.

Feldstein, Y.I., and Starkov, G.V., Dynamics of Auroral Belt and Polar Magnetic Disturbances, Planetary and Space Science, 15, 1967, 209.

Goerke, V.H., Infrasonic Observations of a Fireball, Sky and Telescope, 32, 1966, 313.

Herrin, Eugene and McDonald, John A., A Digital System for the Acquisition and Processing of Geoacoustic Data, The Geophysical Journal of the Royal Astronomical Society, 26, 1971, 13-20.

Hines, C.O., et.al., Physics of the Earth's Upper Atmosphere, Englewood Cliffs, New Jersey: Prentice-Hall, Inc., 1965, 271-298.

Iijima, Takesi, and Fukushima, Nasohi, World-wide Geomagnetic Change Preceding the Onset of Auroral Electrojet, Report of Ionosphere & Space Research in Japan, 22, 1968, 161-172.

_____, Nagata, Takesi, Signatures for Substorm Development of the Growth Phase and Expansion Phase, Planetary and Space Science, 20, 1972, 1095-1112.

Ivliyev, D. Ya., et.al., Development of an Elementary Magnetic Disturbance, Geomagnetism and Aeronomy, 2, 1970, 231-234.

Johnson, R.E., An Infrasonic Pressure Disturbance Study of Two Polar Substorms, Planetary and Space Science, 20, 1972, 313-329.

Kamide, Yohsuke, et.al., Microstructure of Auroral-Zone Electrojet, Report of Ionosphere and Space Science in Japan, 23, 1969, 185-208,

Kim, J.A., and Currie, B.W., Further Observations of the Horizontal Movements of Aurora, Canadian Journal of Physics, 38, 1960.

Kisabeth, Jerry L., and Rostoker, Gordon, Development of the Polar Electrojet during Polar Magnetic Substorms, Journal of Geophysical Research, 76, 1971, 6815-6828.

Khorosheva, O.V., and Darchiyeva, L.A., Development of a Polar Substorm, Geomagnetism and Aeronomy, 10, 1970, 228-230.

Larson, R.J., et.al., Correlation of Winds and Geographic Features with Production of Certain Infrasonic Signals in the Atmosphere, The Geophysical Journal of the Royal Astronomical Society, 26, 1971, 201-214.

Liszka, Ludwik, and Westin, Hans, Detection of 2 Hz Infrasound Produced by Moving Auroral Electrojets, KGO Report #727, Kiruna, Sweden: Kiruna Geophysical Observatory of the Royal Swedish Academy of Science and the University of Umea, April, 1972.

Lyon, G.F., and Kavadas, A., Horizontal Motions in Radar Echoes from Aurora, Canadian Journal of Physics, 36, 1958.

Maeda, K., and Young, J.M., Propagation of the Pressure Waves Produced by Auroras, Journal of Geomagnetism and Geoelectricity, 18, 1966, 275-299.

_____, and Watanabe, T., Pulsating Aurorae and Infrasonic Waves in the Polar Atmosphere, Journal of the Atmospheric Sciences, 21, 1964, 15-29.

Mcnish, A.G., Heights of Electric Currents Near the Auroral Zone, Terrestrial Magnetism and Atmospheric Electricity, 43, 1938, 67-79.

McPherron, R.L., Growth Phase of Magnetospheric Substorms, Journal of Geophysical Research, 75, 1970.

Nicparenko, S., Aurorally Associated Infrasonic Waves, Master's Thesis, Geophysical Institute, University of Alaska, Fairbanks, Alaska, 1967, unpublished.

Procunier, R.W., Observations of Acoustic Aurora in the 1-16 Hz Range, The Geophysical Journal of the Royal Astronomical Society, 26, 1971, 183-189.

Pusovkin M.I., et.al., Development of Magnetic Storms and the State of the Magnetosphere According to the Data of Ground-based Observations, Annales De Geophysique, 3, 1970, 761-770.

Rostoker, Gordon, Midlatitude Transition Bays and their Relation to the Spatial Movement of Overhead Current Systems, Journal of Geophysical Research, 71, 1966.

_____, Polar Magnetic Substorms, Reviews of Geophysics and Space Physics, 10, 1972, 157-211.

_____, Geomagnetic Indices, Reviews of Geophysics and Space Physics, 10, 1972, 935-950.

_____, The Study of the Dynamic Motion of the Aurora Borealis, Killam Earth Sciences Report, The University of Alberta, Edmonton, Canada, 1972.

Sachdev, R.N., Microbarograph Oscillations Associated with Geomagnetic Activity, Journal of Geophysical Research, 74, 1969, 5413-5417.

Swift, D.W., The Generation of Infrasonic Waves by Auroral Electrojets, Preprint, Geophysical Institute, University of Alaska, Fairbanks, Alaska, 1973.

Takesi, Iijima, Relationship of Magnetospheric Substorms on the Ground and the Distant Magnetotail, Report of Ionosphere and Space Research in Japan, 26, 1972, 149-157.

Westcott, E.M., et.al., Auroral and Polar Cap Electric Fields from Barium Releases, Particles and Fields in the Magnetosphere, Dordrecht, Netherlands: D. Reidel, 1970.

Wilson, C.R., Infrasonic Pressure Waves from the Aurora: a Shock Wave Model, Nature, 216, 1967, 131-133.

_____, Auroral Infrasonic Waves, Journal of Geophysical Research, 74, 1969a, 1812-1836.

_____, Infrasonic Waves from Moving Auroral Electrojets, Planetary and Space Science, 17, 1969b, 1107-1120.

_____, Two Station Auroral Infrasonic Wave Observations, Planetary and Space Science, 17, 1969c, 1817-1847.

_____, Auroral Infrasonic Wave-Generation Mechanism, Journal of Geophysical Research, 77, 1972, 1820-1843.

_____, Auroral Infrasonic Waves and Poleward Expansions of Auroral Substorms at Inuvik, N.W.T., Canada, The Geophysical Journal of the Royal Astronomical Society, 26, 1971, 179-181.

_____, and Nichparenko, S., Evidence of Two Sound Channels in the Polar Atmosphere from Infrasonic Observations of the Eruption of an Alaskan Volcano, Nature, 211, 1966, 163-165.

_____, Infrasonic Waves and Auroral Activity, Nature, 214, 1967, 1298-1302.

Young, Jesse M., Acoustic Waves Associated With Aurora, Unpublished Preprint, Environmental Science Services Administration, Research Laboratories, Wave Propagation Laboratory, Geoacoustics Group, 1968.

World Data Center A, High Altitude Meteorogical Data, VI, Asheville, North Carolina: U.S. Dept. of Commerce, 1970.